Old Dominion University

ODU Digital Commons

Summer 2019

Endogenous Force Transmission Between Epithelial Cells and a Role for α-Catenin

Sandeep Dumbali
Old Dominion University, sdumb001@odu.edu

ENDOGENOUS FORCE TRANSMISSION BETWEEN EPITHELIAL CELLS AND A ROLE FOR α-CATENIN

by

Sandeep Dumbali
B.E. July 2009, Solapur University, India
M.Tech. December 2011, Visvesvaraya Technological University, India

A Dissertation Submitted to the Faculty of
Old Dominion University in Partial Fulfillment of the
Requirements for the Degree of

DOCTOR OF PHILOSOPHY

MECHANICAL ENGINEERING

OLD DOMINION UNIVERSITY
August 2019

Approved by:

Venkat Maruthamuthu (Director)

Shizhi Qian (Member)

Krishnanand Kaipa (Member)

Robert Bruno (Member)

ABSTRACT

ENDOGENOUS FORCE TRANSMISSION BETWEEN EPITHELIAL CELLS AND A ROLE FOR α-CATENIN

Sandeep Dumbali
Old Dominion University, 2019
Director: Dr. Venkat Maruthamuthu

In epithelial tissues, epithelial cells adhere to each other as well as to the underlying extra-cellular matrix (ECM). E-cadherin-based intercellular junctions play an important role in tissue integrity. These junctions experience cell-generated mechanical forces via apparent adaptor proteins such as beta (β) catenin, alpha (α) catenin and vinculin. Abnormalities in these junctions may result in skin related diseases and cancers. Here, I devised methods to determine the endogenous intercellular force within cell pairs as well as in large epithelial islands. I further ascertained the factors that affect the level of inter-cellular tension.

Experiments with pairs of epithelial cells exogenously expressing either of two altered E-cadherin constructs on top of endogenous E-cadherin showed that the inter-cellular tension for these cases was similar to wild type cells. This implied that the endogenous E-cadherin was dominant in setting the level of cell-cell contact tension. To analyze intercellular force transmission within large islands, I extended the traction force imbalance method to large micro-patterned islands. It was shown that colony level intercellular forces exerted at the midline by one half of the colony on the other were tensile in nature and showed significant anisotropy with respect to the midline orientation. Finally, to determine what molecular factors set the level of tension transmitted through single cell-cell contacts, I determined the inter-cellular tension in pairs of cells with

perturbed α-catenin. I found that α-catenin knockout not only decreased inter-cellular tension but also the traction forces exerted at the cell-ECM interface. This may be due to roles outside of cell-cell junctions for α-catenin. However, α-catenin mutants with altered binding to vinculin binding did not show significant differences in inter-cellular tension compared to wild type cells. Thus, α-catenin is essential for normal levels of intercellular tension, but the forces transmitted at cell-cell contacts are not very sensitive to the level of vinculin at the cell-cell contact in cell pairs. This may be because vinculin can also be recruited to cell-cell contacts by molecules other than α-catenin, such as β-catenin. These results highlight some essential and non-essential molecular factors regulating cell-cell junctional tension level.

This dissertation is dedicated to my parents, Geeta Dumbali and Prakash Dumbali.

ACKNOWLEDGEMENTS

I would like to express my deep gratitude to my advisor Dr. Venkat Maruthamuthu, for his relentless efforts and valuable guidance throughout my PhD career. I would like to thank him for giving me the opportunity and believing in me, to work under him at Old Dominion University, in a field which was slightly new to me. His sincerity and dedication towards research have inspired me to build my research career and motivated me to strive for excellence. I am extremely grateful for his invaluable pointers and suggestions which have helped me for being a better speaker.

I would like to thank my committee members Dr. Shizhi Qian, Dr. Krishnanand Kaipa and Dr. Robert Bruno for their guidance and suggestions in my research. Finally, I thank my parents and cousins for their never-ending love, support and motivation throughout my PhD career.

Table of Contents

LIST OF TABLES

LIST OF FIGURES

CHAPTER

1. INTRODUCTION

In a multicellular organism, the most fundamental physical interaction between cells is that they cohere together to form an organized multicellular structure. This interaction is through cell-cell junctions wherein cells adhere to one another as well as an attachment to the extracellular matrix (ECM) that they secrete, which consists of a complex network of proteins and polysaccharide chains. One important example of multicellular structure is that found in epithelial tissue, wherein cells are closely bound together into quasi-2D sheets or multi-layered collectives. Epithelia cover all the inner and outer cavities in the body [1]. Epithelial sheets sit on the basal lamina, a thin mat-like layer of the extracellular matrix (ECM). Depending on the tissue, the ECM, which is a network of cross-linked proteins and carbohydrates, can include different constituents, including collagen, laminin, elastin and fibronectin fibers.
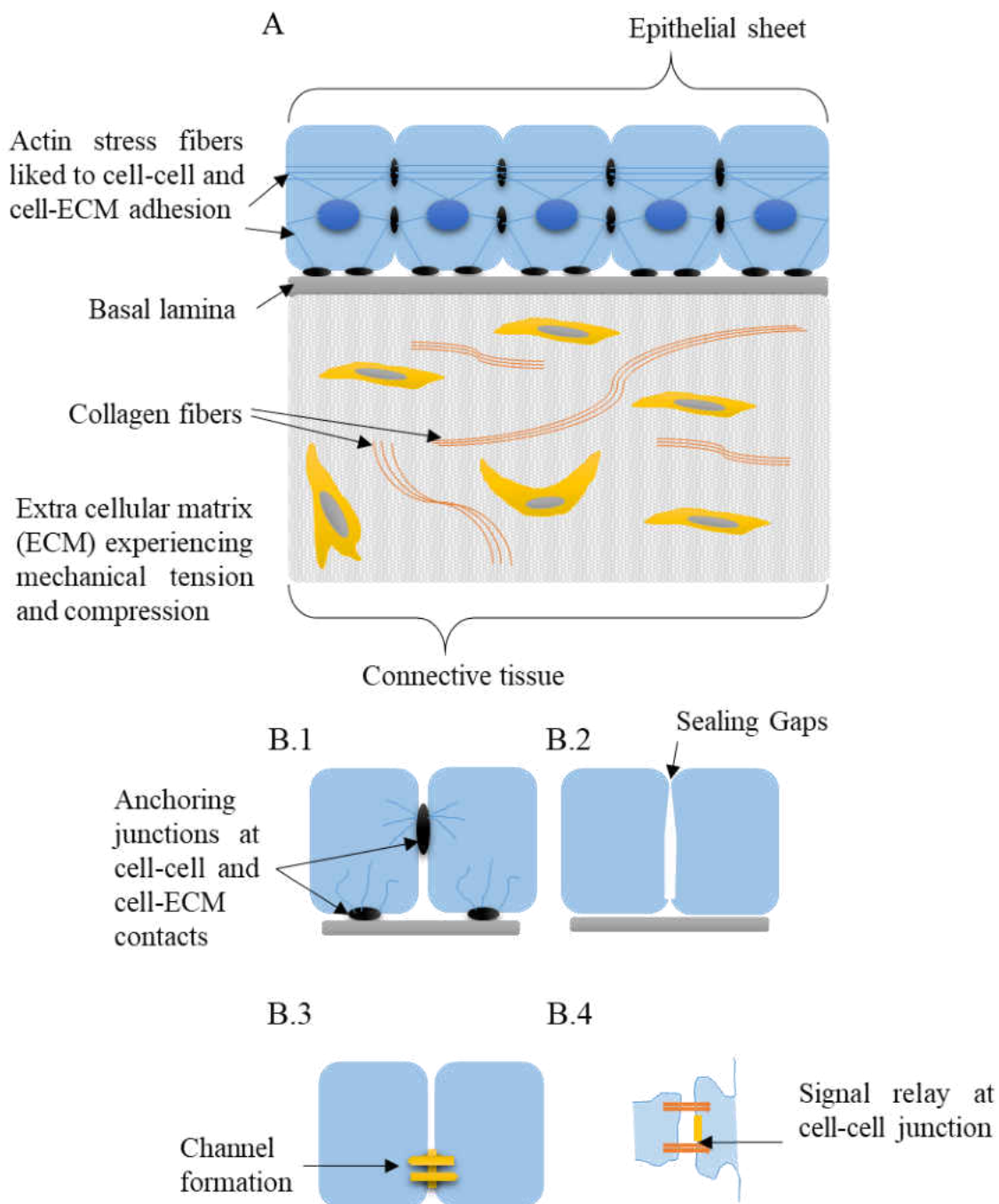
Figure 1: Schematic depiction of epithelial tissues and the junctions involved in epithelial cell-cell contacts. (A) Multicellular cartoon showing epithelial tissue. (B.1) Anchoring junctions. (B.2) Occluding junctions. (B.3) Channel forming junctions. (B.4) Signal relaying junctions.

In an epithelium, cells are directly attached to each other by cell-cell contacts where actin cytoskeletal filaments are anchored, transmitting stresses across the interior of each cell from one adhesion site to another, as shown in Figure 1. Cell-cell or cell-ECM junctions are diverse in structure and have different functions other than transmitting cell-generated or external stress. Based on their structure and functions, these are classified into four junctions: (B.1) Anchoring junctions, which are attached to the cytoskeleton and include both cell-cell adhesions and cell-ECM adhesions – these are involved in force transmission. (B.2) Occluding junctions help in sealing the gaps between epithelial cells and making a sheet, which serves as an impermeable barrier. (B.3) Channel-forming junctions link to the cytoplasm of neighboring cells, thereby creating passageways. (B.4) Signal-relaying junctions transmit signals from one cell to another across their plasma membrane at cell-cell contact site [1].

1.1 Introduction to Endogenous Force Generation by Epithelial Cells

Epithelial cells are either constantly in contact with adjacent cells or with the ECM. They experience external forces and exert internal forces. External forces can be the forces applied by neighboring cells, by the moving surrounding liquid media or the forces from ECM substrate, while the internal forces are generated within the cell by the cytoskeleton [2]. These internal forces are generated by actomyosin linkages which consist of non-muscle myosin II motor protein linking to filamentous actin. Various processes in multicellular organisms like changes in shape, size, position and proliferation are due to both these forces generated by molecular motors and transmitted via cytoskeletal elements and adhesive molecules [3]. Cell-generated forces in epithelial cells are transmitted through the plasma membrane to the ECM mainly by integrins and

to the other cells mainly by cadherins. Transmission of these forces will be efficient only if the bonds between the actomyosin network and the adhesions are strong [4].

The cytoskeleton is a vastly dynamic cellular scaffolding assembly composed of filamentous actin (F-actin, 6 nm in diameter), intermediate filaments (10 nm in diameter) and microtubules (23 nm in diameter), which provide a fundamental structure for mediating force transmission [5]. These cytoskeletal elements consist of many monomers, rather than single proteins, that are able to span large distances within the cell. Microtubules are formed by polymerization of tubulins into hollow cylindrical structures that provide a track for motor proteins such as kinesins and dyneins to travel between different cell compartments [6]. Intermediate filaments are formed by the polymerization of vimentin, keratin and lamin monomers that connect the nucleus with the endoplasmic reticulum, mitochondria and golgi apparatus. This provides structural integrity to the cell. To form the cytoskeletal contractile apparatus, actin monomers assemble into filamentous actin (F-actin) together with myosin motors. The actomyosin assembly plays an important role in connecting multiple parts of the cell membrane and cell membrane to the nucleus [7]. These filaments at the cell's plasma membrane anchor into clusters of proteins that include focal adhesions which link the actin cytoskeleton, through transmembrane integrin receptors, with the ECM as well as with cadherin adhesions that couple neighboring cells.
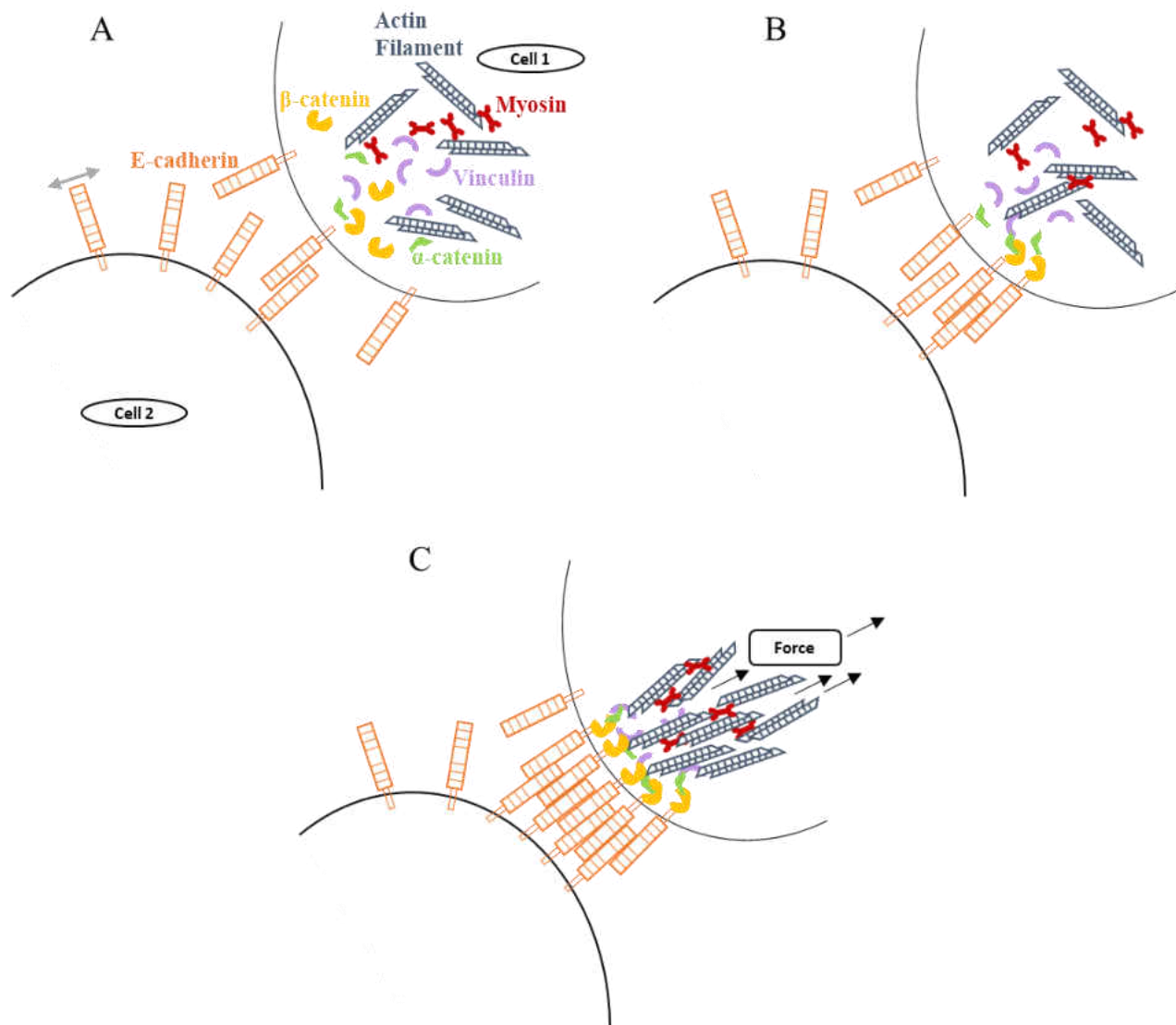
Figure 2: Cell-cell adhesion clusters and their interaction with the actomyosin network. (A) Homophilic binding of E-cadherin primarily initiates cell-cell adhesion between two epithelial cells. (B) E-cadherin binds actin filaments through adaptor proteins such as β-catenin, α-catenin and vinculin. (C) Actomyosin contractility produces pulling forces on adhesion complexes. These forces can induce conformational changes in α-catenin, thereby exposing buried vinculin-binding sites. In turn, vinculin binding promotes further binding of actin filaments to adhesion clusters.

This feedback mechanism enhances the mechanical coupling between the actomyosin network and adhesion clusters.

Force transmission by newly formed E-cadherin-based cell-cell adhesions has been depicted in Figure 2. E-cadherin interacts with cytoplasmic proteins, which modulates cluster formation. E-cadherin constitutively binds to β-catenin. α-catenin binds to β-catenin and mediates interaction with the actin cytoskeleton. Actomyosin contractility initiates pulling forces on the adhesion. This actomyosin tension at cell-cell adhesions opens a binding site in α-catenin for vinculin. Vinculin binding promotes further binding of actin filaments. Stability of α-catenin increases with vinculin recruitment, thereby strengthening mechanical coupling at adhesion sites [4].

1.2 Significance of E-cadherin in Cell-Cell Contacts

E-cadherin, being a type I classical cadherin, is an important protein which mediates interactions between neighboring cells. E-cadherin influence morphogenetic changes that leads tissue remodeling and differentiation [8] Cell-cell contacts with cadherin junctions are considered to be mechanically active structures [9]. Cadherin adhesion not only functions in binding cells together but also coupling together the contractile cortices of adjacent cells to provide transmission of tension at the adhesion site [10]. Intercellular adhesion mediated by E-cadherin plays crucial roles in tissue repair, integrity, cell proliferation [11] and morphogenesis [12]. The actin cytoskeleton is closely associated with E-cadherin adhesion receptors and influences the regulation of cell-cell junction dynamics [13]. For functional cadherin adhesion, an intact actin cytoskeleton is required. Establishing a physical coupling with the actin cytoskeleton is necessary for classical cadherins to build junctions that can resist mechanical stress. An initial model postulated that α-catenin

mediated stable association between the cadherin- β-catenin complex and F-actin [14-18]. A later study demonstrated that, as a monomer, α-catenin binds to β-catenin but showed high affinity for F-actin only as a homodimer [19]. It was also suggested that there couldn't be any interaction between β-catenin and F-actin via α-catenin due to the overlap of β-catenin binding site and homodimerization domain of α-catenin [19-22]. This has helped in setting a molecular premise for the regulation of cadherin-catenin-actin but was unable to provide upfront clarification of the ways in which the actin cytoskeleton transmits tensile forces via E-cadherin adhesions. A possible role for α-catenin then emerged in a study with Drosophila embryos, where the lateral movement of cadherin clusters within the membrane was increased due to the depletion of α-catenin [23]. A more recent study showed that α-catenin can directly mediate the link between the cadherin- β-catenin complex and F-actin under force [24]. Thus, α-catenin plays an important role in binding E-cadherin receptors to actin cytoskeleton despite the fact that some other aspects of cellular behavior can be affected by α-catenin, independently of its role in cadherin adhesion [25, 26].

1.3 Importance of Cell-ECM Traction and Intercellular Forces

For efficient transmission of forces, strong links are required between the actomyosin network and adhesions. The composition and the size of the adhesion are critical parameters for such efficient force transmission. Adhesion adapts to mechanical stress by modifying the size and shape of individual adhesion clusters. Thus, the adhesion structure depends on both internally generated and external forces. For example, cytoskeleton generated forces on integrin adhesions induce an opposing balancing force from the ECM. This means that stresses cannot develop properly at focal adhesions if the ECM is not rigid enough [4]. The traction forces exerted by cells at focal adhesions are directly proportional to the rigidity of the ECM. On the other hand, adhesions can change cell-

generated forces by influencing actomyosin assembly. Cell adhesions nucleate actin assembly and activate myosin II, thereby modifying actomyosin organization and dynamics. Integrin and cadherin adhesions have common signaling components that regulate actomyosin assembly. Due to this, mechanical and biochemical cross-talk exists between them. This cross-talk can either enhance or suppress adhesion, depending on the environmental and cellular context. This has important implications in morphogenesis as well as in tumor invasion and metastasis [4]. In vitro studies have shown that high traction forces exerted on cell-ECM contacts can disturb cell-cell contacts, which implies that actomyosin tension at cell-cell junctions is integrin dependent. Adaptive transmission of the forces allows cell movement, cell shape changes and tissue morphogenesis [4].

Why is it necessary to study cell generated or applied mechanical forces in cell biology? The fundamental reasonable answer is that numerous studies have illustrated that cells constantly experience mechanical forces that directly affect their functions *in vivo* [27]. The concept that forces can regulate tissue remodeling and development was proposed in the year 1892 by Dr. Wolff [28]. According to his study, the structure of bone tissue adapts to the mechanical environment under the observation that the principal stress lines were matched within a trabecula due to consistent physical loading [28]. Even researchers from the same era proposed that mechanical forces were responsible for shaping tissues and organs throughout embryonic development [29, 30]. However, due to the lack of suitable tools, these scientists were unable to directly test these ideas experimentally. After a century passed, these mechanobiological concepts and their development now appear to be closely associated to the advent of facilitating technologies. The initial observations signifying that mechanical forces drive embryogenesis and bone structure were

a natural result of newfound microscopy methods. The recent resurgence in reviewing the role of mechanics in cell biology has largely been facilitated by a suite of tools to measure and influence such forces *in vitro*. Aspects of mechanically-induced anabolic bone growth *in vivo* were studied *in vitro*, wherein application of strains that would be experienced by bone during physical movement increases cell proliferation [31], osteogenic differentiation [32, 33] and bone deposition [34]. The first illustration that non-muscle cells can generate contractile forces on their own in addition to externally applied forces, by Harris and Stopak, showed that cells cultured on soft polymer substrates would wrinkle the substrate surface [35, 36]. Based on various studies over the past three decades, it is now clear that intracellular forces can be generated by most eukaryotic cells that are associated with a surrounding extracellular matrix or neighboring cells and that these contractile forces are critical for a number of biological processes, such as cell migration, mitosis, stem cell differentiation and self-renewal. These forces are clearly essential for physical processes like mitosis and migration [37, 38].

To study how mechanical forces regulate cellular functions, it is important to consider the cell not in isolation but rather in direct physical contact with the ECM or with neighboring cells. This is because adhesion of cells to the matrix affects the structural organization of the cell itself. The changes in cell shape and cytoskeletal architecture is partly due to integrin binding and clustering against ECM ligands [27]. As the cytoskeleton is connected to the nuclear membrane, forces experienced or generated by the cell-ECM module are consequently transmitted and sensed all over as a coordinated system.

1.4 Factors that Regulate the Cellular Forces

During adhesion by cadherins and integrins, activities like robust actin cytoskeletal rearrangements, activation of GTPase RhoA and enhancement of myosin II activity are triggered by the forces applied to adhesion receptors, resulting in the generation of a cell contraction force through the mutual sliding of actin and myosin II filaments, as shown in Figure 3 [39].
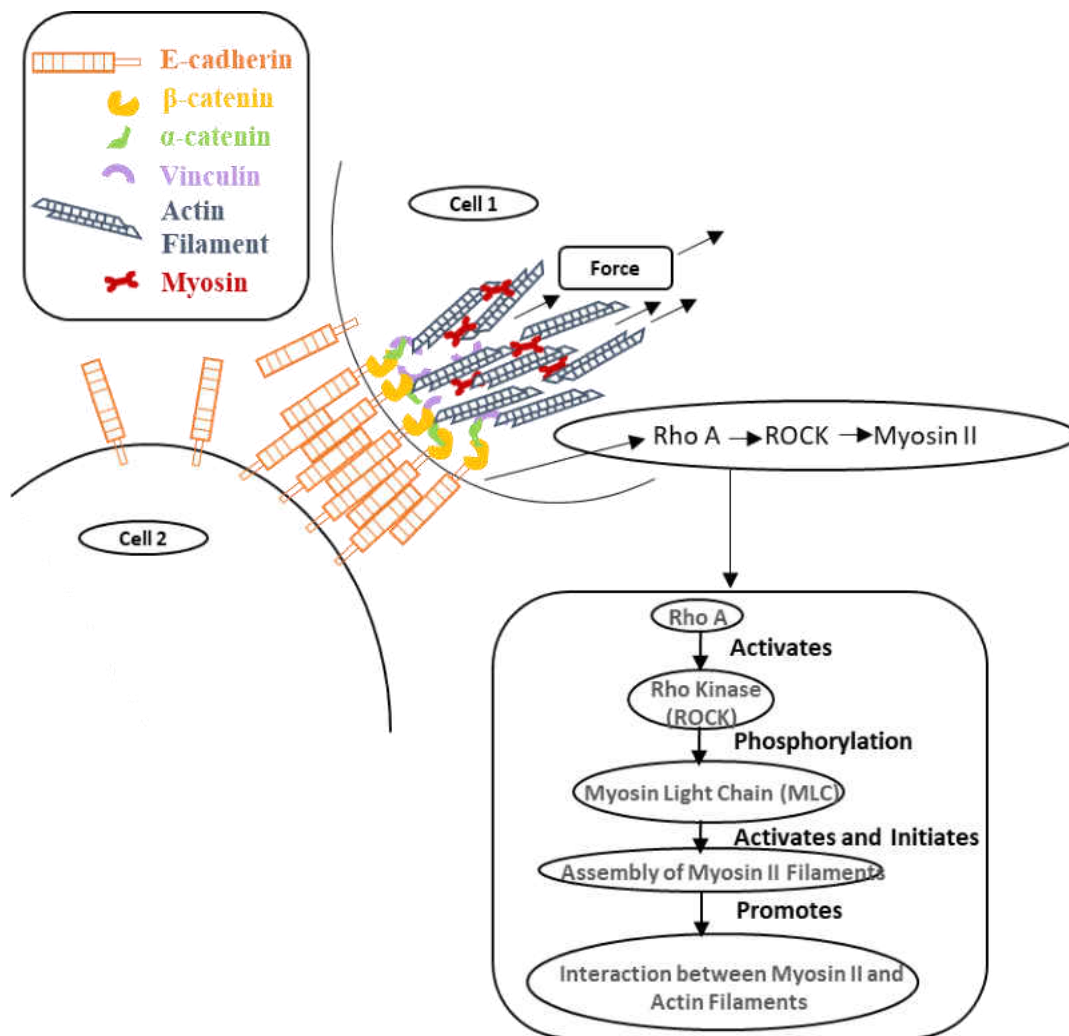
Figure 3: Cadherin-RhoA mediated force transmission. E-cadherin junction formation initiating RhoA activity, thereby activating its effector ROCK. ROCK then promotes the formation of actomyosin stress fibers.

At E-cadherin adhesions, the catenins and other adapter molecules modulate force transmission. α-catenin deficient cells, which do not directly bind to vinculin, have revealed an altered force response [40]. It is still unclear how α-catenin regulates cell-cell force transmission, although it is known to regulate forces transmitted during collective cell migration [41]. Interestingly, in epithelial cells, the affinity of E-cadherin is drastically reduced with α-catenin depletion, suggesting that there may be some contribution by α-catenin in modulating force-activated adhesion and strengthening of the adhesion [40]. Due to application of shear stress, β-catenin constantly folds and unfolds its armadillo [42], a binding domain, and is also phosphorylated. β-catenin deficient cells fail to strengthen their adherens junctions in response to externally applied stress [43]. At cell-cell adhesions, non-muscle myosin II is activated by RhoA, a Rho GTPase. When cadherins from two adjacent cells engage, RhoA is activated [44, 45] and this leads to sustained mechanical force exertion on the cell-cell adhesions [46]. Moreover, indirectly inhibiting RhoA by depletion [47] or directly inhibiting the RhoA [48], effector ROCK have both been shown to significantly decrease adherens junctional tension [49].

The traction or intercellular forces are influenced by other factors, such as the ECM. To measure these forces, it is important to understand the mechanical properties of the substrate or ECM. The cell traction measurement methods assume that the substrate's material properties are the same in all directions, i.e., isotropic as well as linear elastic. A solid material deforms under the application

of force and there is a certain relationship between force and deformation. The effect of force depends on the area of deformation which can be defined in terms of stress, the force per unit area and strain, the fractional change in length of a material. This stress, for linear elastic materials, linearly increases with an increase in strain, and the relation therein is defined by stiffness or Young's Modulus, E [50]. These linear elastic and isotropic substrates are also often assumed as infinite or semi-infinite in size compared to the cell size. For many methods, polyacrylamide (PAA) hydrogels and polydimethylsiloxane (PDMS) are used as cell substrates which are helpful in measuring traction forces exerted by cells. Increasing the rigidity of ECM or in vitro substrate showed considerable increase in cell-ECM traction forces and inter-cellular forces [51]. Moreover, different ECM ligands like collagen I or fibronectin under constant rigidity can affect traction and inter-cellular force magnitudes [51].

1.5 Methods used to Measure Cellular Forces

The role of mechanical force in cell biology can be examined using a limited number of techniques which significantly vary in their assumptions, ease of use and in the technical and experimental setup required for a specific application. These techniques are mainly categorized based on the measurement of tissue generated forces versus single cell (or collection of cell) generated forces, measurement of deformation versus those that translate this deformation into cellular forces and the measurement of forces in two dimensions versus three dimensions [52].

To illustrate the existence of cellular forces, the easiest method is to measure the deformation of tissues, cells or substrates without correlating any of these deformations to actual forces. For instance, stromal cells implanted within collagen gels will compact the gel over a period of hours

to days, similar to the contractions that occur during wound closure [53-57]. The compaction, which is measured, considers the change in the diameter of the cell-laden gel polymerized in a well, driven in part by cellular forces. This compaction was shown to be substantially reduced by inhibiting myosin-based contractile activity [58]. Another technique involves ablating cell-cell junctions, such as in Drosophila embryos, using a laser and results in the apparent retraction of ablated edges, providing a qualitative measure of the magnitude of contractile forces transmitted by adjacent cells [49, 59, 60]. Even though these approaches sometimes converted the deformations to force using some assumptions, they are limited by complexities due to plasticity, viscoelasticity and fracture [50].

Another method uses the incorporation of cantilevers of predefined stiffness that bend in response to tissue contraction. Using optical microscopy, the displacement of the free end of the cantilever can be imaged and the displacement values be used for the calculation of contractile forces with the help of beam theory [61]. These vertical cantilevers are microfabricated from silicone elastomer – PDMS - which allows the measurement of forces from constructs with a smaller number of cells (around 100-600 cells) [62-65].

Since forces transmitted through cell-cell and cell-ECM adhesions impact many cell processes, understanding and quantifying cell-cell or cell-ECM forces is very important. Many studies have used atomic force microscopy [66, 67], micropipette aspiration [68], magnetic cytometry [5], and fluorescence resonance energy transfer (FRET) based on molecular force sensors to measure cell mechanics, adhesion forces and molecular tension in cultured cells [69]. The technique called traction force microscopy can be carried out using substrates made of polyacrylamide (PAA)

hydrogels or elastic micropillars to quantify traction forces transmitted by cultured cells through cell-ECM adhesions [51, 70]. In traction force microscopy (TFM), the approach is to characterize the deformation of a substrate induced by traction forces by the cell and to use the deformation field to calculate the traction forces exerted by the cell at each point on the substrate. For tracking the deformation in gels, sub-micron sized fluorescent beads are placed within the substrate to act as displacement markers. This is the most widely used technique for the measurement of cellular forces [52].

 In vivo, cells exist in a surrounding 3D ECM with a 3D shape that is unusually distinct compared to the cells plated on 2D surfaces [71]. Scientists are interested in understanding the nature of cellular traction forces that lie beneath these phenotypic variances in a 3D environment. It is difficult to measure tractions of cells in 3D, not only because of the requirement to track fiduciary markers in 3D, but also because the material properties of biologically relevant 3D ECM is much more complex than the synthetic materials used for measuring tractions in 2D [52].

1.6 Techniques to Measure Cell-Cell Adhesion Forces

Several methods have been used to examine cell-cell adhesion biochemistry and biophysics, such as light microscopy with antibody staining or GFP-fused protein expression, optical tweezers [72] and shear flows [73]. High-resolution images of adhesion sites and underlying protein linkages can be obtained using electron microscopy [74]. With the help of techniques such as centrifugation assays [75], shear flow [76], cell poking [77] and micropipette assays [78] cell adhesion strength can be determined. Atomic force microscope (AFM)-based assays have been used for the direct measurement of the forces necessary to disunite contacts between adjacent living cells [79]. AFM

has been used for characterizing the mechanical junctions between cells at the molecular level, stretching and unfolding individual molecules and adhesion strength measurements [80, 81]. Although such approaches have progressed our cognizance of cell-cell adhesion, they do not provide any insight on the endogenous force which is present at the cell-cell adhesion.

Förster/Fluoroscence resonance energy transfer (FRET), a molecular fluorescence technique, has been used to examine the proximity of fluorescent tags on a single or adjacent molecule to report on molecular-scale deformation [82]. FRET-based tools have been employed to quantify numerous parameters of the cell-material interface pertinent to cell responses, including molecular changes in cytoskeletal proteins induced by interactions with surfaces, such as changes in the crosslink density of hydrogel synthetic ECM equivalents [82]. Recent studies have shown how mechanical forces exerted at cadherin contacts can be visualized by converting them into optical signals using a FRET-based molecular tension sensor [83]. In these studies, in the cytoplasmic domain of E-cadherin, between plasma membrane and catenin binding domain, a tension sensor was introduced. Due to the highly sensitivity of a FRET signal toward the distance between the fluorophores, increased tension resulted in low FRET efficiency [84]. The FRET efficiency of E-cadherin tension sensor module (EcadTSMod) at cell–cell contact sites, as shown in figure 4, was significantly decreased compared to constructs lacking the cytoplasmic domain of E-cadherin, like for vinculin at cell-matrix sites [85]. This indicated that the EcadTSMod is under tension in cell–cell adhesions and is dependent on the catenin-binding domain of E-cadherin [84]. It was also noted that the E-cadherin cytoplasmic domain is under 1 to 2 pN of constitutive load from the cytoskeleton. This suggested that at the cortical actomyosin cytoskeleton, the cadherin-catenin linkage could act as a constitutive membrane anchor [83].
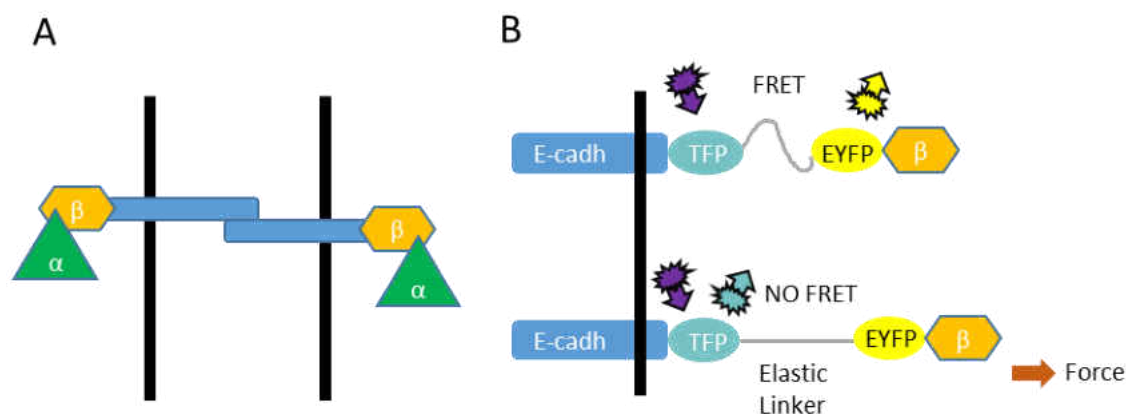
Figure 4: Schematic depiction of E-cadherin FRET molecular tension sensor. (A) Model showing the E-cadherin-catenin-actin linkage. Mechanical tension transmission by E-cadherin between cells via the extracellular domain to the actin cytoskeleton through β-catenin, α-catenin and other proteins is depicted. (B) The tension sensor module is made of monomeric teal fluorescence protein (mTFP)/monomeric enhanced yellow fluorescence protein (mEYFP) separated by an elastic linker. This tension sensor module is inserted in the cytoplasmic domain of E-cadherin, which transmits force. High and low FRET indices correspond to low and high tension respectively.

Inter-cellular forces have been measured more directly using a technique called the traction force imbalance method. This method is based on the measurement of traction forces, followed by computation of the force exerted at the cell-cell contact using physical force balance. This approach is detailed more in Chapter 3.

CHAPTER

2. FLEXIBLE CELL SUBSTRATES AND THEIR STIFFNESS MEASUREMENT

[Portions of this chapter having been adapted directly from the following published article:

Bashirzadeh Y.*, Chatterji S.*, Palmer D.*, Dumbali S.*, Qian S., Maruthamuthu V., Stiffness Measurement of Soft Silicone Substrates for Mechanobiology Studies Using a Widefield Fluorescence Microscope. J. Vis. Exp. (137), e57797, doi:10.3791/57797 (2018).] (* These authors have contributed equally.)

2.1 Introduction

2.1.1 The Extracellular Matrix

The effects of the extracellular matrix (ECM) on epithelial cells are mediated via specific receptors called integrins located on the surface of the cells, particularly on the basal surface of the cells. This cell surface contacts the basal lamina, a layer of basement membrane (a specialized ECM) comprised of numerous proteins and glycoproteins, typically including laminins, collagen, entactin, along with different proteoglycans [86]. As shown in Figure 5, the basement membrane underlies the typical epithelium or vascular endothelium and consists of two thin structural layers: a basal lamina, which is synthesized by epithelial or endothelial cells [87] and a reticular lamina, secreted by fibroblasts [88]. With the use of the electron microscope, it was found that the basal lamina is subdivided into a clear lamina lucida, which rests directly beneath the epithelial cells, and a structurally opaque lamina densa [89, 90]. The nature of ECM is controlled by the cell's

nucleus through its transcriptional events and, reciprocally, the ECM modulates these same events, acting through cell surface receptors and the cytoskeleton [91].

Epithelial cell

Plasma membrane

Lamina lucida

Integrins
Laminins 1, 5, 6, 10
Collagens XVII and IV
Dystroglycans

Basal lamina

Lamina densa

Collagen IV
Entactin/Nidogen
Perlecan
Heparin sulfate proteoglycans

Lamina reticularis

Collagen I, III, V

Proteoglycans

Plasma membrane

Fibroblast
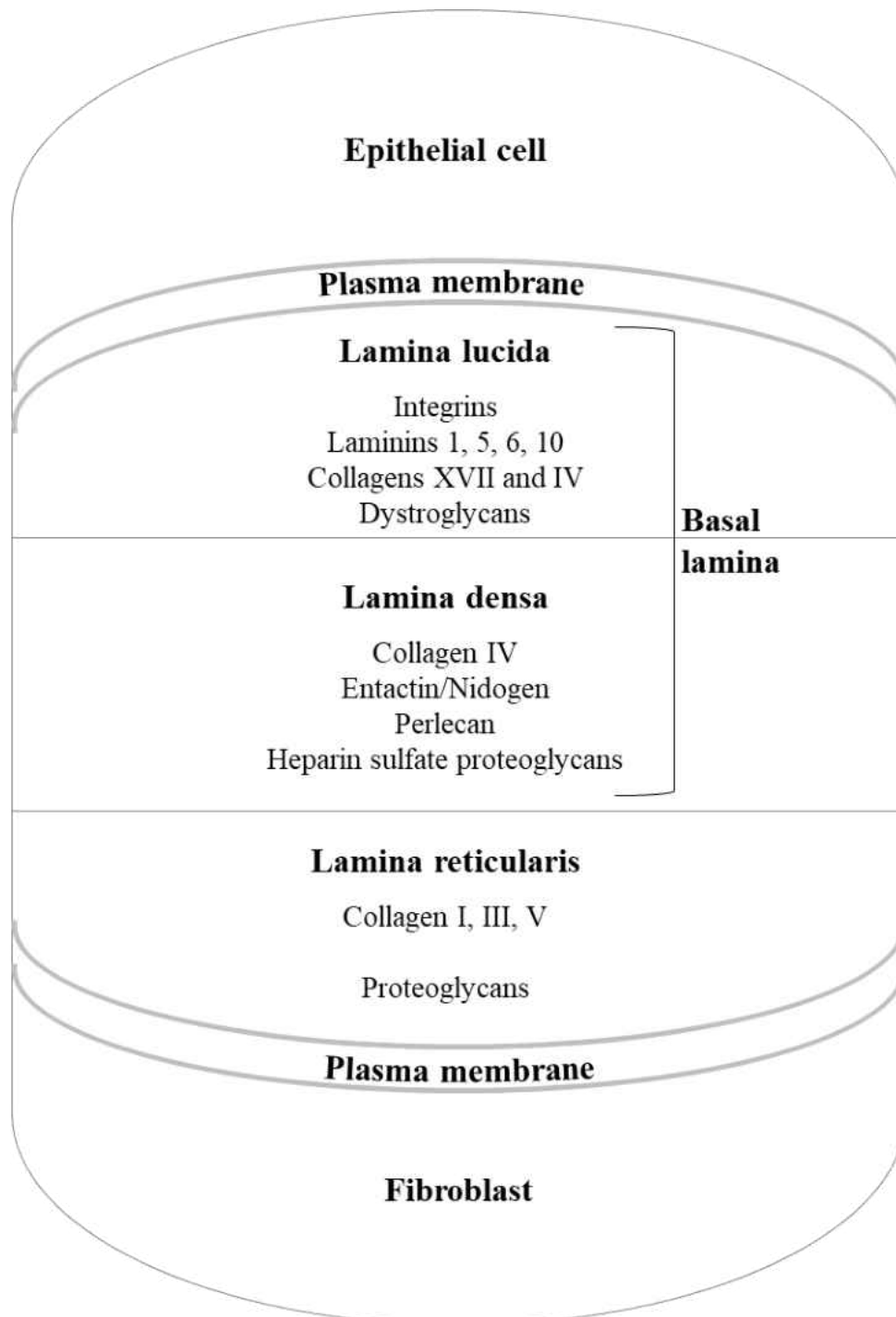
Figure 5: Basement membrane. The basement membrane underlies the typical epithelium or vascular endothelium and consists of two thin structural layers. One layer is the basal lamina made by epithelial or endothelial cells. The second layer is the reticular lamina made by fibroblasts. Electron microscope data show that the basal lamina consists of a clear lamina lucida next to epithelial cells and an opaque lamina densa. The lamina lucida contains integrins, laminins (1, 5, 6 and 10), and collagen XVII, as well as type IV collagen, and dystroglycans. The lamina densa contains type IV collagen fibers, entactin/nidogen-1, perlecan, and heparan sulfate proteoglycans. The reticular lamina contains collagens I, III, and V and various proteoglycans. (The legend is adopted from the review article [87].)

2.1.2   Stiffness of Cell Substrates as a Relevant Parameter Stiffness

In vivo, the microenvironment of cells consists of a complex, but vastly organized environment, with a diverse collection of proteins, sugars, other cells. The cell's local mechanical environment is dictated by spatial orientation of the cell and the composition of a cell's microenvironment [91]. The mechanical environment is composed of endogenous forces generated by the cells themselves, as well as exogenous forces that are applied to cells by the surrounding microenvironment. Cytoskeletal contractility is responsible for the endogenous forces generated by cells while exogenous forces subsist in a variety of forms, including gravity, shear as well as tensile and compressive forces [92, 93]. These exogenous forces are exerted by the ECM through interaction with cells. Thus, an important mechanical effector of cell behavior is the local stiffness of the ECM [91].
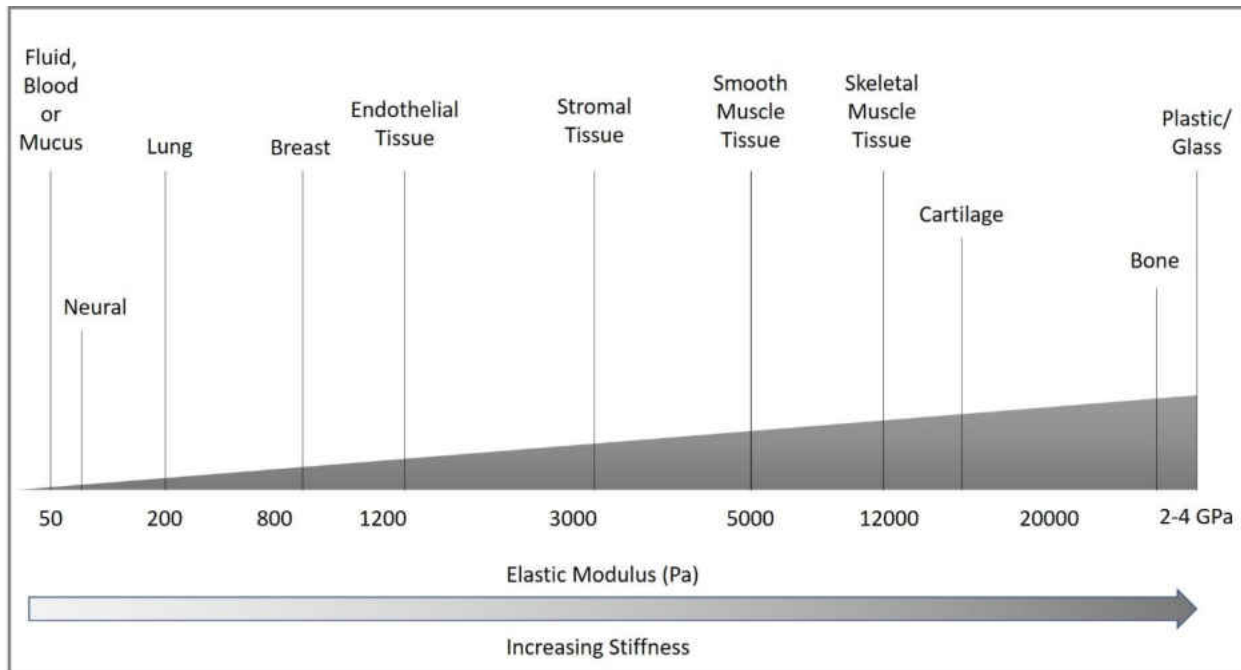
Figure 6: Different tissues in the human body with their specific stiffness. The biomechanical properties of a tissue in terms of elastic modulus (stiffness), measured in pascals (Pa), vary markedly between organs and tissues. Stationary tissues such as brain, or compliant tissues such as lung, show low stiffness, whereas tissues exposed to high mechanical loading, such as bone or skeletal muscle, exhibit higher stiffness.

The property of a material that enables it to resist deformation in response to an applied force is called as stiffness. Stiffness is used to specify whether a material is compliant or rigid. Our tissues are comprised of different types of ECM molecules that feature a wide range of elastic moduli, and each tissue/organ has specific stiffness (Figure 6) for fulfilling physiological needs. For

example, bone provides structure and protects all internal organs; hence, it is much stiffer compared to other tissues in the body [91].

In vitro cell research is mostly conducted on tissue culture polystyrene, which has the stiffness of ~1 GPa, while that of the tissues in the body ranges from 100 Pa (for brain) to 100 kPa (for muscle tissue) [94]. This stiffness disparity significantly affects the way cells respond to their microenvironment. The majority of researchers are thus committed to explicating the effect of substrate stiffness on the functions of various cell types [95], including stem cells and their fate [96]. In an effort to aid a better understanding of stiffness-dependent cell dynamics, different types of gels such as polyacrylamide (PAA) hydrogels [97, 98], polyethylene glycol (PEG) [99], polydimethylsiloxane (PDMS) [100] and soft silicone [101] have been developed. Many studies of stiffness regulated cell responses employ PAA gels, which are not only less expensive and simple to implement, but also display a physiologically appropriate stiffness range of 0.3 – 300 kPa [95, 102, 103].

2.2 Methods

2.2.1 Polyacrylamide Gel Substrates and ECM Coupling of ECM and Fiducial Markers

Polyacrylamide hydrogels are widely used as cell culture substrates to understand cell responses to the physical characteristics of their microenvironment [104, 105]. Polyacrylamide hydrogels are a network of cross-linked acrylamide units. The Young's Modulus of the material can be tweaked by varying the amount of bis-acrylamide cross-linker with the total acrylamide monomers in the gel precursor solution [105]. Polyacrylamide is considered as a linearly elastic material [106, 107] as it exhibits a constant storage modulus throughout a wide range of strains [108]. Hence, the

mechanical characterization of these gels by time-independent recovery after mechanical loading, is possible [109]. Moreover, the basic assumption of linear elasticity also implies that materials that undergo reversible deformation are also not affected by the rate of loading [110].

Alterations in polyacrylamide substrate stiffness influence cell shape [95], cell proliferation [102], functional maturation [111], and cell differentiation [112]. To control cell adhesion, polyacrylamide substrates can be selectively coated with ECM proteins [113]. Protein coated gels can further be used to quantify cellular forces with the help of traction force microscopy (TFM), by recording the displacement of microbeads embedded within the gel [114].

2.3 Measurement of Polyacrylamide Gel Substrate Stiffness Using a Widefield Fluorescence Microscope

[Portions of this chapter having been adapted directly from the following published article:

Bashirzadeh Yashar, Chatterji Siddharth, Palmer Dakota, Dumbali Sandeep, Qian Shizhi, Maruthamuthu Venkat. Stiffness Measurement of Soft Silicone Substrates for Mechanobiology Studies Using a Widefield Fluorescence Microscope. J. Vis. Exp. (137), e57797, doi:10.3791/57797 (2018).

Epithelial and other cells in soft tissues adhere to a microenvironment whose stiffness typically falls in kilopascal range [91]. Flexible substrates such as polyacrylamide [115] and silicone [116] gels have proven to be excellent biomimetic substrates for cell culture. Several methods have been used to measure the stiffness of flexible substrates, including atomic force microscopy,

macroscopic deformation of whole samples upon stretching, rheology and indentation using spheres and spherically tipped microindentors [117]. While each technique has its own advantages and disadvantages, indentation with a sphere is an especially simple yet fairly accurate method that only requires access to a widefield fluorescence microscope. Recently, confocal microscopy has also been used for an elegant characterization of the indentor method [118]. Here, we show that a widefield microscope may be sufficient, provided a suitable protocol is used to confine fluorescent beads to the top surface or to a thin slice in the top region of the substrate. To characterize the Young's moduli of isotropic linear elastic substrates, this simple method only employs a widefield fluorescence microscope for the actual stiffness testing. Use of suitable indentors and methods to restrict fluorescent marker beads to the substrate top surface enable this method [101].

2.3.1   Methods and Measurement Protocol

In order to fabricate the polyacrylamide hydrogel, a 22 x 22 mm coverslip was treated with hydrophobic reagent (we use the commercial product Rain-X). The mixture of acrylamide and bisacrylamide is then polymerized between the hydrophobic coverslip and an activated coverslip (activated by treating successively with 2% 3-aminopropyltrimethyoxysilane in isopropanol and 1% glutaraldehyde in distilled water) [48], as shown in Figure 7. The same procedure is repeated to polymerize another layer of PAA gel; this time the volume is 20% of the former gel mixture. This second gel mixture also contains micron sized fluorescent beads. This gel is then ready for the measurement of its stiffness using a widefield fluorescence microscope.
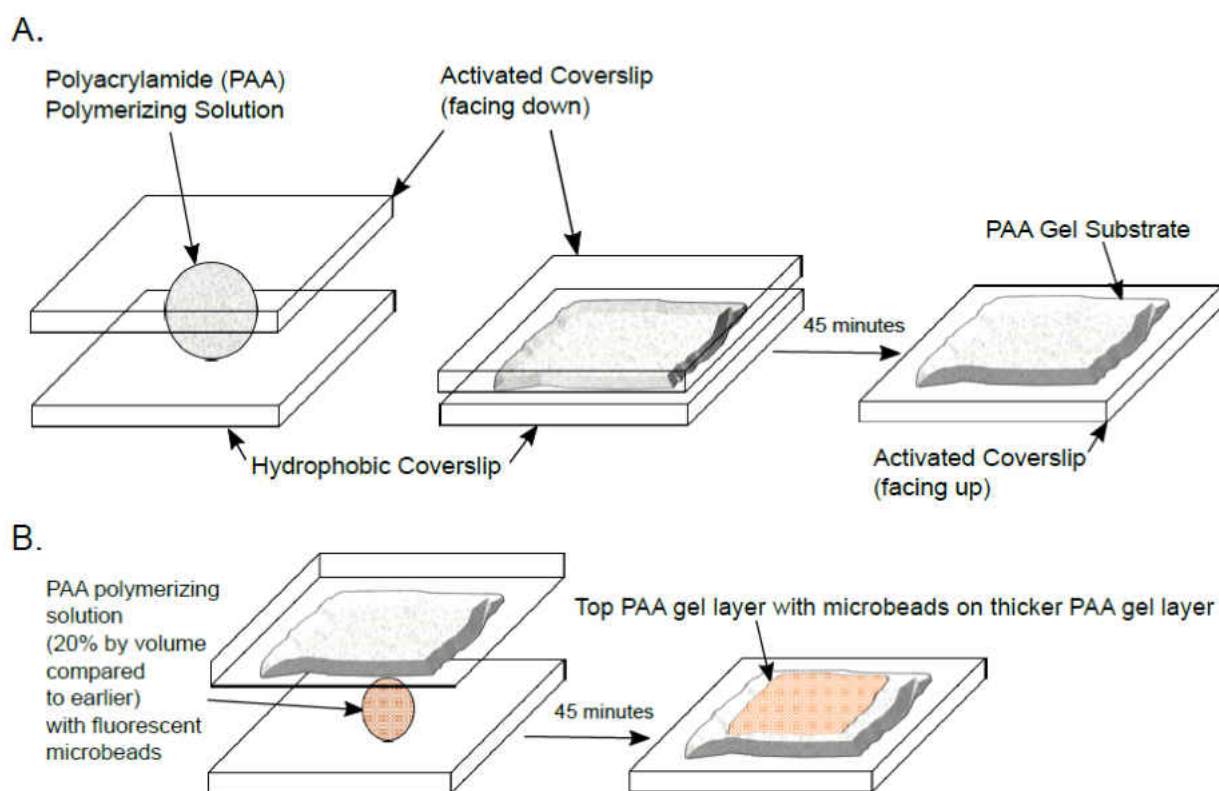
Figure 7: Schematic depiction of the procedure for the preparation of PAA gel substrate and coupling of fluorescent microbeads to the top surface. (A) Polyacrylamide gel preparation using polymerizing mixture: A drop of the polymerizing solution is placed on a hydrophobic coverslip and sandwiched with an activated coverslip on the top. After 45 minutes of polymerization, a PAA gel is obtained. This step is repeated one or more times if a thicker PAA gel is required. (B) Using 20% of the volume for the first layer, but with fluorescent microbeads incorporated, a thinner PAA layer is polymerized on the top of the thicker PAA gel layer below.

2.3.1.1 Measurement of PAA gel with Sphere Indentation using a Widefield Fluorescence Microscope

The following is the procedure for measuring PAA gel stiffness:

a) Place the gel in the Petri dish and ensure that it contains at least 1 mL of PBS to have the gel surface several mm below the liquid surface.

b) Using pointed tweezers, drop five 1 mm zirconium sphere indentors on the gel. Immerse the spheres into the liquid medium and drop them, away from the edges of the gel layer and at least 5 indentor diameters away from the location of the other indentors.

   Note: When dropped above the liquid surface, the spheres may fail to enter the liquid medium (float) due to the liquid medium's surface tension.

c) Place the Petri dish with the gel on the microscope stage so that it is possible to image through the Petri dish base.

d) Using phase imaging with a 10X objective (such as a dry 10X objective of NA 0.30), locate and bring a sphere indentor into focus.

e) Take a phase image of a part or the whole of the indentor and save this image. Use a tile scan if available. If the indentor has any visible defects, discard and replace it with another indentor.

f) Under live phase imaging, pan to the left of the indentor's edge so that the left edge of the frame is at least a distance of ~1.5 R from the indentor center. Ensure that the center of the indentor remains visible on the right side, close to the right edge of the image frame. Take a phase image and save it.

g) Switch the microscope light source to the illumination for the red fluorescent channel. With the x- and y-coordinates unchanged (the x-y position of the indentor center within but near the right edge of the frame), focus down (decrease Z) until the red fluorescent microbeads under the sphere indentor's center just go out of focus.

h) Take a z-stack with an image for every z-increment of 0.5 μm till the microbeads in the top layer of the gel far from the indentor (near the left edge of the imaging frame) go out of focus.

i) Repeat steps d) – h) with the other indentors on the sample.

2.3.1.2 Calculating PAA Gel's Stiffness (Young's Modulus)

The following is the procedure for calculating PAA gel stiffness:

i. Open the phase image of the indentor using ImageJ, click on the line tool, and measure the indentor's diameter in pixels. Click and hold on a point on the indentor edge; move the cursor to a diametrically opposite point on the edge and note the length in pixels displayed on the status bar of the ImageJ main window before releasing the cursor.

   a. Ensure that the unit of length is set to pixels by clicking **Analyze | Set Scale** and checking the Unit of length.

   b. Convert the indentor's radius in pixels to μm by taking into account the objective magnification and the CCD camera pixel size (R in μm = R in pixels x the CCD camera pixel size in μm / the objective magnification).

ii. Open the red channel z-stack of microbead images (if the microbeads are red fluorescent) in ImageJ by clicking on File | Import | Image Sequence and select any image in the stack and click OK to open the stack.

Note: F1 is the frame number at which the microbeads under the indentor center are in the best possible focus and F2 is the frame number at which the microbeads (at a region of ~1.5 R away from the bead center) near the left edge of the frame are in the best possible focus. The z difference between the two frames is the indentation depth δ.

a. Using the line tool in ImageJ, draw a line across a well-defined microbead in the image. Click on Analyze | Plot Profile and click on the Live button to obtain the updated line scan intensity across the bead while selecting different frames. The frame that gives the highest value of the maximum intensity can be chosen as the frame in focus.

b. Since the z-increment between the frames in the z-stack is 0.5 μm, calculate the indentation depth in μm as δ = (F2-F1) x 0.5.

iii. Calculate the force exerted on the gel by the indentor due to its weight (minus the opposing buoyant force), that is, the indentation force F, as the volume of the indentor x (the density of the indentor - the density of the liquid medium) x the acceleration due to gravity. Use the equation:

$$F = \left(\frac{4}{3}\right) \times 3.142 \times R^3 \times (\rho_{indentor} - \rho_{medium}) \times g)$$

where,

R – radius of the indentor;

$\rho_{indentor}$ – density of the indentor;

ρ_{medium} – density of the liquid medium and

g – acceleration due to gravity (9.81 m/s2).

All quantities on the right-hand side in SI units to obtain F (in N).

iv.   Calculate the Young's modulus (E) of the gel using a modified [119] Hertz Model [120] equation:

$$E = c\,\frac{3(1 - \vartheta^2)F}{4R^{0.5}\delta^{1.5}}$$

Where:

c = a correction factor that modifies the Hertz model expression;

ϑ = Poisson's ratio of the PAA gel (taken as 0.5 as for incompressible materials7);

F = the indentation force;

R = the indentor radius; and

δ = the indentation depth.

All quantities on the right-hand side in SI units to obtain E in Pa.

2.4 Results and Discussion

Various parameters that characterize the spherical indentation of the gel surface are shown in Figure 8A. Phase imaging is used to capture either (A) the entire image of the indentor as shown in Figure 8B (using image stitching, if necessary) or (B) part of the image of the sphere. The only parameter to be derived from the indentor's image is its diameter. For example, for the indentor we used in this protocol, different individual indentors from the same lot had diameters that ranged from 950 μm to 1,200 μm with a mean value of 1,037 μm and a standard deviation of 47 μm (8 indentors). Note that the diameter measured for a particular indentor (rather than the mean diameter

for many indentors) should be used for the stiffness calculation for the indentation-induced by that particular indentor.
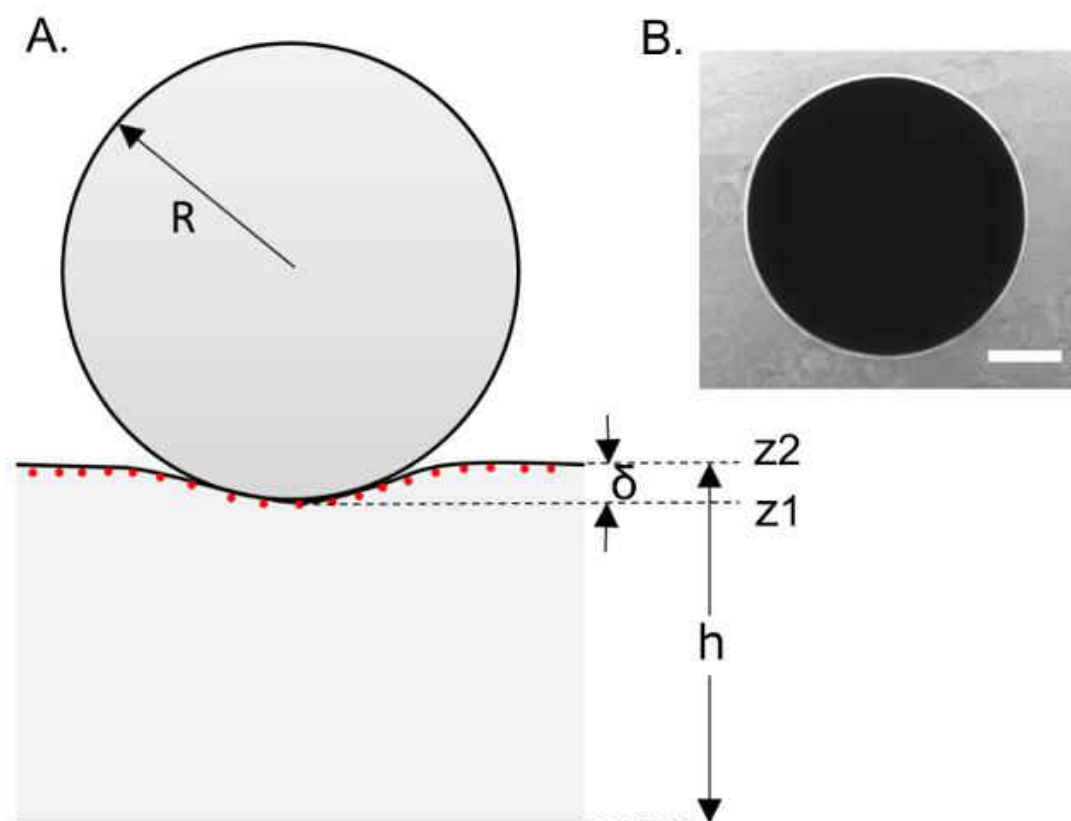
Figure 8: Schematic illustration of sphere indentation of the PAA gel surface. (A) This schematic depiction shows a spherical indentor on the surface of a PAA gel sample. Various parameters of interest are indicated. (B) This panel shows an image of a 1 mm indentor (on a gel sample) obtained via phase imaging. The scale bar indicates 250 µm. {The figure and the legend have been adapted from [101].}

Fluorescent images of the microbeads in the top surface of the gel are taken at an x-y frame position so that the region under the indentor is in the far-right part of the frame. The region in the far-left part of the frame is chosen to be the region away from the indentor as shown in Figure 9. Z-stack images of the regions under the indentor and away from the indentor are shown in Figure 10 as well. For the 1 mm diameter zirconium indentor used with PAA gel, the z-values at which the 2 regions come into focus differed by about 20 μm (δ). This is much smaller than the thickness of the gel, which could be around 400-500 μm. Using the density (4.66 g/cm3) of the zirconium indentor (which is actually made of a mixture of zirconium dioxide and silicon dioxide) and the density of the liquid medium (for PBS: 1.01 g/cm3), the net force exerted on the gel can be computed. For the case under consideration, it was in the 20 - 25 μN range. Using the sphere indentation method of this protocol using a widefield microscope, polyacrylamide gel was made with an acrylamide to bisacrylamide ratio of 7.5%:0.1% was found to have a Young's modulus of 22.1 ± 4.2 kPa. Finally, to validate the sphere indentation method that uses a widefield microscope as we described in this protocol, we also measured the Young's moduli of a polyacrylamide gel of the same composition with a rheometer – this yielded a Young's modulus of 21 ± 3 kPa.

A. Image of fluorescent micro-beads

location
of indentor

B. Region under the indentor

z1 + 5 μm   z1 - 5 μm

z2   z1   z

z2 + 5 μm   z2 - 5 μm
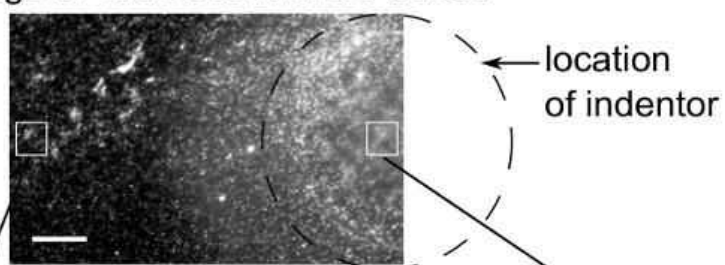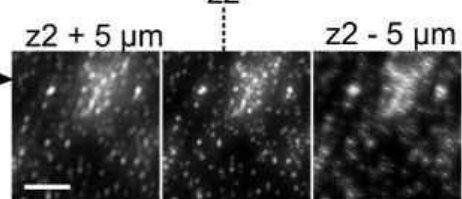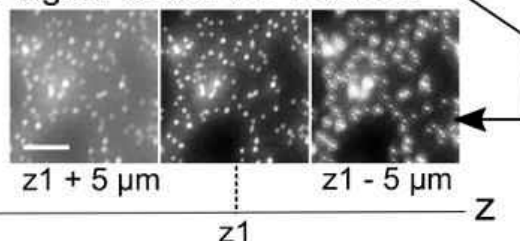
C. Region away from the indentor

D. Line scan across a bead (0.5 μm z increments)

z > z1
z = z1
z < z1

Intensity (A.U)

Pixel along line
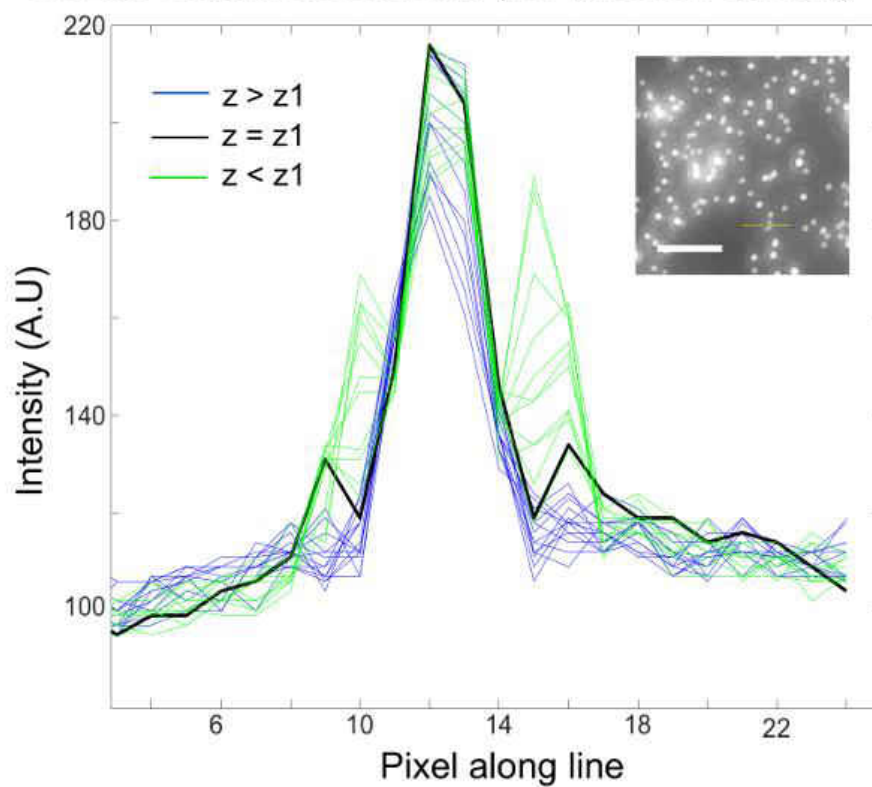
Figure 9: Bead image acquisition and determination of the in-focus image. (A) This fluorescence image shows microbeads on the top surface of a gel sample (the data for this figure was obtained with a silicone gel) and the desired x-y location of its frame relative to the indentor (dotted line). The scale bar indicates 150 μm. Panels B and C show z-stack fluorescence images of regions on the PAA gel surface (B) under the indentor and (C) away from the indentor (boxed regions in the top image). The indicators z1 and z2 correspond to the z-values at which the region under the indentor and the region away from the indentor are in focus, respectively. The scale bars indicate 20 μm. The monochrome images shown are those obtained in the red channel, since nominally pink microbeads were used whose excitation and emission profiles fit the red channel. (D) This panel shows an intensity line scan across a micro-bead (shown in the inset image with a yellow line across it) as the focus is varied in z-increments of 0.5 μm. The focus (z-value) corresponding to the in-focus image can be objectively chosen based on the z-value corresponding to the line scan with the highest maximum intensity. The scale bar in the inset indicates 20 μm.

While the sphere indentation method is easy to implement, careful attention must be paid to the choice of indentor and the thickness of the gel sample. The equation used to calculate the Young's modulus is valid under a set of conditions and these are typically satisfied when the thickness of the gel sample is > 10% of the indentor radius and < ~10x the indentor radius. We found that a gel thickness was 5-10x the indentor radius was a good choice, wherein the sample thickness was not too high (i.e., the objective working distance does not become a limitation) and the calculated stiffness was also not too sensitive to the exact value of the gel thickness. The choice of spherical indentor should also be such that the indentation depth δ is < 10% of the gel thickness as well as

< 10% of the indentor radius. With these considerations in mind, indentors of both different material and diameter can be used to measure the stiffness of softer and stiffer gel. The determination of the indentation depth is the most critical step of this protocol. The method suggested in this protocol to identify in-focus images should help determine the indentation depth reliably. It should also be noted that the stiffness calculation used for the sphere indentation method uses Hertzian theory, which assumes frictionless contact.

2.5 Q Gel Substrates and Coupling of ECM and Fiducial Markers

Q gel was prepared in a petri dish by mixing A and B solutions at a 0.5:1.1 ratio, followed by curing at 100 degrees C for an hour. Fluorescent beads of 0.46 micrometer diameter were coupled to the silicone top surface using shallow UV treatment followed by EDC/NHS chemistry. A millimeter-scale sphere was used to intend the top surface (by gravity); fluorescent beads on the indented silicone surface were imaged using a fluorescent microscope and the resultant images were analyzed to calculate the Young's Modulus of the silicone substrate as specified in the 2.4 section.
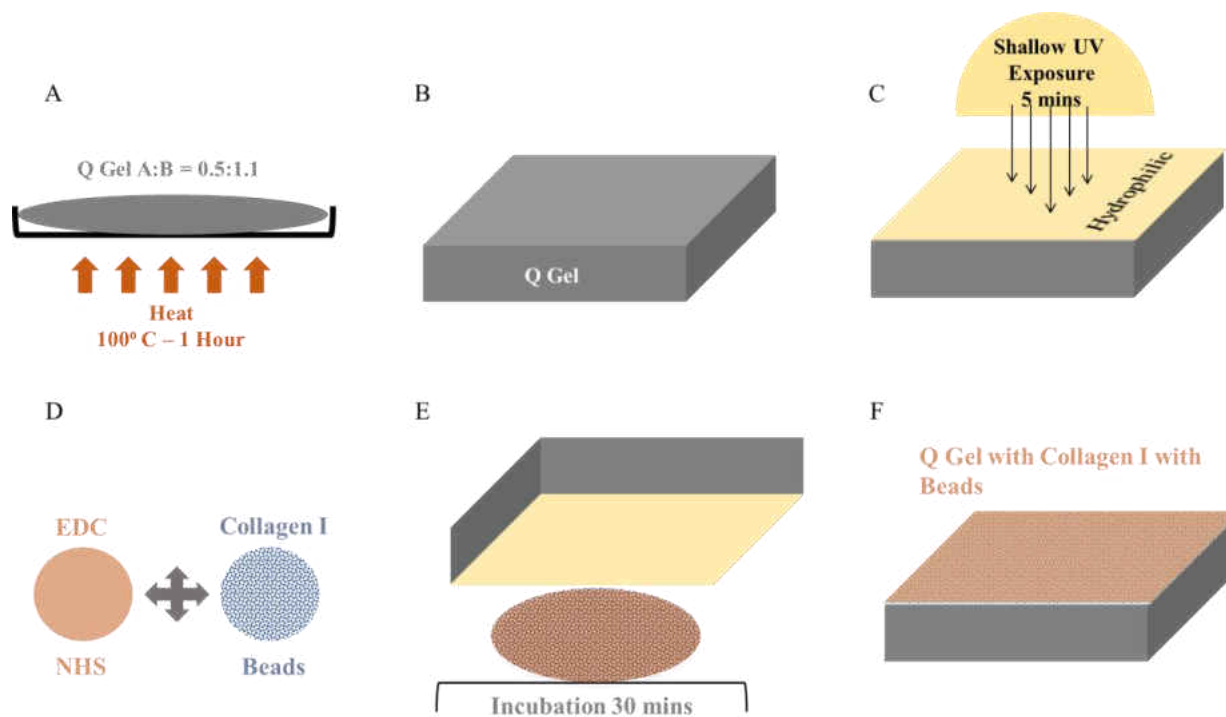
Figure 10: Schematic representation of coupling collagen I and fluorescent beads on the top surface of Q gel. (A) Making of Q gel and curing it for 1 hour at 100º C. (B) Cured Q gel (C) Shallow UV Exposure. (D) EDC-NHS-Collagen I-Beads (ENCB) mixture. (E) Gel incubation with ENCB mixture for 30 minutes. (F) Final Q gel coupled with collagen and beads.

CHAPTER

3. TRACTION FORCE MICROSCOPY AND INTERCELLULAR FORCE MEASUREMENT WITH E-CADHERIN MUTANTS

3.1 Introduction

3.1.1   Traction Force Microscopy

Within the multiple disciplines of biomedical research, mechanobiology is, relatively, an emerging perspective. Earlier studies have shown that cells exert and resist forces to enable normal function [112, 121]. Hence, it is important to quantify these cell generated forces across various interfaces of relevance in biology [122, 123]. In addition to the convolution of the mechanical response of cells, cellular force analysis is innately challenging due to the sometimes involved physics of mechanical force quantification [124]. The approach of traction force microscopy remains the principal technique for investigating cell-exerted forces. Broadly speaking, traction force microscopy experiments and quantifications involve capturing surface displacements and computing tractions exerted by cells on an *in vitro* fabricated elastic substrate [125].

TFM has proven to be a leading technique owing to its ease of implementation and flexibility to biomimic cellular environments, along with an established analysis procedure. These experiments can be performed with the help of a widefield fluorescent or confocal microscope [124]. In general, cells are seeded on a thin elastic ECM coated hydrogel, which has fluorescent beads as fiducial markers. Imaging of the bead positions followed by image processing helps quantify 2D or 3D displacement of the gel. With a knowledge of the mechanical properties of the hydrogel or substrate and these displacements, forces applied by cells on the substrate can be quantified [124].

3.2 Methods

3.2.1   Computation of Traction Forces

Previous studies have investigated cellular tractions using traction force imbalance method. The idea was to calculate the endogenous force at cell-cell interface using the balance of traction forces applied on the substrate. Using experimental and analytical methods, traction force microscopy was carried out (Figure 11). The displacement of the fluorescent beads embedded within PAA gel were very much less than 10% of the gel thickness. For the computation of bead displacement, particle imaging velocimetry was used to calculate displacements on a specified grid [51].
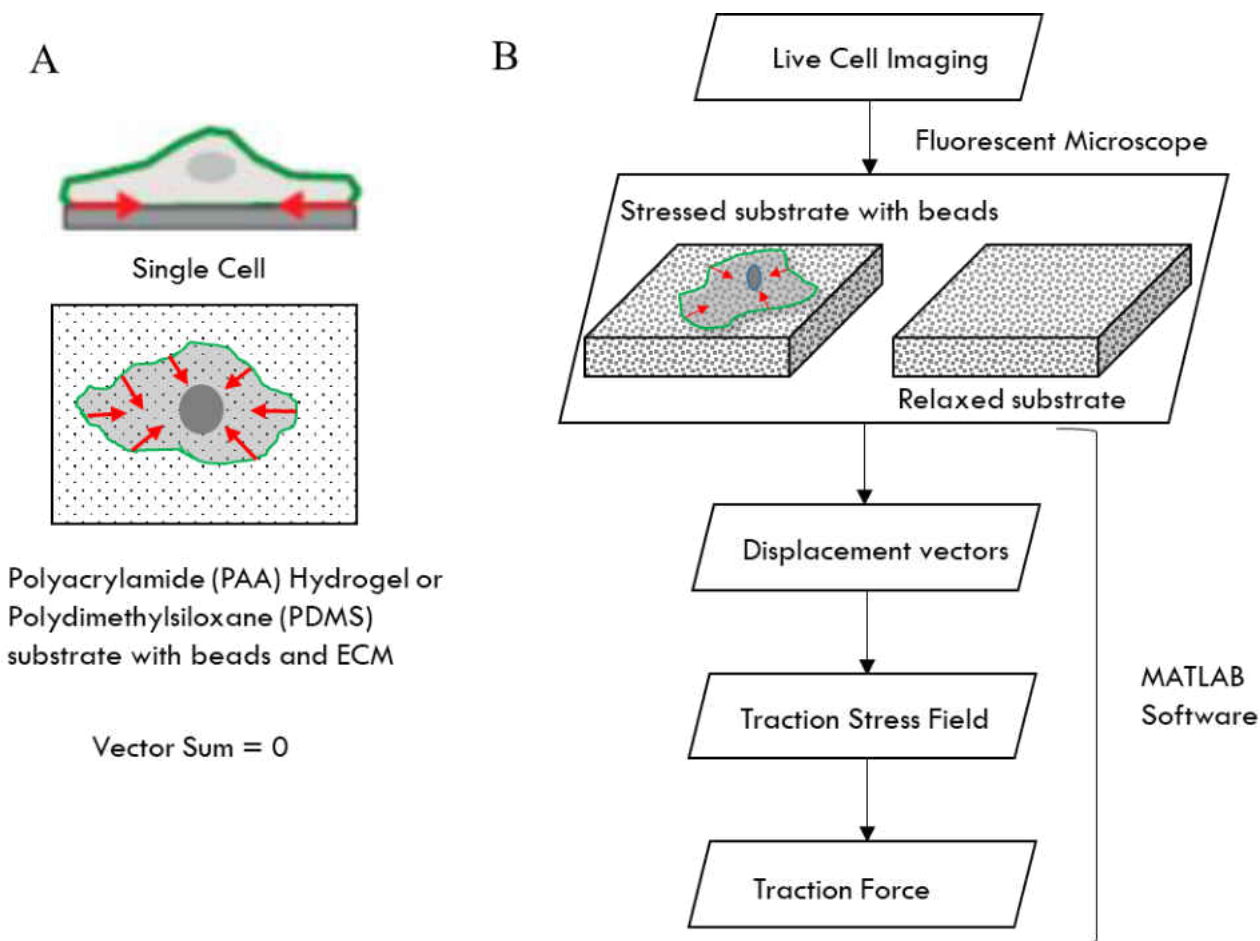
Figure 11: Experimental and Analytical Schematic of Traction Force Microscopy. (A) Side view with corresponding top view of a single cell on the substrate with fluorescent beads. The red arrows are the contractile forces applied by the cell on the substrate. The vector sum of the traction forces exerted by a single cell is zero [51]. (B) Steps within traction force microscopy. The sample with cells on the substrate with beads is imaged using a widefield microscope (here) for imaging. The images of cell and the beads (2 images for the beads: one with the cell and other without the cell) under stressed and relaxed conditions are taken. These images are then aligned using image

processing software so as to calculate displacement field. Using custom scripts in MATAB, the traction stresses are then calculated.

With the help of this displacement field, the stress field was calculated with the assumption of the substrate as a linear elastic half-space. Fourier transform traction cytometry (FTTC) was then used to get the solution of the force-displacement relationship involving the Green's function, with zeroth-order regularization [126-128]. In order to obtain promising solutions, which can, in turn, significantly improve FTTC method, regularization was carried out [127]. To obtain the stress field in real space, the problem was first solved in Fourier space and then inverted back to real space [127, 128]. This FTTC analysis enabled the reconstruction of traction stress at a selected grid spacing. The traction force vector at any that location was simply calculated as the product of unit grid area and the traction stress vector [51] (note that even though stress is a tensor, it can be considered as a vector once the area is specified).
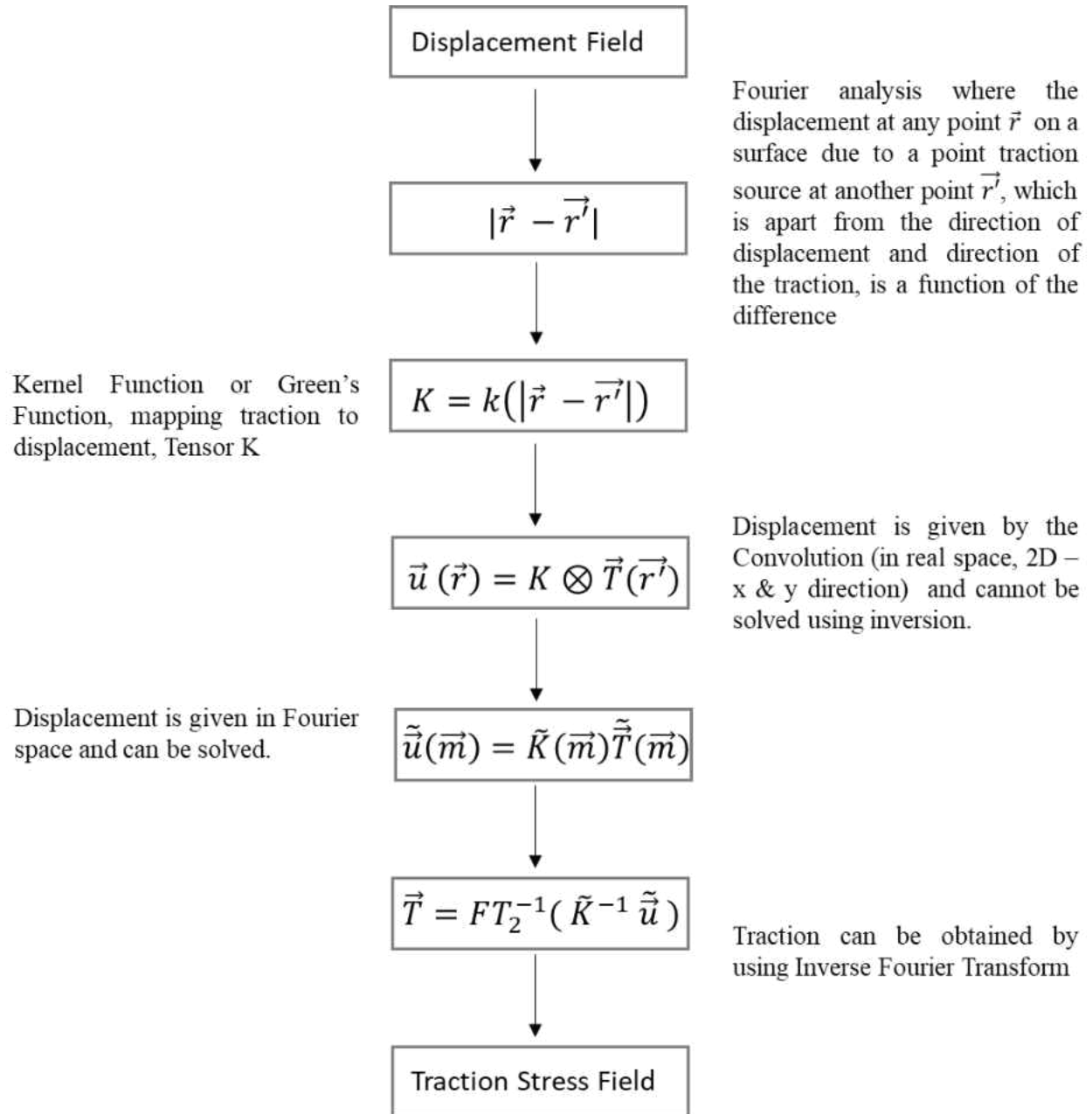
Figure 12: Fourier transform traction cytometry [129]: equations involved in the calculation of traction stress field.
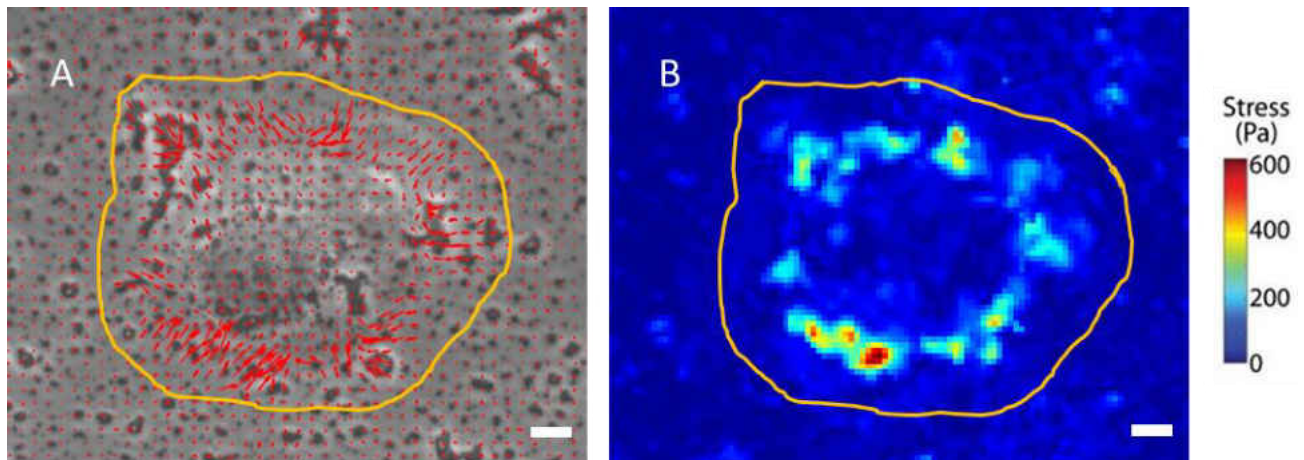
Figure 13: Traction forces within a single cell. (A) Phase image of a Madin Darby Canine Kidney (MDCK) single cell. Red arrows indicate stress vectors. Yellow boundary specifies the region used to calculate summation of the traction forces. (B) Heat map plot indicating the magnitudes of the traction stresses in (A). (Scale bar, 5µm)

As shown in Figure 13, MDCK single cells were considered in which the majority of the traction stresses were exerted near the cell boundary and were directed towards the center of the cell. These stresses exhibited a distribution similar to that of focal adhesions in single cells without the colocalization of E-cadherin at cell-ECM based adhesion, as expected. The traction force vector, $\vec{T_i}$ was found by multiplying the traction stress by the unit grid area. The total cell-ECM endogenously generated force was the sum of traction force magnitudes across the cell, $\sum|\vec{T_i}|$. The sum of traction force magnitudes across the cell was previously found to be around 250 nN [51]. The unbalanced traction force was calculated using the vector sum of the traction forces across the

cell, $\sum \vec{T_i}$. In order to distinguish the magnitude of unbalanced force to the total sum of cell-ECM force, the ratio $|\sum \vec{T_i}|/\sum |\vec{T_i}|$ was considered. This unbalanced force for single cells was previously found to be around $5 \pm 3\%$ of the total cell-ECM force [51].

3.2.2   Intercellular Force Measurement in Cell Pairs

Using the method described in section 3.2, the traction force underneath cell pairs was calculated. The total sum of magnitudes of cell-ECM forces, for the cell pair as a system, was found to be approximately 400 nN [51]. The percent unbalanced traction force observed within cell pairs was similar to that observed in single cells. The sum of traction vectors under a cell within a cell pair was also determined, $\vec{F}_{\text{cell 1}} = \sum_{\text{cell1}} \vec{T_i}$. This imbalance was inferred as the force exerted at the cell-cell contacts by one cell onto the other, within the cell pair, as the cell is in mechanical equilibrium. Thus, in a cell pair, an equal but opposing force was exerted by both the cells on each other.
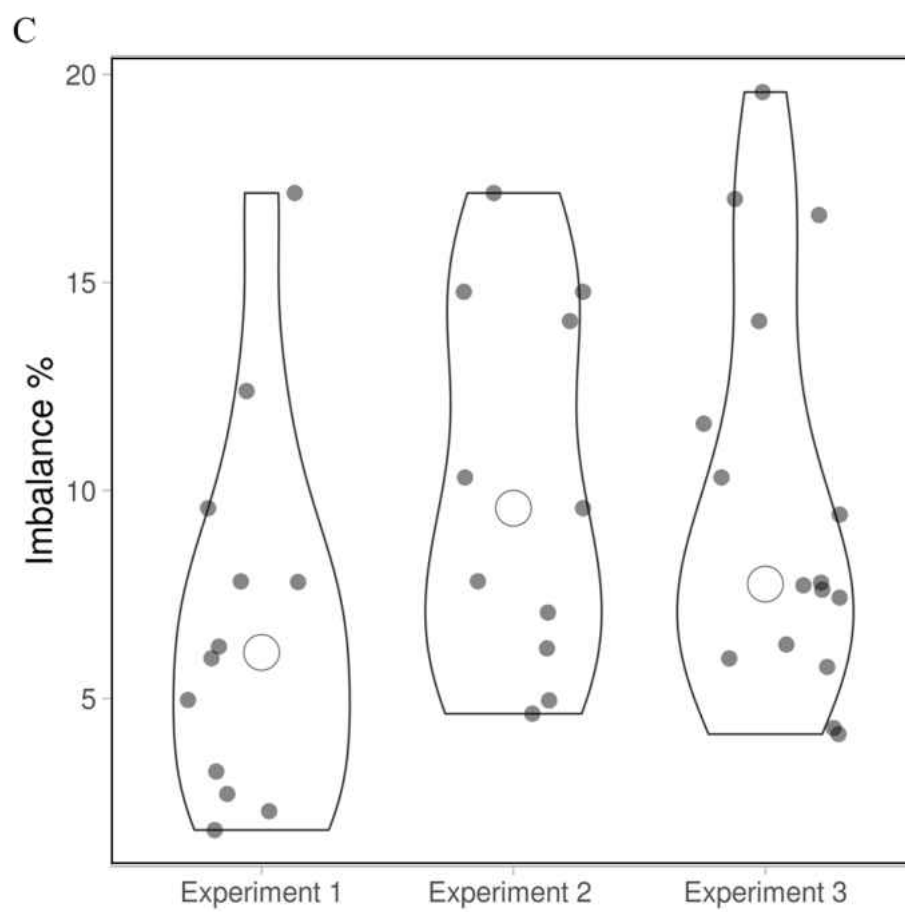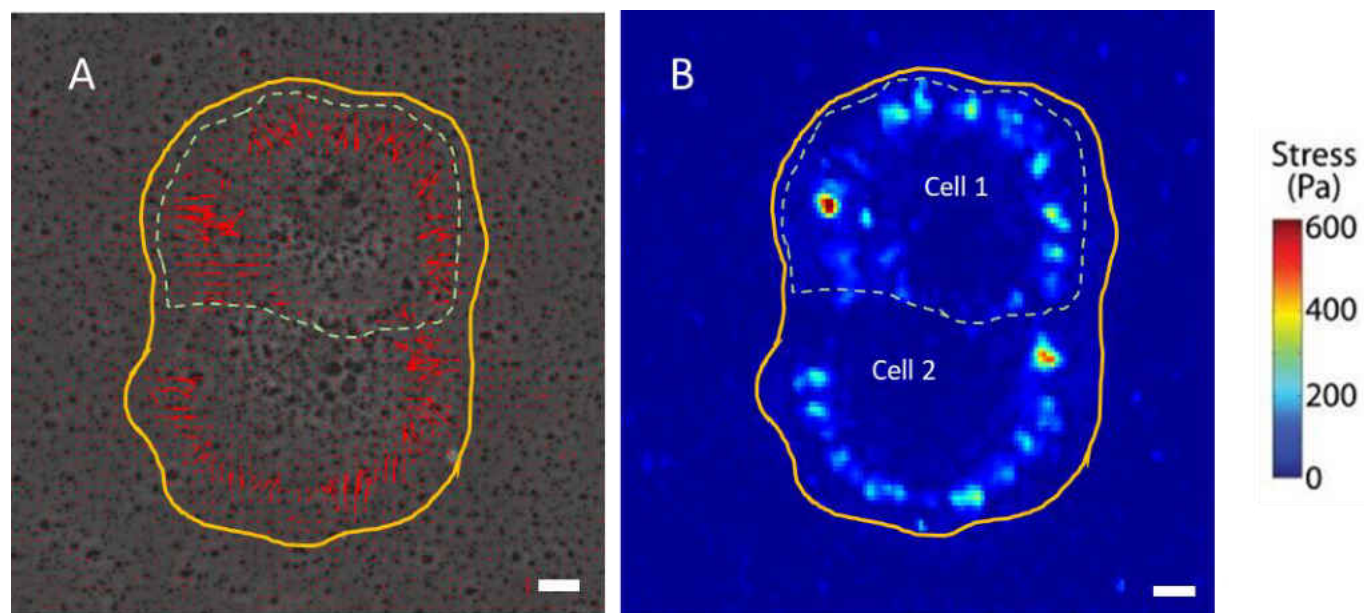
Figure 14: Calculation of intercellular force using the unbalanced traction force. (A) Phase image of a cell pair. Red arrows indicate stress vectors. Yellow boundary is specifying the region used to calculate the total sum of traction force and green dotted line indicates the region used to calculate the traction sum of a single cell within the cell pair. (B) Heat map plot indicating the magnitudes of traction stresses in (A). (Scale bar, 5 μm) (C) Violin plot showing distribution of percent imbalance of traction forces.

3.3 Results and Discussion

3.3.1 Intercellular Force in Cell Pairs Expressing E-cadherin Mutants

Cells constantly experience mechanical tension via intercellular junctions. These junctions are never static. They are dynamic and involve constant turnover of adhesion proteins in various physiological processes. These junctions must also be robust in order to maintain cell-cell contact strength. E-cadherin junctions are calcium dependent junctions. Studies have shown that depleting calcium disrupts intercellular junctions [130]. This tool was used in studies providing insights on how cadherin turnover dynamically controls intercellular junctions. Time dependent calcium depletion caused a percent drop in cell-cell contact area and intercellular forces [51]. Another study demonstrated that, after calcium depletion, cadherins were eliminated by endocytosis [131]. In epithelial cells, cadherin endocytosis critically influences physiological processes.
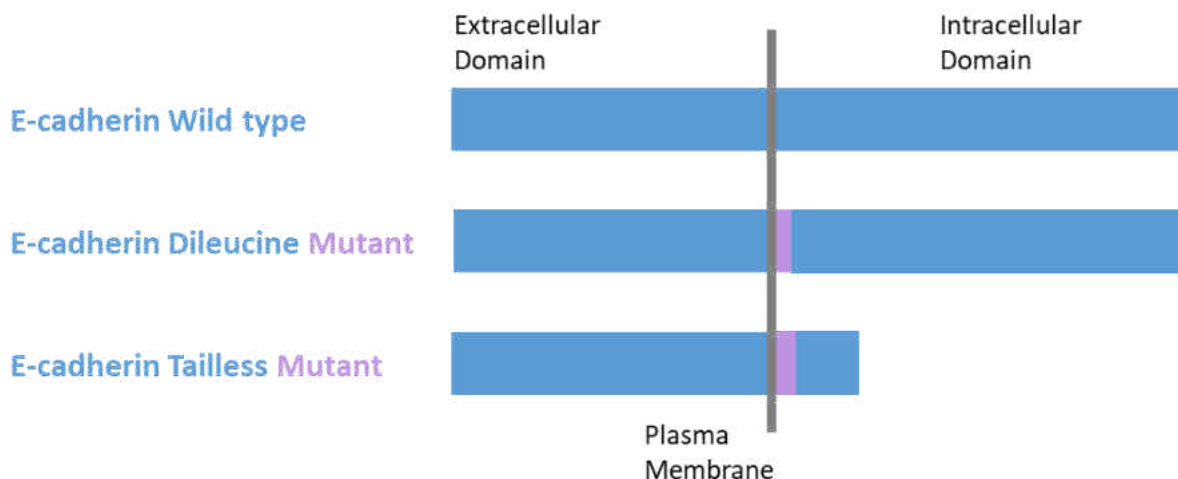
Figure 15: Schematic of E-cadherin constructs: E-cadherin wild type with full length E-cadherin, E-cadherin dileucine mutant with a mutation that inhibits endocytosis but retains cytoplasmic domain and E-cadherin tailless mutant lacking the cytoplasmic domain that binds to β-catenin and other cytoplasmic proteins.

To study the effect of endocytosis on intercellular forces, I examined cells expressing an E-cadherin construct inhibiting endocytosis due to a mutated dileucine motif (LL) and E-cadherin lacking the cytoplasmic catenin binding domain (Figure 15). The expression of these constructs were higher compared to endogenous E-cadherin [129]. E-cadherin endocytosis is known to be driven by the dileucine motif (LL) [130]. Cells stably expressing the 3 constructs shown in Figure 15 were seeded on PAA gels coated with collagen I and fluorescent beads. Using the traction force imbalance method, intercellular forces were calculated and compared with that for wild type cells. As shown in Figure 16, there was no qualitative difference in the cell traction plots of these constructs compared with wild type E-cadherin. We expected the average intercellular force for

the cells expressing the dileucine E-cadherin construct and the E-cadherin construct without the cytoplasmic domain to be lower compared to cells expressing the full-length E-cadherin construct (all with fluorescent protein tags for FRET). Instead, we found that the difference was statistically non-significant (Figure 16G). What might explain our result? We suspect that the endogenous E-cadherin, which is expressed in all three cell lines, still dominates in terms of transmitting force at the cell-cell contact. However, it is possible that other types of cell-cell adhesion molecules (for e.g., other classic cadherins and desmosomal cadherins) may also be playing a role in cell-cell contact force transmission, especially if E-cadherin-based force transmission is impacted.
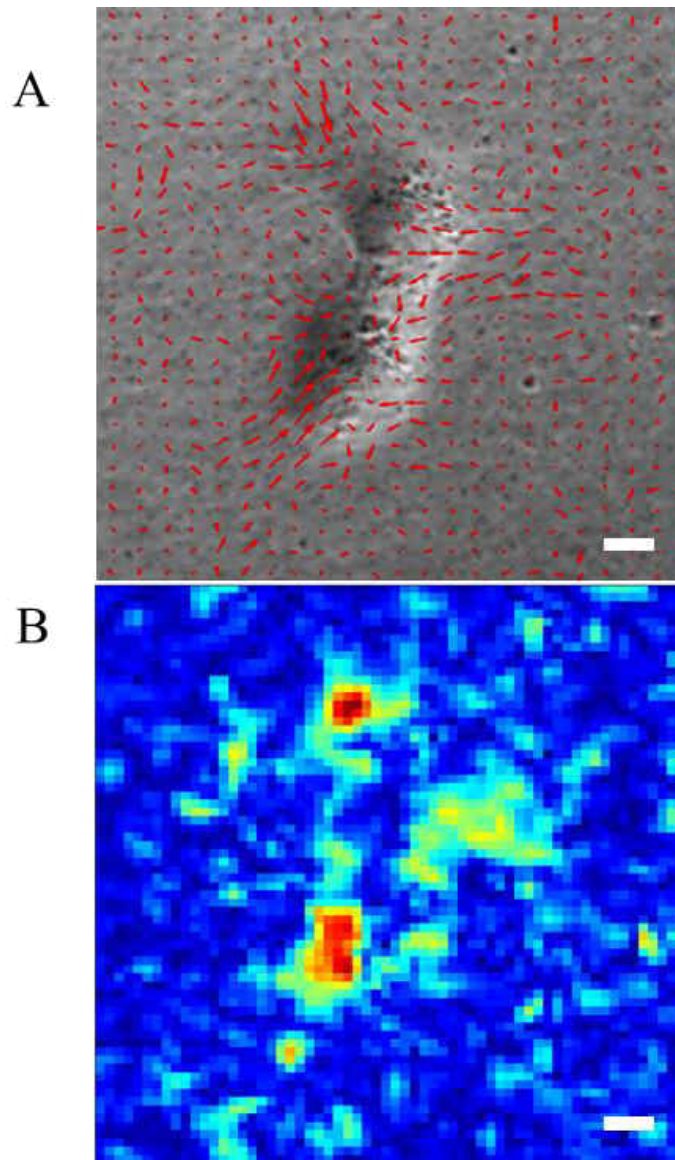
Figure 16 (A-G): Qualitative and quantitative analysis of intercellular forces between E-cadherin constructs. (A) Phase images of E-cadherin wild type (B) corresponding traction heat map. (C) Phase images of E-cadherin dileucine mutant and corresponding (D) traction heat maps. (E) Phase images of E-cadherin dileucine mutant and corresponding (F) traction heat maps. Scale bar 5 μm.

(G) Histogram of average intercellular forces between E-cadherin constructs. (E-cadherin wild type n = 11, E-cadherin dileucine mutant n = 10, E-cadherin tailless mutant n = 13).
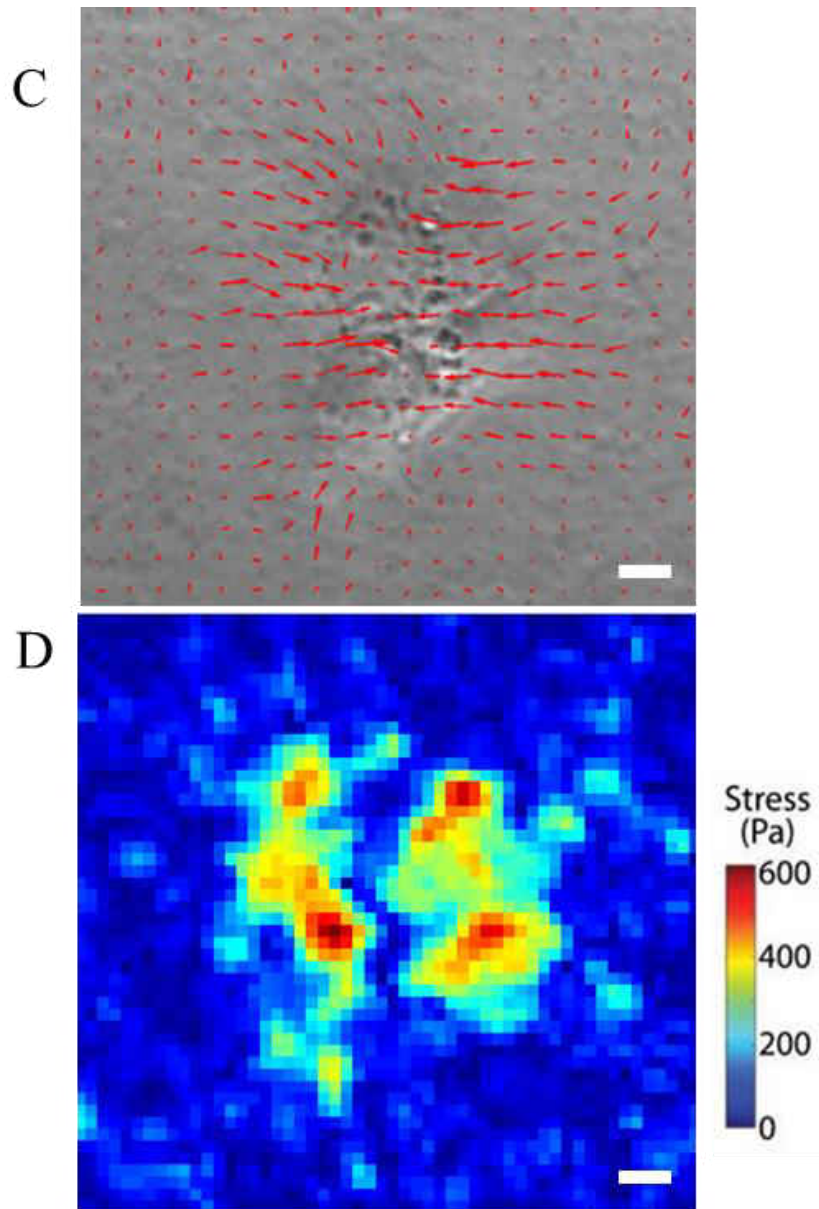
Figure 16 (C-D): Qualitative and quantitative analysis of intercellular forces between E-cadherin constructs. (C) Phase images of E-cadherin dileucine mutant and corresponding (D) traction heat maps. Scale bar 5 μm.
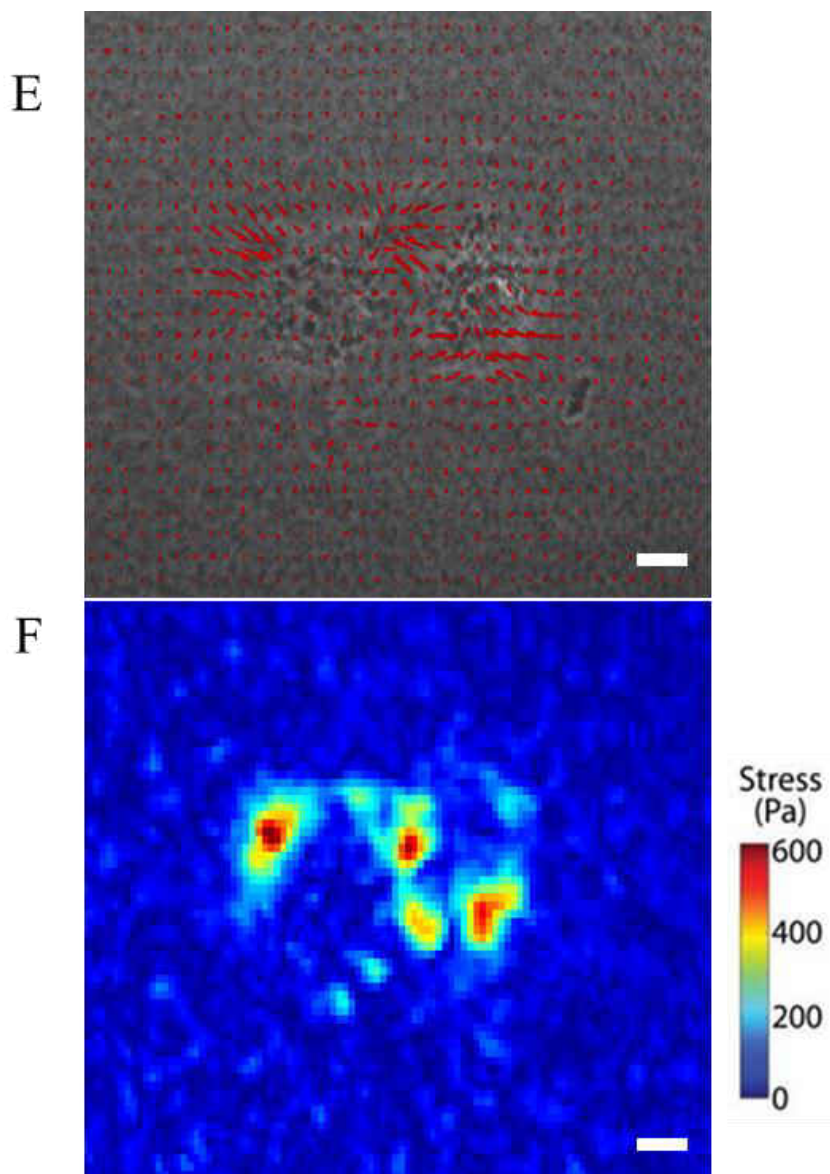
Figure 16 (E-F): Qualitative and quantitative analysis of intercellular forces between E-cadherin constructs. (E) Phase images of E-cadherin dileucine mutant and corresponding (F) traction heat maps. Scale bar 5 μm.
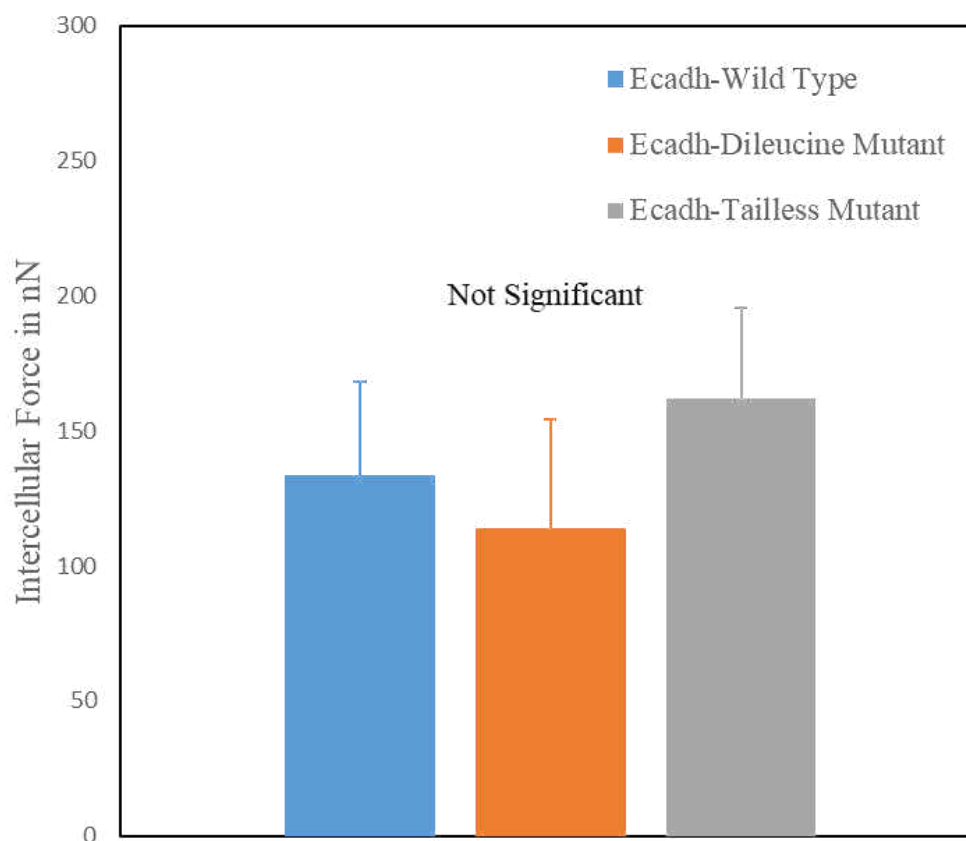
Figure 16 (G): Qualitative and quantitative analysis of intercellular forces between E-cadherin constructs. (G) Histogram of average intercellular forces between E-cadherin constructs. (E-cadherin wild type n = 11, E-cadherin dileucine mutant n = 10, E-cadherin tailless mutant n = 13).

CHAPTER

4. ENDOGENOUS SHEET-AVERAGED TENSION WITHIN A LARGE EPITHELIAL CELL COLONY

Note: Contents of this chapter have been published in the Journal of Biomechanical Engineering:

Dumbali SP, Mei L, Qian S, Maruthamuthu V. Endogenous Sheet-Averaged Tension Within a Large Epithelial Cell Colony. J Biomech Eng. 2017;139(10):1010081–1010085.

The following contents, published in the Journal of Biomechanical Engineering, are based on the experiments conducted to examine endogenous tension within a large epithelial cell colony.

Abstract

Epithelial cells form quasi-two-dimensional sheets that function as contractile media to effect tissue shape changes during development and homeostasis. Endogenously generated intrasheet tension is a driver of such changes but has predominantly been measured in the presence of directional migration. The nature of epithelial cell-generated forces transmitted over supracellular distances, in the absence of directional migration, is thus largely unclear. In this report, we consider large epithelial cell colonies which are archetypical multicell collectives with extensive cell–cell contacts but with a symmetric (circular) boundary. Using the traction force imbalance method (TFIM) (traction force microscopy combined with physical force balance), we first show that one can determine the colony-level endogenous sheet forces exerted at the midline by one half of the colony on the other half with no prior assumptions on the uniformity of the mechanical properties of the cell sheet. Importantly, we find that this colony-level sheet force exhibits large variations with orientation—the difference between the maximum and minimum sheet force is comparable

to the average sheet force itself. Furthermore, the sheet force at the colony midline is largely tensile, but the shear component exhibits significantly more variation with orientation. We thus show that even an unperturbed epithelial colony with a symmetric boundary shows significant directional variation in the endogenous sheet tension and shear forces that subsist at the colony level.

Keywords: epithelial colony, traction force, endogenous sheet tension, cell–cell contact

4.1 Introduction

The contractility of epithelial cells and the transmission of endogenous cell-generated forces over supracellular distances are important drivers of morphological changes at the tissue-level and beyond [132, 133]. In fact, epithelial sheets can use biochemical cues to break in-plane symmetry and generate anisotropic endogenous tension [134]. However, the nature of supracellular force transmission in epithelial sheets, even in the absence of developmental cues, is largely unclear. In this regard, in vitro cell collectives such as cell colonies, in spite of their limited size and presence of free boundary, are an accessible model system to understand the fundamental nature of endogenous forces and how they are transmitted in a multicellular context.

Cell-generated forces are transmitted through multicellular epithelial sheets via cell–cell contacts bound by cell–cell adhesion structures, such as adherens junctions [133]. Forces transmitted through epithelial cell–cell contacts have been measured using multiple techniques local to the cell–cell contact [83, 135, 136] by using molecular tension sensors, oil droplets, and laser ablation. On the other hand, traction force microscopy-based methods [51, 137-141] have provided a complementary picture with quantitative measures of cellular force generation and transmission in

single cells, small islands, and expanding monolayers. However, our knowledge of force transmission in quiescent, large epithelial cell colonies is limited.

While multiple studies have reported on forces transmitted in small islands of two or more cells [51, 137, 142, 143], studies on monolayers [140] have provided information on local forces, but with assumptions such as homogeneous cell mechanical properties across the monolayer. However, the dependence of cell stiffness on cell prestress suggests that cell mechanical properties may not be homogeneous across cell sheets [144]. Here, we consider a large epithelial cell colony (large in the sense that the extent of cell–cell contacts is much larger than the free cell colony boundary) that is also circular in shape. While the effect of the free boundary is itself not eliminated, the circular shape does eliminate directional cues due to asymmetric free boundaries. Without assuming uniform cell mechanical properties, while we cannot obtain local forces, we demonstrate that the endogenous forces within the cell sheet can be determined at the whole epithelial colony level. We also uncover significant variation of this large tensile force with orientation.

4.2 Methods

4.2.1 Cell Culture

Dulbecco's modified Eagle's medium (Corning Inc., Corning, NY) supplemented with L-glutamine, sodium pyruvate, 1% Penicillin/streptomycin, and 10% fetal bovine serum (Corning Inc., Corning, NY) was used to grow Madin Darby canine kidney (MDCK) cells under 5% CO_2. For plating micropatterned polyacrylamide (PAA) hydrogels, about 10^5 cells were plated on 35-mm culture dishes with hydrogels and the medium was replaced within 0.5 h after plating.

4.2.2 Preparation and Micropatterning of Polyacrylamide Hydrogel Substrates

Polyacrylamide gels were made with an acrylamide to bisacrylamide ratio of 7.5%:0.1%. Red fluorescent beads of diameter 0.44 μm (Spherotech Inc., Lake Forest, IL) were included as fiducial markers. For micropatterning the PAA gels [145], a 22mm x 22mm glass coverslip (no. 1.5) was first treated with deep UV light to render it hydrophilic. The coverslip was then incubated with a solution of 0.1 mg/ml poly(L-lysine)-poly(ethylene glycol) at pH 7.4 for 30 min. Then, it was exposed to deep UV light with a quartz chrome photomask (Toppan, Round Rock, TX) (with the 500 μm clear circle in the light path) for 5 min. The coverslip was then incubated with 0.02 mg/ml collagen 1 protein (at pH 8.5) for 30 min. The PAA gel was then polymerized and sandwiched between the collagen-coated coverslip and an activated coverslip (activated by treating successively with 2% 3-aminopropyltrimethyoxysilane in isopropanol and 1% glutaraldehyde in distilled water). The resultant PAA gel had a thickness of ~150 μm as determined from z-stacks of images of fluorescent beads within the gel (Figure 17).

A

- Deep UV exposure of Glass Coverslip

  UV Exposure

  Glass Coverslip
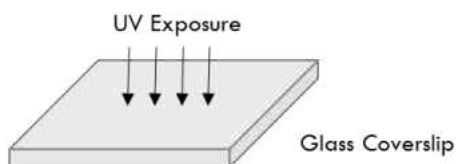
- Incubation with Poly-L-lysine – Polyethylene Glycol (PLL-PEG)

  PLL-PEG coating
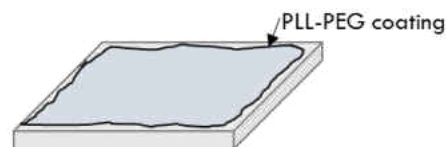
B

- Exposure to Deep UV along with Quartz Chrome Photomask

  UV Exposure   Photomask

  500 μm clear circles
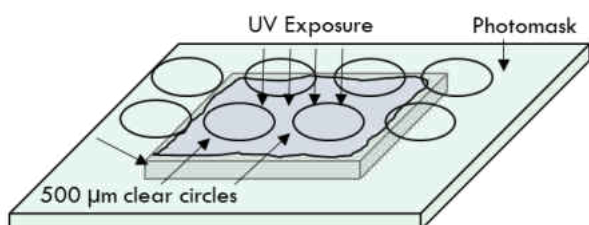
C

- Incubation with Collagen 1 Protein (ECM)
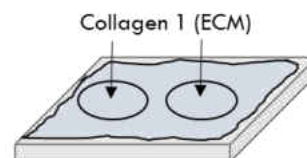
  Collagen 1 (ECM)

D

- PAA gel (with micron-sized Fluorescent Beads) Polymerization between Collagen 1 coated coverslip and Activated Coverslip

  Activated Coverslip
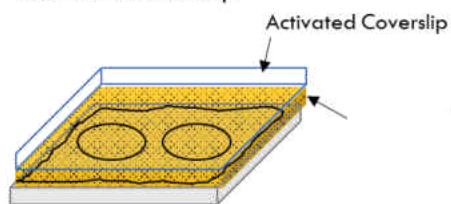
- Collagen Coupled Micro-patterned Gel Transferred to Activated Coverslip
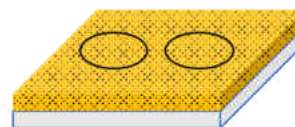
- Epithelial Cells Plated on 500 μm Micro-patterned Collagen Coated PAA Gel

  Epithelial Cell Island
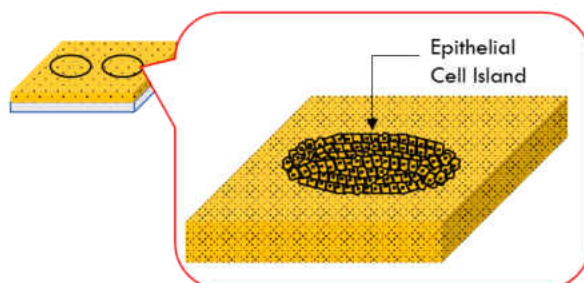
Figure 17: Micropatterning of Polyacrylamide Hydrogel Substrates. (A) Glass coverslip is made hydrophilic by exposing it under deep UV. It is then incubated with the crosslinker protein Poly-L-Lysine Polyethylene Glycol for 30 minutes. (B) This coverslip is placed on quartz chrome photomask containing 500 um circular patterns. The mask is inverted upside down and exposed to deep UV to make the 500 um circular patterns hydrophilic. The chrome film outside the circular pattern blocks UV and helps forming hydrophilic surface only through the clear circular patterns. (C) The coverslip with circular micropatterns is incubated with collagen I protein for 30 minutes. (D) The PAA gel is polymerized between micropatterned coverslip and activated coverslip. After 45 minutes of polymerization, cells can be plated on collagen coated micropatterned activated coverslip.

4.2.3 Traction Force Measurements

An imaging system consisting of a Leica DMi8 epifluorescence microscope (Leica Microsystems, Buffalo Grove, IL) with a 10 x 0.3 NA objective, HQ2 cooled CCD camera (Photometrics, Tucson, AZ) and an airstream incubator (Nevtek, Williamsville, VA) was used to obtain phase images of MDCK cell colonies and red bead images (from the top surface of the gel) beneath them. Bead images were also obtained after the colonies were removed using 10% sodium dodecyl sulfate. After image alignment using Image J [146], the displacement of the beads was calculated using MATLAB (MathWorks, Natick, MA) with code available at the website [4]. Traction forces were then reconstructed from the displacements of the gel surface using Regularized Fourier Transform Traction Cytometry, which employs the Boussinesq solution [127, 129, 147, 148].

4.2.4 Sheet Force Calculations

The epithelial sheet force at the colony mid-line was calculated similar to what was implemented for TFIM of cell pairs previously [51], except that the colony mid-line demarcated the two parts of the colony here. A binary mask (dilated by 10%) based on the micro-pattern diameter (0.5 mm) was used to select all traction forces exerted by the colony (to calculate the scalar sum Σ(colony)|$\mathbf{Ti}$| or vector sum Σ(colony)$\mathbf{Ti}$) so that noise contributions from regions away from the colony, as well as that due to the frame boundary, were avoided. Two half masks on either side of the colony midline (which in turn was constructed at an angle θ with respect to the horizontal) were used to select traction forces exerted by the two halves of the colony. The sheet force exerted on half 1 (by the other half, half 2) is $\mathbf{F_{12}} = \Sigma$(half1)$\mathbf{T_i}$ and the sheet force exerted on half 2 (by the other half , half 1) is $\mathbf{F_{21}} = \Sigma$(half2)$\mathbf{T_i}$. The sheet force $\mathbf{F}_{sheet}$ is thus the average ($\mathbf{F_{12}}$ - $\mathbf{F_{21}}$)/2 (the difference is used as $\mathbf{F_{12}}$ is directed roughly opposite to $\mathbf{F_{21}}$), with an associated error of ($\mathbf{F_{12}}$ + $\mathbf{F_{21}}$)/2 (as explained in ref [51]). If the angle made by the sheet force to the colony mid-line is α, the sheet tension at the mid-line is $\mathbf{F}_{sheet}$ sinα and the sheet shear is $\mathbf{F}_{sheet}$ cosα. All binary masks were created using ImageJ and all force calculations mentioned above were using custom-written scripts in MATLAB (MathWorks, Natick, MA).

4.2.5 Finite Thickness Traction Computation

The traction force under the epithelial cell colony was also computed (from the experimentally measured displacement field) taking into account the finite thickness of the substrate using a commercial finite element package, COMSOL. For this, substrate of dimensions width 3 mm, length 3 mm, and height 150 µm was assumed, with the experimentally measured displacement field applied on the top surface and the bottom surface fixed (zero displacement). We assumed

hydrogel properties of Young's modulus 13.5 kPa and Poisson's ratio 0.49. Tetrahedral mesh was employed with denser mesh on the top surface where the displacement field is imposed, with a total of 38,423 units in the mesh. The system was numerically solved using the Solid Mechanics module in COMSOL Multiphysics (COMSOL Inc., Burlington, MA) and the computation was carried out on a high-performance computing cluster at ODU, Norfolk, VA.

4.3 Results

We micropatterned collagen I as a half millimeter-wide filled circle on PAA gel and then plated MDCK cells on them, resulting in a cohesive circular epithelial cell colony (Figs. 18(A) and 18(B)). Using TFIM, which has previously been used to determine the endogenous force exerted at a single cell–cell contact, we sought to determine the endogenous sheet force exerted within a large epithelial cell colony. Here, based on the position of submicron fluorescent beads in the PAA gel with and without the colony on it, we first determined the displacement field of the gel under the cell colony using particle image velocimetry and then computed the traction force field using regularized Fourier transform traction cytometry [51, 127, 148]. The traction stress field is depicted superimposed on the phase image of the epithelial cell colony in Fig. 18(B), with the corresponding traction stress heat map in Fig. 18(C).
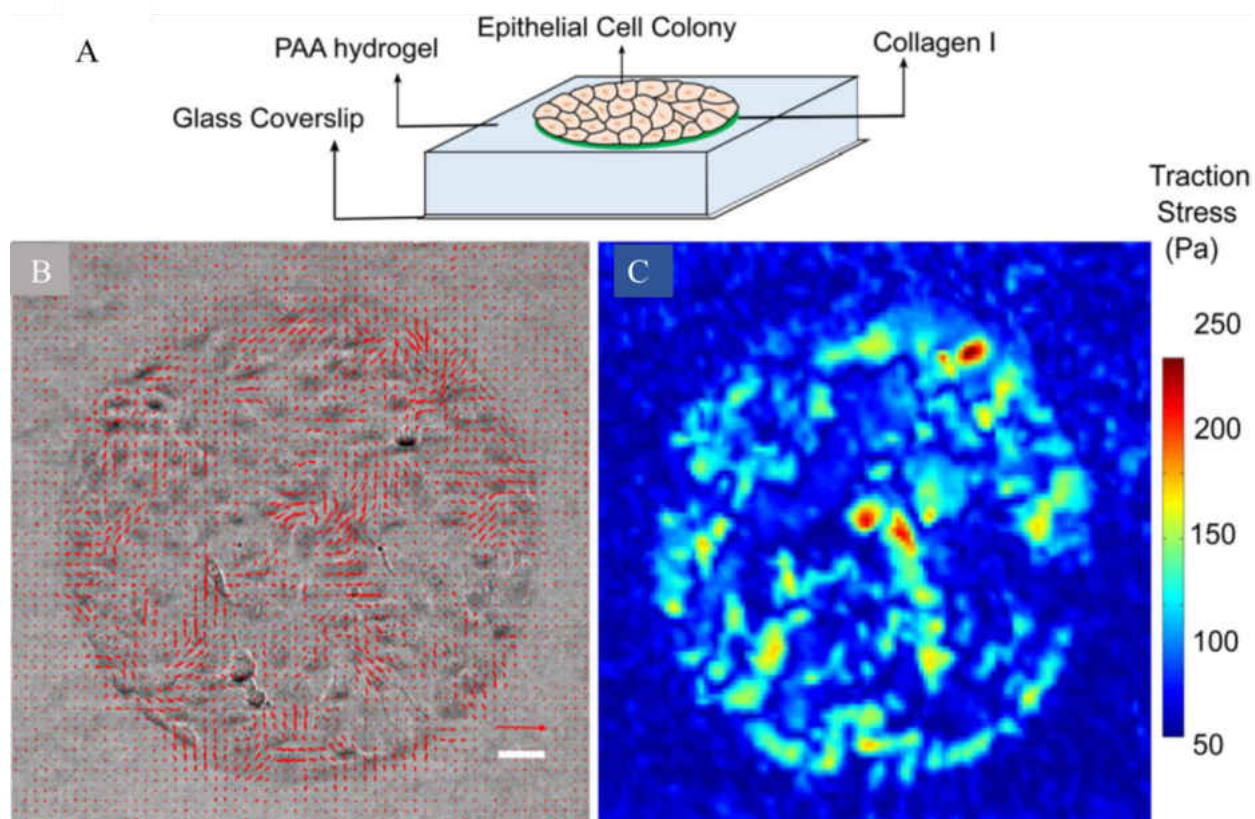
Figure 18: (A) Schematic depiction of the epithelial cell colony on the PAA hydrogel. (B) Phase image of the circular MDCK cell colony with the traction stress vectors overlaid. Scale bar for distance is 50 μm and for traction vector is 1000Pa. (C) Heat map representation of the traction stress under the colony.

The epithelial cell colony we consider exerts traction forces in a manner qualitatively different from small cell islands considered in many previous studies. While small cell islands (wherein the extent of free edge boundaries are comparable to that of cell–cell contacts) have been previously shown to predominantly exert large traction stresses only near the islands edges [51, 139, 142, 143], the larger colony considered here (wherein the contour length of free edge boundary is much less than the contours of all the cell–cell contacts within the colony) exerts large traction stresses

at the edges as well as in the interior regions of the colony (Fig. 18(C)). In fact, when we considered

above average traction stresses as a proxy for large traction stresses, we found that their frequency

distribution (Fig. 19(A)) was similar in the central, medial, and distal regions across the colony

(pooled from n¼6 epithelial colonies). Next, in order to be able to apply TFIM, the vector sum of

traction forces exerted by the cell colony should vanish (or be close to zero, subject to experimental

error). We thus determined the vector sum of traction forces as well as the scalar sum (sum of the

magnitudes) of traction forces exerted by the cell colonies (Fig. 19(B)). The magnitude of the ratio

of the vector sum to the scalar sum of traction forces under the colony was 562%, comparable to

that for the case of single cells or cell pairs [51].
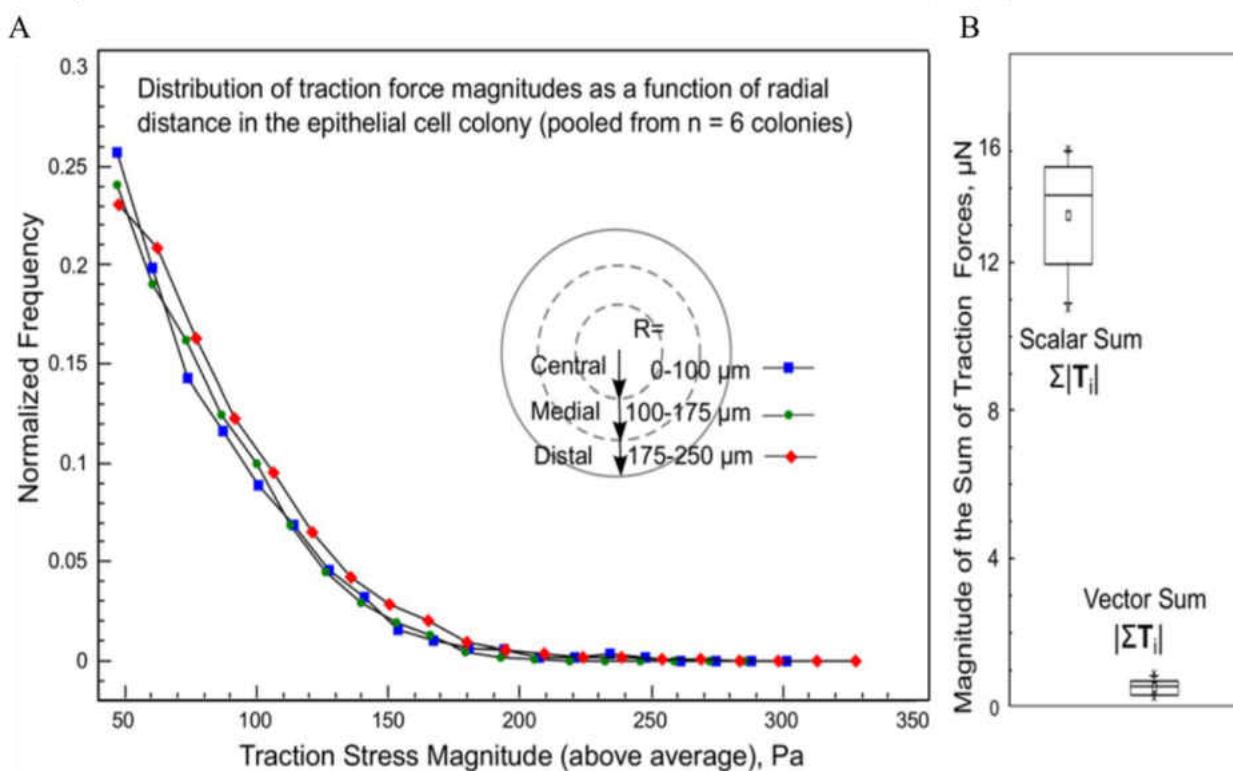
Figure 19: (A) Distribution of the magnitudes of traction stresses exerted under the central, medial, and distal regions within the colonies. Only above average traction stresses (used as a proxy for significant/large traction stresses) are considered in this plot. Data are pooled from n = 6 colonies. (B) Traction forces under each epithelial cell colony are balanced. The vector sum for each of the colonies is close to zero relative to the scalar sum of the traction forces that are shown for comparison. n = 6 colonies.
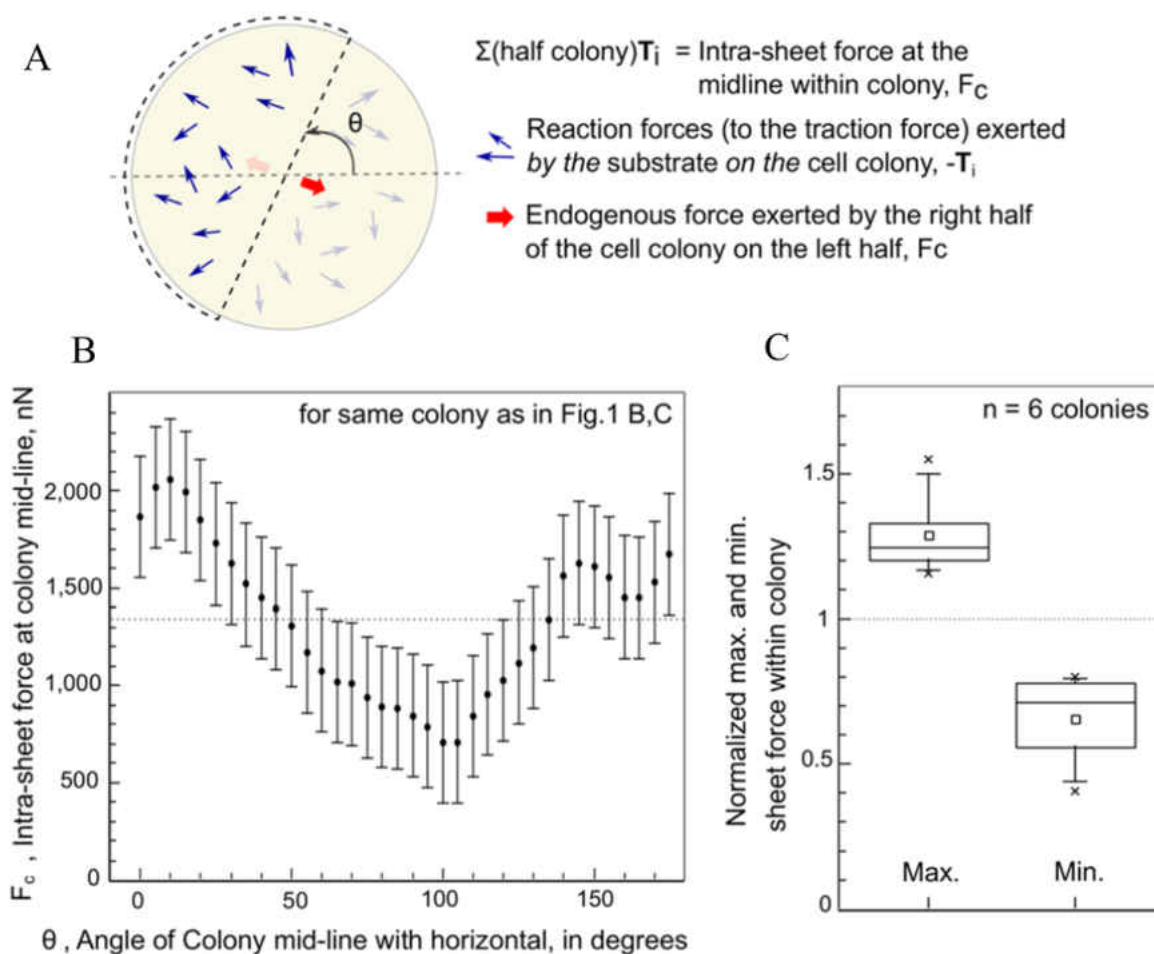
Figure 20: (A) Schematic depiction of the physical force balance used to determine the intrasheet force at the colony midline. (B) Variation of the intrasheet force at the colony midline as a function

of the orientation of the midline for the colony shown in Figs. 1(A) and 1(C). (C) The maximum and minimum sheet force in a colony normalized by its average sheet force across all orientations (n = 6 colonies).

Traction force imbalance method is premised on the balance between (the reaction to) traction forces exerted by the substrate on the part of the cell island under consideration and the endogenous forces exerted on this part of the cell island by the rest of the cell island [51]. Using TFIM, we sought to determine the endogenous sheet force exerted at the colony midline by one half of the colony on the other. Figure 20(A) illustrates the external forces acting on one half of the cell colony and the force balancing principle underlying TFIM as applied to the colony. However, as evident in Fig. 20(A), the orientation of the midline can vary over 180 deg (i.e., the angle of the midline with the horizontal can be anywhere between 0 deg and 180 deg). Thus, we calculated the endogenous sheet force within the colony as a function of the orientation of the midline. For the colony shown in Fig. 18(B), we found that, remarkably, the endogenous sheet force (which was largely perpendicular to the midline, as mentioned further below) varied between a minimum of 700 ± 310 nN to a maximum of 2060 ± 310 nN as a function of the midline orientation (Fig. 20(B)) (see Sec. 4.2 for method of error estimation). Thus, the range of variation of the endogenous sheet force was comparable to the average sheet force of the colony (1330 nN, averaged over all midline orientations). For n = 6 colonies, the average endogenous sheet force at the colony midline, averaged over all orientations for each colony, was found to be 1310 ± 400 nN (see Sec. 4.2 for method of error estimation) and the maximum and minimum endogenous sheet force differed, on average, by 63% of the average sheet force of each colony (Fig. 20(C)).
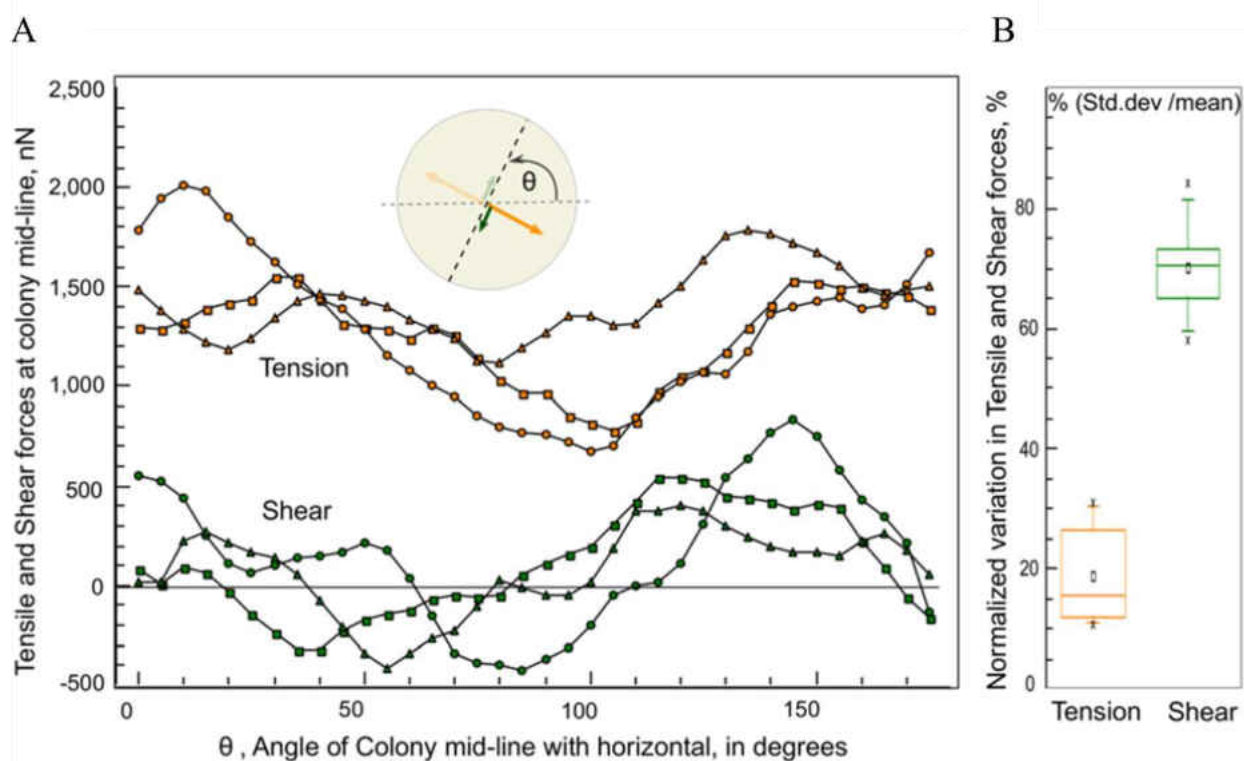
Figure 21: (A) Variation of the tensile and shear components of the endogenous sheet force at the colony midline with the orientation of the midline, shown for three representative colonies with similar average sheet force. (B) Normalized variation in the sheet tension and shear within each colony in % (n = 6 colonies).

In order to further explore the nature of the endogenous sheet force, we resolved it into tensile and shear components (as schematically depicted in Fig. 21(A) inset). Figure 21(B) shows the variation of the tensile and shear components with the midline orientation in three separate colonies with similar endogenous sheet forces. We found that, first, the endogenous sheet force is largely tensile in nature (i.e., the sheet force is largely perpendicular to the corresponding colony midline). Second, although smaller, whole colony-level shear forces persist at the midline. As evident in Fig. 21(A), the absolute variation in the tensile and shear forces was comparable. But since the

shear forces are smaller in magnitude, the normalized variation (standard deviation/mean) in shear forces far exceeded that in the sheet tension at the midline (Fig. 21(B), n = 6 colonies). Thus, even though the net shear force vanished for specific orientations of the midline, they persist at the colony level in general, with an average magnitude of about one-fifth that of the sheet tension.

To demonstrate that the traction forces as well as the intrasheet tension that we determined here are ultimately due to cell-generated contractility and are not simply an experimental artifact, we determined their dependence on Rho-kinase activity. Rho-kinase is a Rho-GTPase effector that indirectly promotes myosin activity and hence contractility [149]. We used Y27632, a pharmacological inhibitor of Rho-kinase to reduce cell contractility and tested the effect of this on the measured traction and endogenous sheet forces. As shown in Fig. 22(A), treatment with 50 lM Y27632 for 1 h reduced the traction forces to near-background levels. The anisotropic endogenous sheet forces also concomitantly reduced drastically (Fig. 22(B)). For n = 4 colonies, 1 h of treatment with Y27632 reduced the endogenous sheet forces by 79 ± 5%.
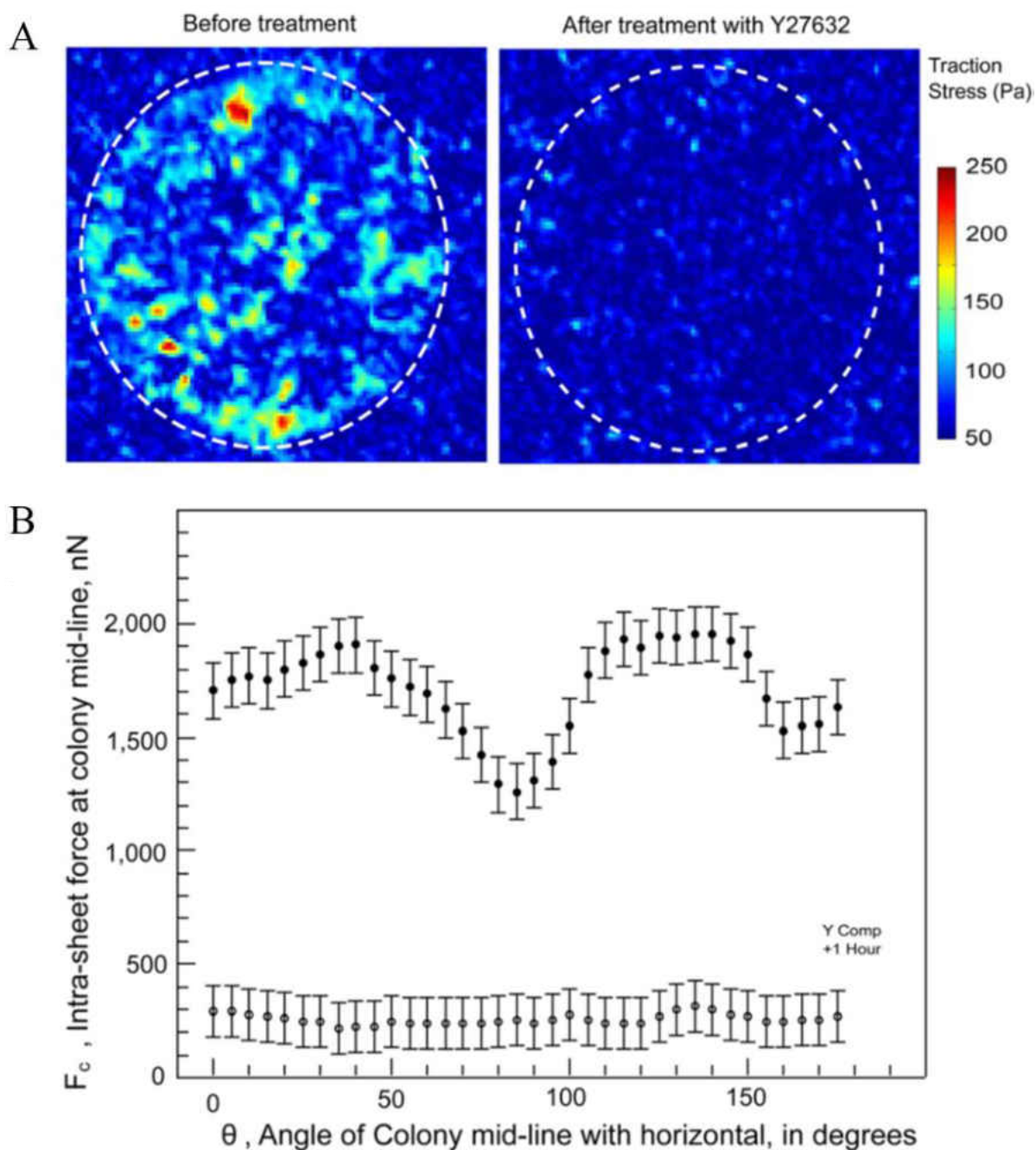
Figure 22: Traction and sheet forces are Rho-kinase sensitive. (A) Heat map representation of the traction stress under the MDCK cell colony before and after 1 h of treatment with 50 μM of the Rho-kinase inhibitor Y27632. (B) Variation of the intrasheet force at the colony midline as a function of the orientation of the midline before and after 1 h treatment with Y27632.

A FEM result taking into account finite thickness of substrate   Traction Stress (Pa)

B

FEM result taking into account finite thickness of substrate

Boussinesq solution

F_c , Intra-sheet force at colony mid-line, nN

θ , Angle of Colony mid-line with horizontal, in degrees
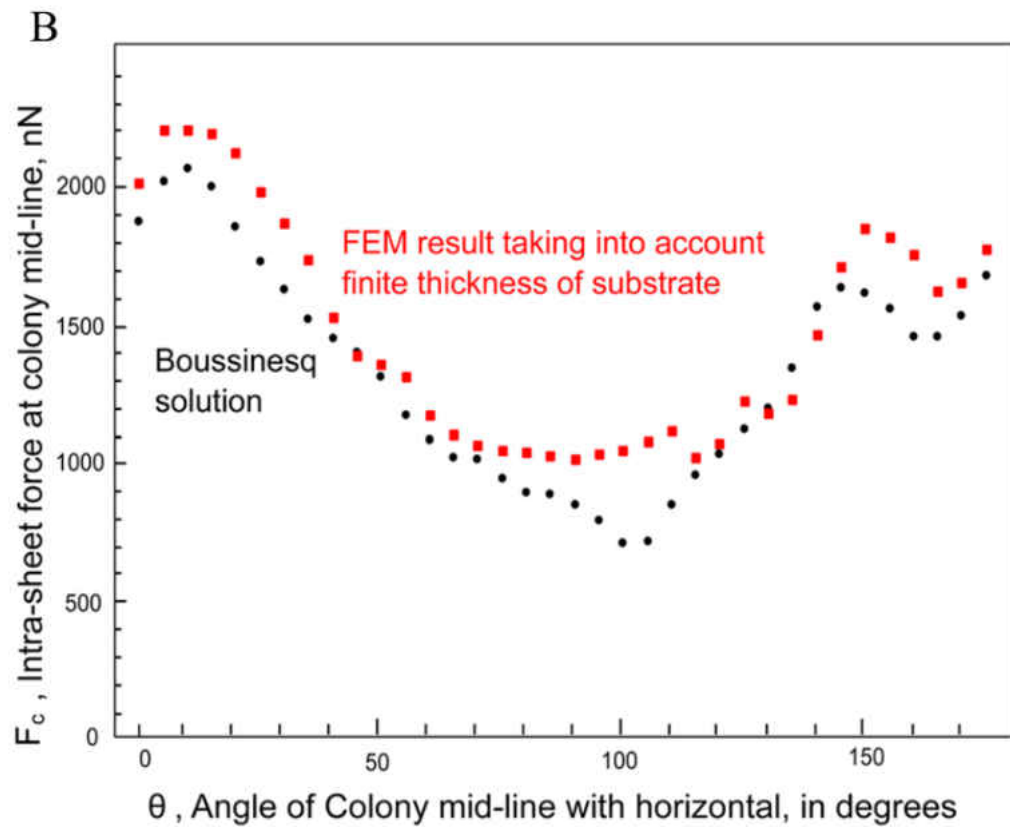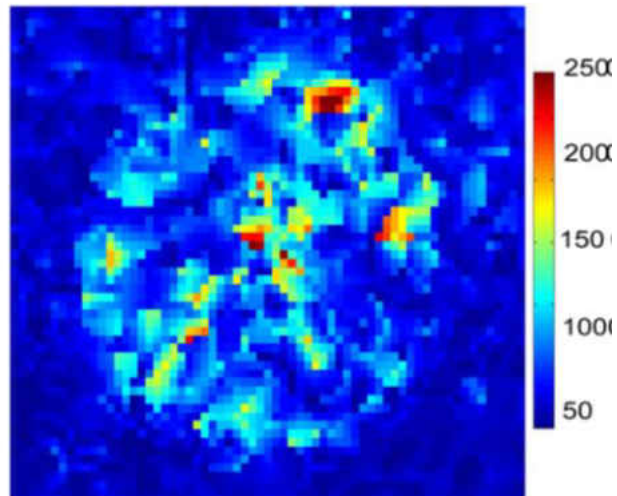
Figure 23: (A) Heat map representation of the traction stresses under the colony computed using a finite element model of the substrate as a linear, isotropic elastic medium of finite thickness (of 150 μm). Compare with the Boussinesq solution in Fig. 18(C). (B) Comparison of the intrasheet force at the midline obtained using the Boussinesq solution and the FEM result considering the finite thickness of the substrate. Estimated errors (not shown in the figure) in the Boussinesq solution sheet force are 310 nN and in the FEM results sheet force are 670 nN.

Since we used the Boussinesq solution in traction force calculations, we finally wanted to assess whether the finite thickness of the substrate (that varied between 150 and 200 μm) influenced the central result of this paper. To do this, we performed finite element method (FEM) computations taking into account finite substrate thickness (see Sec. 3.2) and compared this with the Boussinesq solution. As shown in Fig. 23(A), the traction heat map of the same colony as in Fig. 18(B) was largely similar. More importantly, the FEM results (that took finite substrate thickness into account) also yielded similar anisotropy in the endogenous sheet tension (Fig. 23(B)). Comparison of the sheet tension calculated using traction values obtained from the Boussinesq solution and the traction values obtained using the FEM with finite substrate thickness showed that they differed by ~15%, comparable to the error in the computation of the sheet tension itself. Thus, the key finding of this work (i.e., anisotropy of the sheet force, which is predominantly tensile) was also exhibited by the sheet force calculated using the traction forces from the FEM computation which took finite substrate thickness into account.

4.4 Discussion

We found that the endogenous sheet forces within large epithelial colonies display high tension and anisotropy. The average magnitude of the endogenous sheet tension normalized by the sheet diameter, i.e., the average sheet tension per unit length that we find for the colony, is 2.5 ± 0.8 nN/µm. This is comparable to a similar measure recently reported for a unidirectionally expanding MDCK sheet along the direction of expansion [150] and to the local cell–cell tension calculated in much smaller islands with the assumption of uniform cell island mechanical properties [151]. This suggests that even quiescent epithelial cell colonies (not engaged in directed migration) are in a highly tense state and this tensional state may be expected to regulate multiple biochemical processes that maintain homeostasis of the cell colony.

It is worth noting that, unlike for cell pairs [51, 137, 142], the endogenous sheet tension within the colony determined here using TFIM involves contributions from tension both perpendicular and parallel to individual cell–cell contacts, as the cell–cell contacts themselves are multiply oriented in an unrestrained manner near the colony midline. Thus, the endogenous sheet tension reported here is a useful metric to characterize the tensional state of an epithelial colony and it reflects tension transmitted through cell–cell contacts and the cells themselves with a colony.

The large circular epithelial cell colony and its sheet forces determined here using TFIM can help bridge the gap between studies involving cell pairs/small islands [51, 137, 143] where the extent of free boundary is comparable to the extent of cell–cell contacts and studies of colonies and expanding monolayers [151, 152] where uniform cell mechanical properties have been assumed. While seminal studies of expanding monolayers [140, 152] have the advantage of obtaining local

forces, it involves approximations at the frame boundaries and the assumption of uniform cell mechanical properties [152]. While our current approach has the disadvantage that it does not obtain local forces, but only average sheet forces (which implies that variations along the midline cannot be captured), it has the advantage of obtaining data from a single frame without similar assumptions at the frame boundaries or assumption of uniform cell mechanical properties. Thus, our approach here provides an alternative means to obtain useful mechanical readouts from cell collectives but has the disadvantage that local forces are not obtained. Our experimental model also has a free boundary, but the effect of the boundary is less significant than that for small cell islands in that large traction stresses are no longer limited to the cell island periphery here (as depicted in Fig. 19(A)). Comparison of the average sheet tension obtained here ($\sim$2.5 nN/μm) with a corresponding average measure reported [24] in a unidirectionally expanding monolayer of the same cell type (average of $\sim$2.7 nN/μm) leads us to estimate that the effect due to the free boundary may be causing a difference in the vicinity of 10%. However, sheet tension during individual time points of monolayer expansion [150] varied by as much as -12% to $+28\%$, relative to the average value reported here. Further studies with even larger colonies and monolayers should enable greater comparison between, and integration of, conclusions from the earlier studies and the extent to which anisotropies in sheet tension diminish or persist.

What might cause the directional variation in the endogenous sheet forces observed here? When we quantified the variation in the number of cells in each octant of each colony, we found that the standard deviation in cell number per octant for each colony was in the range of 10–20%. We could also detect no significant spatial changes in cell extracellular matrix deposition when we

assayed for collagen or fibronectin using immunofluorescence (the immunofluorescence was dominated by the cytoplasmic pool, data not shown). While we cannot conclusively rule out spatial variation in cell density or extracellular matrix as contributing factors to the orientation dependence of the sheet tension, we propose that cell-to-cell heterogeneities in force generation and transmission brought about by variations in the architecture and composition of the cytoskeletal, adhesive, and contractile apparatus may well play a major role. Just as determination of the endogenous force at a single cell–cell contact offers insight into the dynamic organization of a cell pair [142], knowledge of colony-level forces and specific biochemical factors inside the cells that lead to their directional variation can be expected to yield insights into larger scale multicellular rearrangements.

CHAPTER

5. α-CATENIN: A KEY REGULATOR OF ENDOGENOUS INTERCELLULAR FORCE TRANSMISSION

5.1 Introduction

5.1.1 Role of α-Catenin in the Catenin-Cadherin Complex

In multicellular organisms, tissue integrity significantly depends on strong adhesion between neighboring cells. As discussed in Chapter 1, this cell-cell adhesion is mediated by protein complexes that are part of junctions, such as an adherens junction, a tight junction and a desmosomal junction. A tight junction facilitates a barrier between either side of the cell layer while a desmosomal junction resists mechanical stress experienced within the epithelium, thereby maintaining the integrity. An adherens junction not only initiates cell-cell contact but also leads formation of the other junctional complexes [153]. Adherens junctions are formed by the assembly classical cadherins, catenins and associated proteins. The cytoplasmic domain of cadherin links to different cytoplasmic proteins including β-catenin, α-catenin and p120 catenin to facilitate the adherens junction. α-catenin is an actin-binding and bundling protein that contains vinculin homology domains [153] (Figure 24).

Earlier studies have shown that mutations in the cadherin-catenin complex or epigenetic modifications related to them may lead to cancer [154]. It has been shown that reduction in α-catenin levels may lead to weak formation of the adherens junction, irrespective of E-cadherin or β-catenin [155]. It was also found that, in human cancerous tissue, the downregulation of α-catenin interfered with the catenin-cadherin complex, thereby weakening the cell-cell junctions [155].

A

B
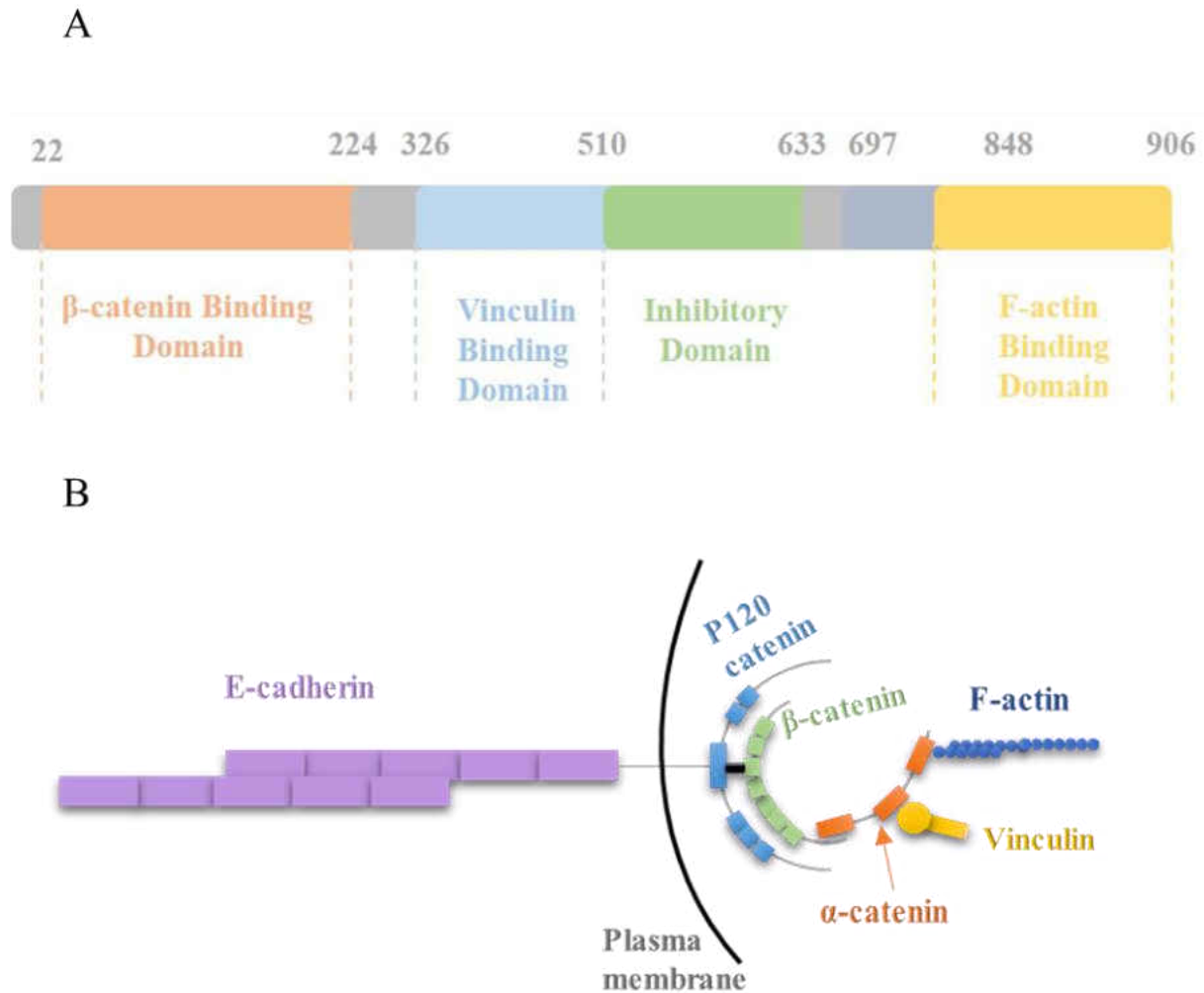
Figure 24. Function of α-catenin in cell-cell contacts. (A) Schematic representation of α-catenin structure showing β-catenin, vinculin and filamentous actin (F-actin) binding regions. (B) Role of α-catenin in the cadherin-catenin complex. During cell-cell contact formation, E-cadherin-E-cadherin binding enhances the linking of the cadherin-catenin complex to actin. α-catenin plays an important role as a linker between β-catenin and filamentous actin. A vinculin homology domain also binds to the head of vinculin.

5.1.2   Importance of α-Catenin in Intercellular Force Transmission

During morphogenesis and in cancer cell invasion, endogenous force transmission between neighboring cells facilitates morphological changes. The transmission of these forces is achieved by strong mechanical coupling between the cells primarily via the adherens junctions [156]. Adherens junction not only serves as a stage to detect variations in tension exerted by the adjacent cells but also helps transmitting this information amongst the cells [83, 157]. The contraction of the peripheral actomyosin ring exerts endogenous centripetal force which is experienced by neighboring cells by means of the E-cadherin-catenin complex. In response to this cortical tension, neighboring cells remodel their cadherin-catenin-actomyosin linkage [156]. This adaptation results in effective transmission of forces to other immediate cells. In order to assess the cellular response, it is important to understand how the mechanical signals are converted into biochemical signals. When a cadherin junction experiences mechanical force, α-catenin undergoes conformational changes thereby activating the domain associated with vinculin binding [158]. Recruitment of filamentous actin at an adherens junction also actively influences the activation of α-catenin. This suggests that α-catenin is a key player in intercellular force variations at the adherens junction. In addition to this, Rho A activation (dependent on α-catenin) influences adherens junction remodeling [156]. Recent studies have shown further how α-catenin can influence adherens junction assembly via vinculin recruitment [41, 159].

5.1.3 Effect of α-Catenin-Vinculin Binding at Cell-Cell Junctions

One of the widely known components of cell-ECM adhesions is vinculin. Vinculin is also present at the site of cadherin junctions. It functions with at least two known conformations: an active conformation when its domains can interact with other ligands and an inactive conformation that prevents any such interactions [160]. The active conformation initiates with disruption of the head-tail interactions [161]. On the other hand, cell-cell junctions require active vinculin binding to proteins like α-catenin that have both signaling capabilities and structural roles [162]. One of the studies showed that α-catenin and actin filaments can initiate an active vinculin conformation. FRET results highlighted the closed conformation of vinculin with high FRET signal, as the two selected fluorophores were close to each other initially, but lower FRET signals were recorded after the addition of α-catenin with just the vinculin binding domain or actin filaments [163]. This was concentration dependent and implied that actin and α-catenin binding to vinculin separates the fluorophores, proving their roles in the activation of vinculin.

Vinculin has been shown to play a crucial role in maintaining the integrity of E-cadherin junctions. Vinculin knockout cells show reduced affinity of E-cadherin adhesions. Immunofluorescence results suggested that these cells have lower expression levels of E-cadherin compared to control cells. This indicated that the presence of vinculin can strengthen E-cadherin junctions.

5.2 Results and Discussion

5.2.1   Intercellular Force Quantification to Study the Effects of α-Catenin

As α-catenin plays a role in adherens junctions and influences intercellular dynamics, I investigated how the level of α-catenin affects intercellular forces. Soft silicone gel with ~10 kPa Young's Modulus was fabricated and was coupled with Collagen I protein. MDCK cells and MDCK cells with α-catenin knocked out (KO) (a gift from the Conway Lab, VCU) were considered initially to test the effect on intercellular forces. The 'α-catenin KO' cells still expressed a truncated version that only did not contain the N-terminal, β-catenin binding domain, but with other binding domains intact. These cells were plated on the soft silicone gel sparsely in order to facilitate cell pair formation. These were then imaged, and the forces quantified using traction force microscopy, as detailed in Chapter 3. Representative images of MDCK and MDCK α-catenin KO cell pairs and the associated traction forces are shown in figures 25-26. Figure 27 shows the distribution and the median intercellular force for MDCK (n=39) and MDCK α-catenin KO (n=30) cell pairs. The average intercellular force for MDCK cells was found to be 55 ± 27 nN while that of MDCK α-catenin KO cells was 39 ± 22 nN. This means that the N-terminal region of α-catenin is necessary for normal intercellular force transmission.

Figure 25: Traction forces within a MDCK cell pair. (A) Phase image of a cell pair. Red arrows indicate traction stress vectors. (B) Heat map plot indicating the magnitudes of the traction stresses in (A). (Scale: 5 μm)

Figure 26: Traction forces within a MDCK α-catenin KO cell pair. (A) Phase image of a cell pair. Red arrows indicate traction stress vectors. (B) Heat map plot indicating the magnitudes of the traction stresses in (A). (Scale: 5 μm)
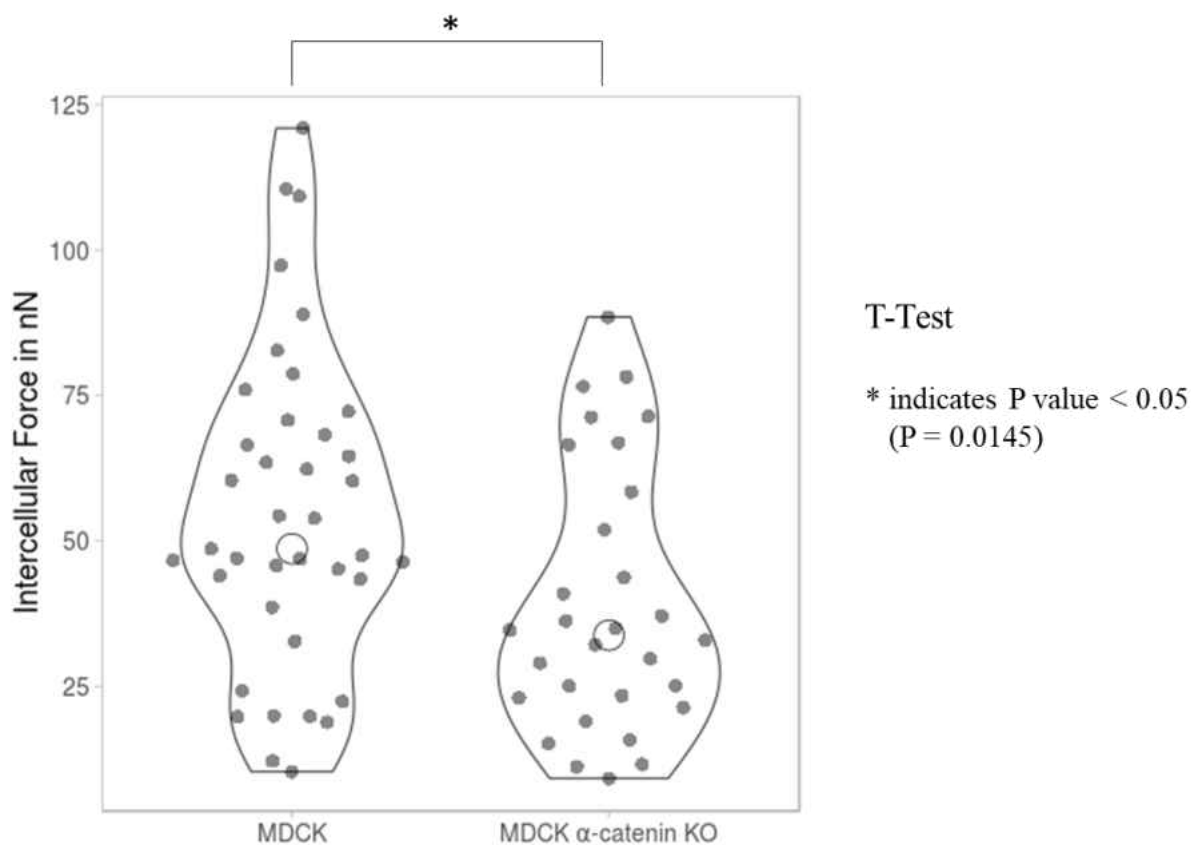
Figure 27: Violin plot showing the comparison of median intercellular forces between MDCK cells and MDCK α-catenin KO cells. The median weight of intercellular force for MDCK is higher that MDCK α-catenin KO. * indicates P value = 0.0145.

The distribution of intercellular force within MDCK cell pairs was pooled form 39 data points, while MDCK α-catenin KO was pooled from 30 data points. The comparison of intercellular forces of MDCK and MDCK α-catenin KO was carried out using a T-test. The *P*-value was found to be 0.0145 ($P < 0.05$) which showed that there is a statistically significant difference between these two cell lines.

A
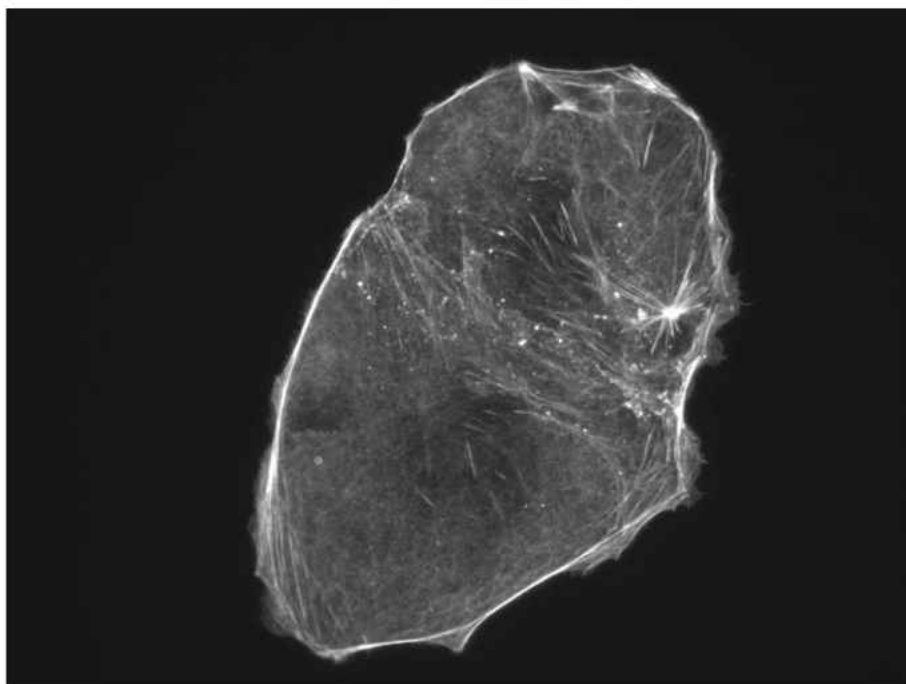
B
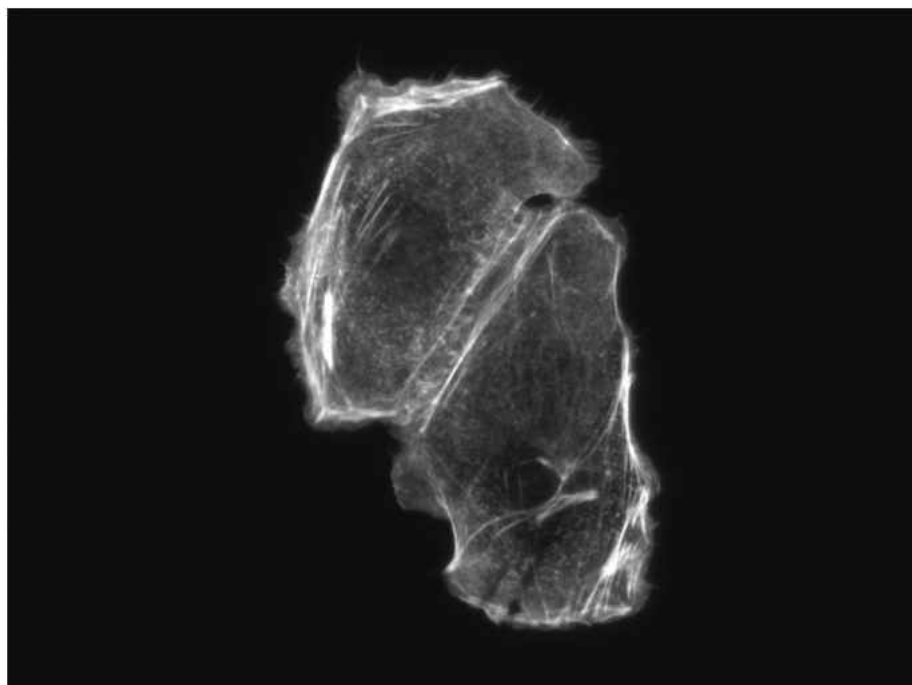
Figure 28: Immunofluorescence images showing actin localization for (A) MDCK cell pairs and (B) MDCK α-catenin KO cell pairs.

In order to ascertain as to why force transmission could be different, I stained for actin in cell pairs. While there were prominent actin bundles perpendicular to the cell-cell contact at either end of the cell-cell contact in MDCK cell pairs, cell-cell contacts in MDCK α-catenin KO cell pairs instead showed prominent actin bundles parallel to the cell-cell contact (Figure 28), indicating that the N-terminal region of α-catenin is required for normal actin bundle organization and force transmission at cell-cell junctions.

5.2.2 Absence of α-Catenin decreases Cell-ECM Traction Forces also

We also measured traction forces in single MDCK and MDCK α-catenin KO cells. Figures 29 and 30 shows phase and traction heat map images of MDCK and MDCK α-catenin KO single cells. We found that cell-ECM forces were also lower in case of MDCK α-catenin KO cells. As α-catenin does not take part in integrin-based cell-ECM adhesion, lower traction forces were indicative of some other phenomenon involving α-catenin. According to one study, absence of α-catenin can promote branched actin nucleation by Arp 2/3 activity [19]. This increase in branched actin filaments, compared to linear actin bundles, can in turn affect cell-ECM traction forces.

A
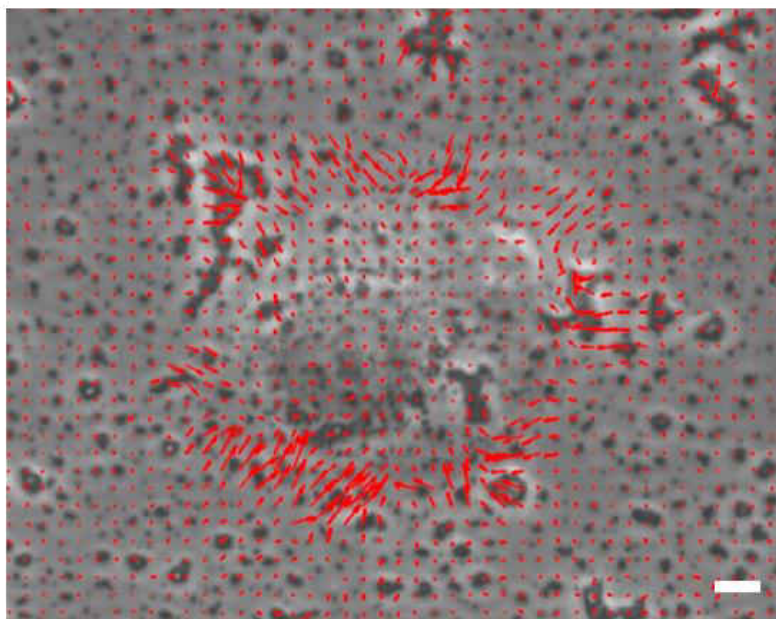
B
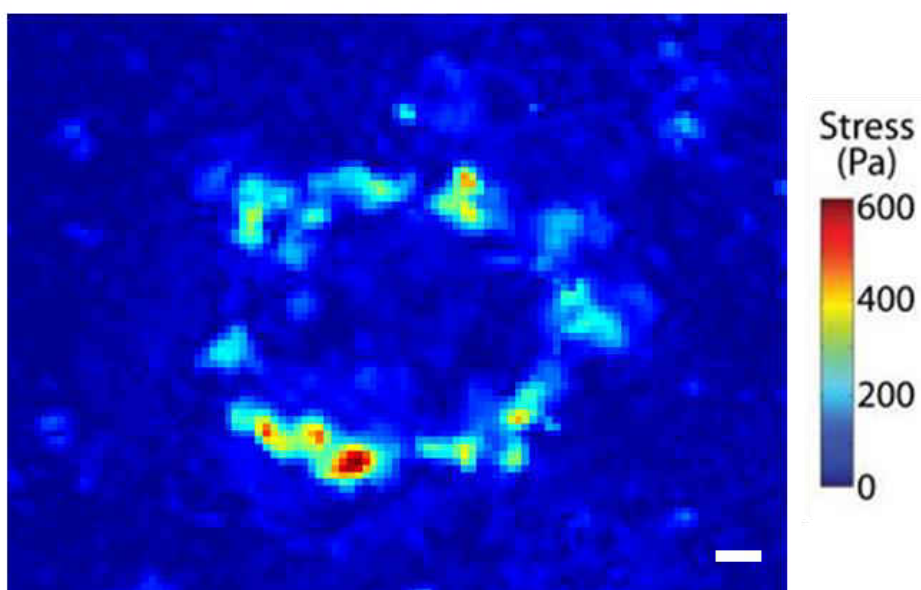
Figure 29: Traction forces within a MDCK single cell. (A) Phase image of a single cell. Red arrows indicate traction stress vectors. (B) Heat map plot indicating the magnitudes of the traction stresses in (A). (Scale: 5 μm)

A

B
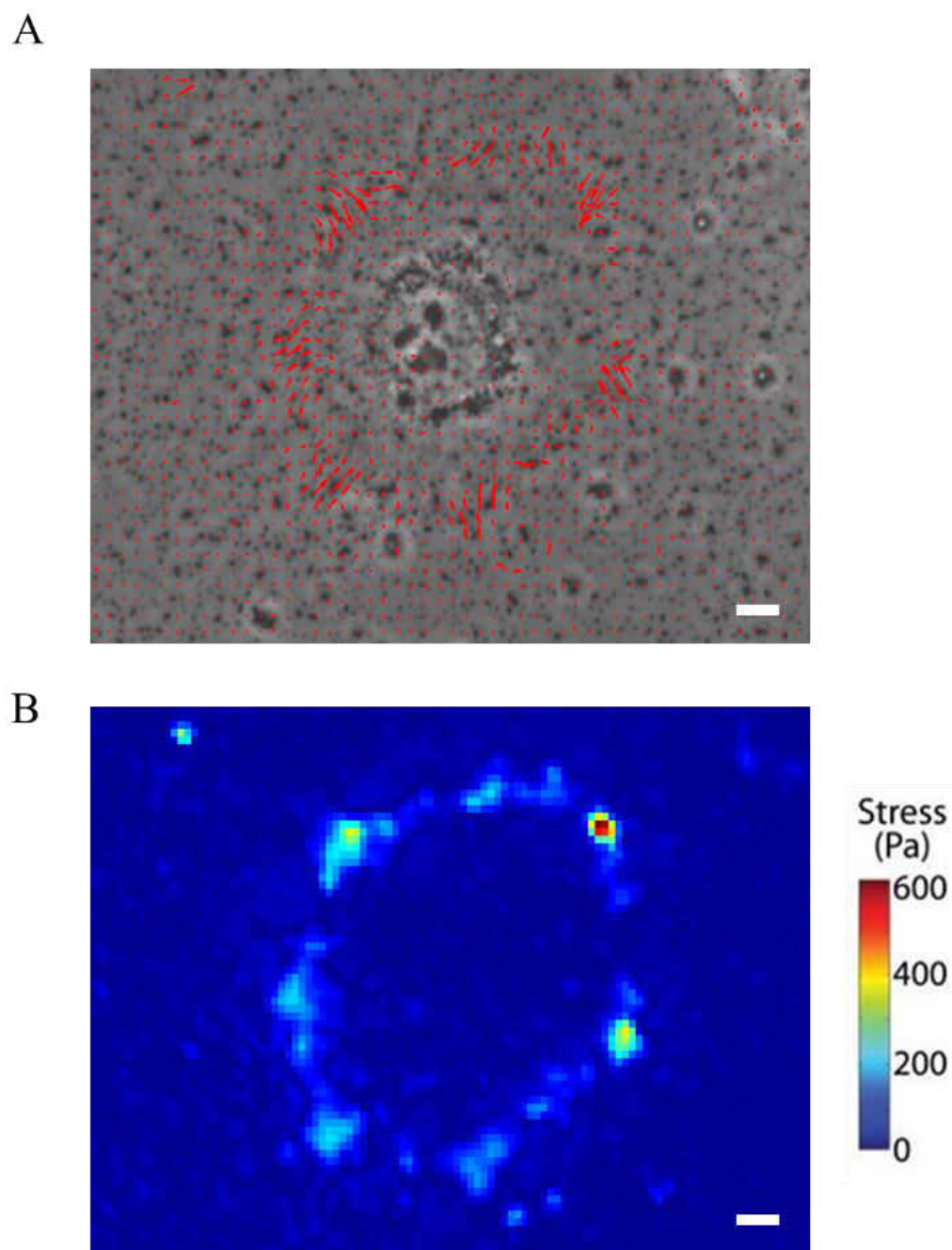
Figure 30: Traction forces within a MDCK α-catenin KO single cell. (A) Phase image of a single cell. Red arrows indicate traction stress vectors. (B) Heat map plot indicating the magnitudes of the traction stresses in (A). (Scale: 5 μm)
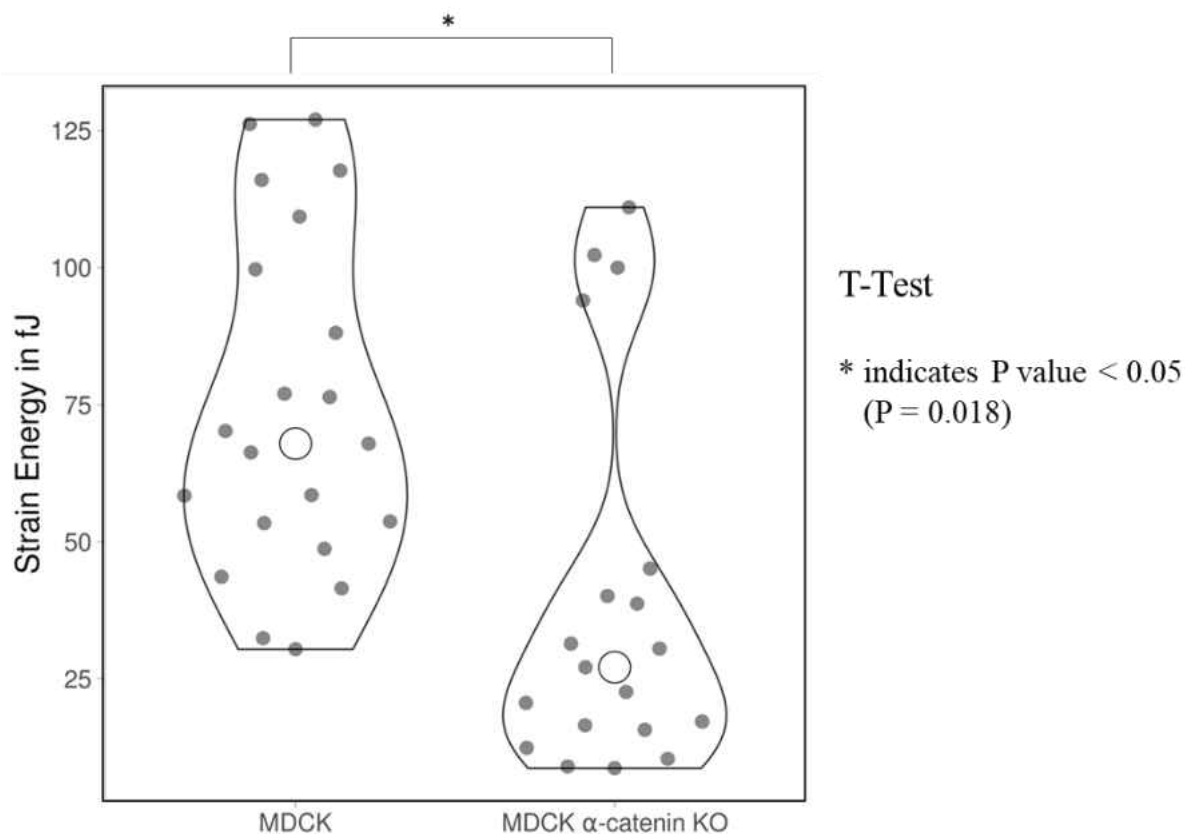
Figure 31: Violin plot showing median of strain energy comparison between MDCK and MDCK α-catenin KO single cells. The median strain energy for MDCK is higher than that for MDCK α-catenin KO. * indicates P-value = 0.0018.

As a reflection of the traction forces, the strain energy stored in the substrate due to its deformation by traction forces exerted by MDCK α-catenin KO cells, is shown to be lower compared to MDCK cells (figure 31). In Figure 31, a violin plot shows that the median of strain energies of MDCK α-catenin KO (n=19) was lower compared to MDCK (n=21). A T-test was carried out to assess statistical significance: a *P*-value of 0.0018 implies a statistically significant difference.

5.2.3   Mutants Influencing Vinculin Binding to α-Catenin

To assess the role of vinculin binding to α-catenin in mediating inter-cellular force transmission at the cell-cell junction, I carried out traction force microscopy experiments using α-catenin KO rescue mutants. α-catenin rescue mutant α-catenin-L344P rescue (substituting leucine 344 by proline) was generated (gift from Conway Lab, VCU), which inhibits vinculin binding and activation [164]. This rescue mutant rescues α-catenin in MDCK α-catenin KO cells with vinculin binding blocked. Another α-catenin mutant, α-catenin-CA rescue was designed, where CA stands for constitutively active α-catenin. This mutant rescues α-catenin KO cells with an 'always active' α-catenin with higher affinity towards vinculin. Finally, the WT rescue consists of α-catenin KO cells that are then made to exogenously express full length α-catenin. Both cell pair and single cell traction measurement results for the above three rescues are presented in what follows.
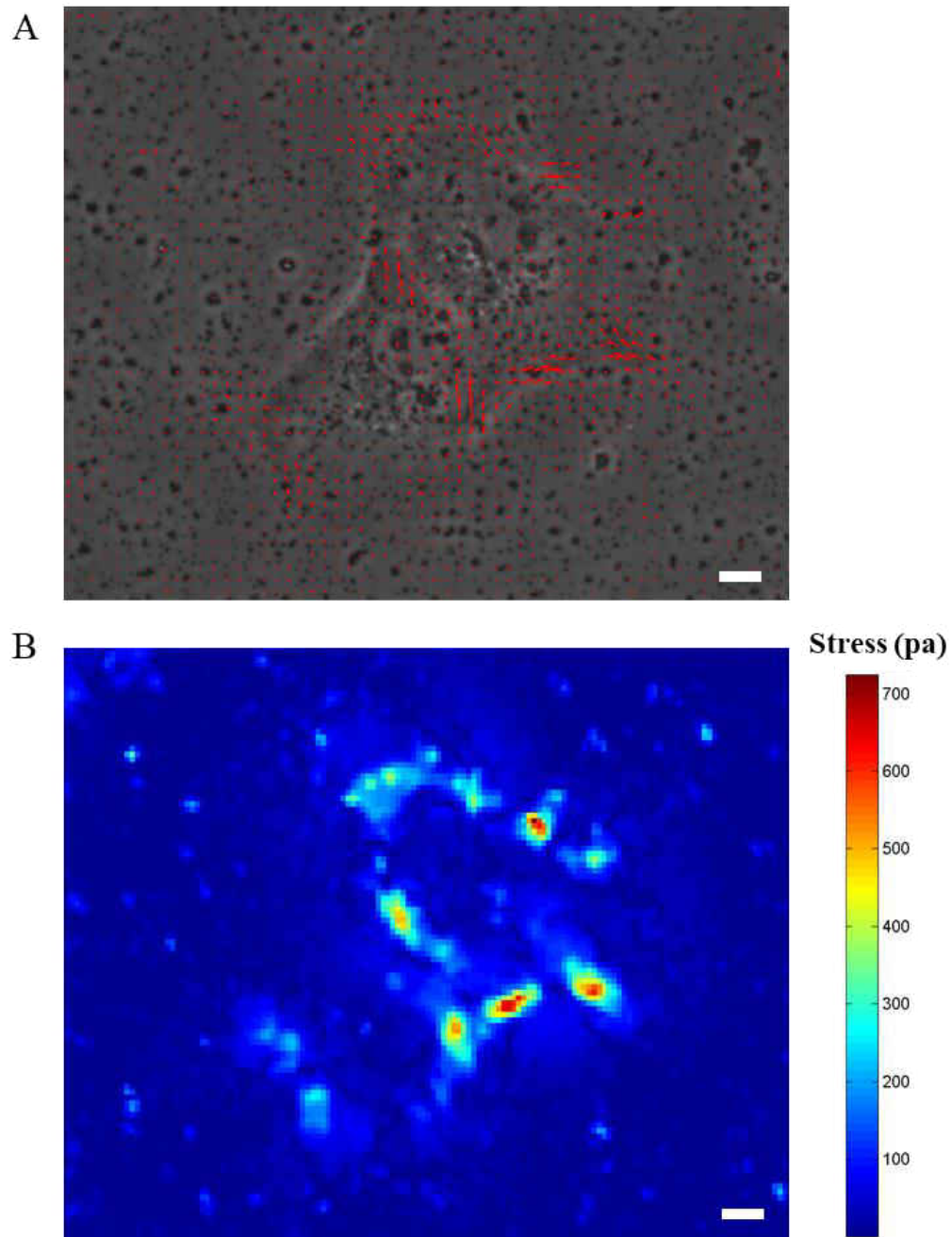
Figure 32: Traction forces within a MDCK α-catenin KO α-catenin-L344P rescue cell pair. (A) Phase image of a cell pair. Red arrows indicate traction stress vectors. (B) Heat map plot indicating the magnitudes of the traction stresses in (A). (Scale: 5 μm)
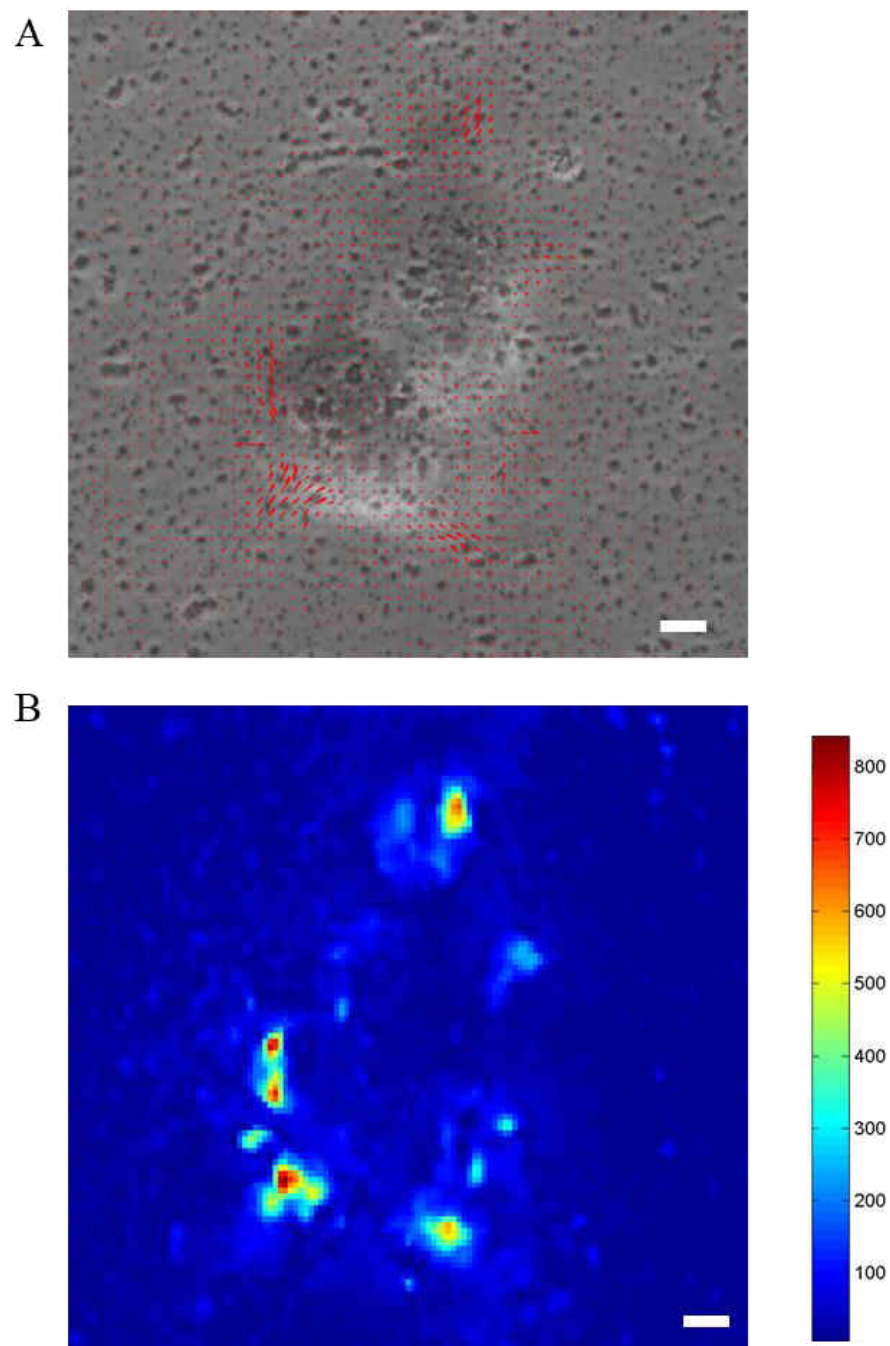
Figure 33: Traction forces within a MDCK α-catenin KO α-catenin-CA Rescue cell pair. (A) Phase image of a cell pair. Red arrows indicate traction stress vectors. (B) Heat map plot indicating the magnitudes of the traction stresses in (A). (Scale: 5 μm)

A

B
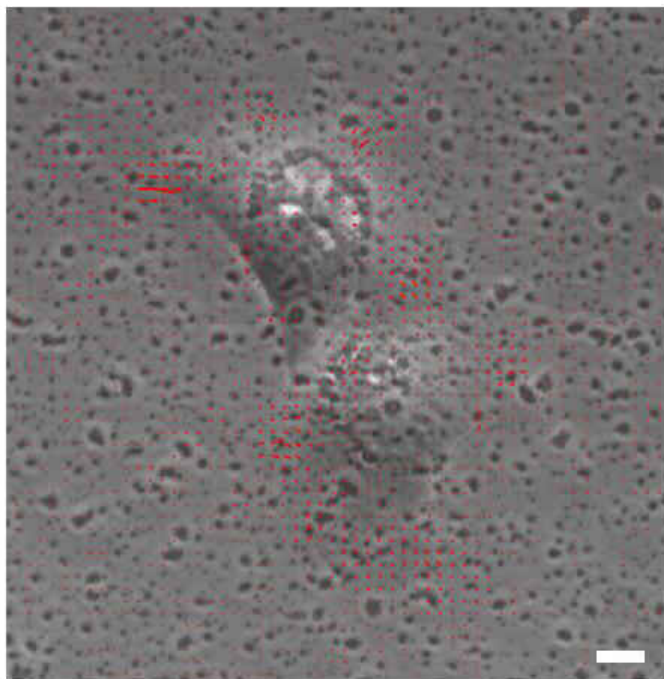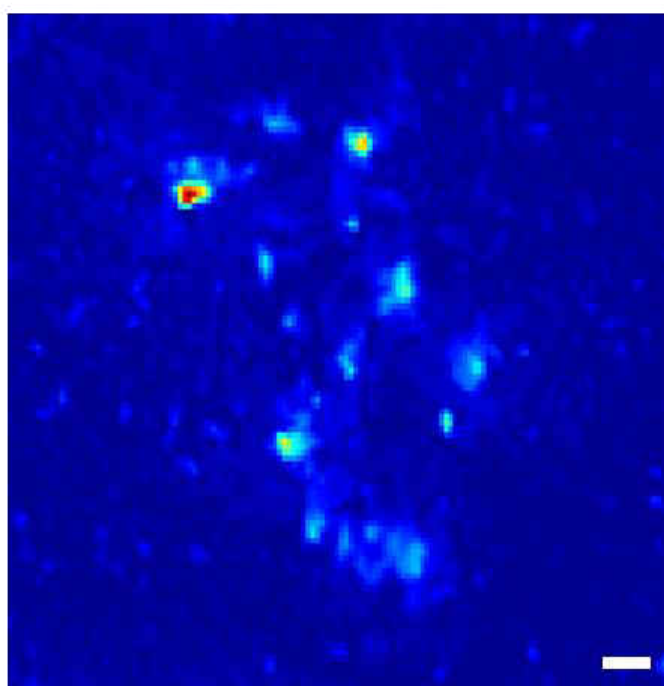
Stress (pa)

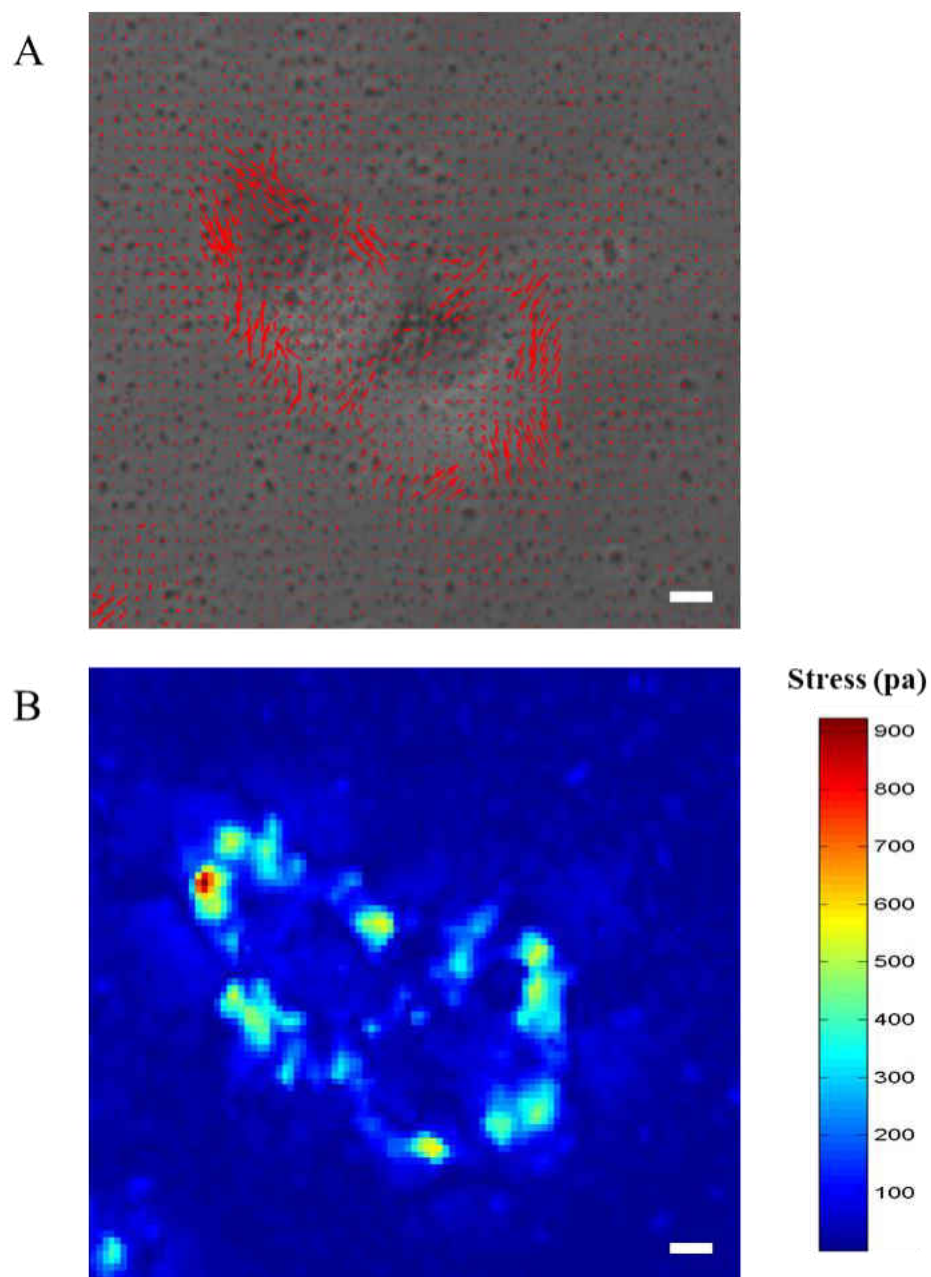Figure 34: Traction forces within a MDCK α-catenin KO α-catenin-WT Rescue cell pair. (A) Phase image of a cell pair. Red arrows indicate traction stress vectors. (B) Heat map plot indicating the magnitudes of the traction stresses in (A). (Scale: 5 μm)
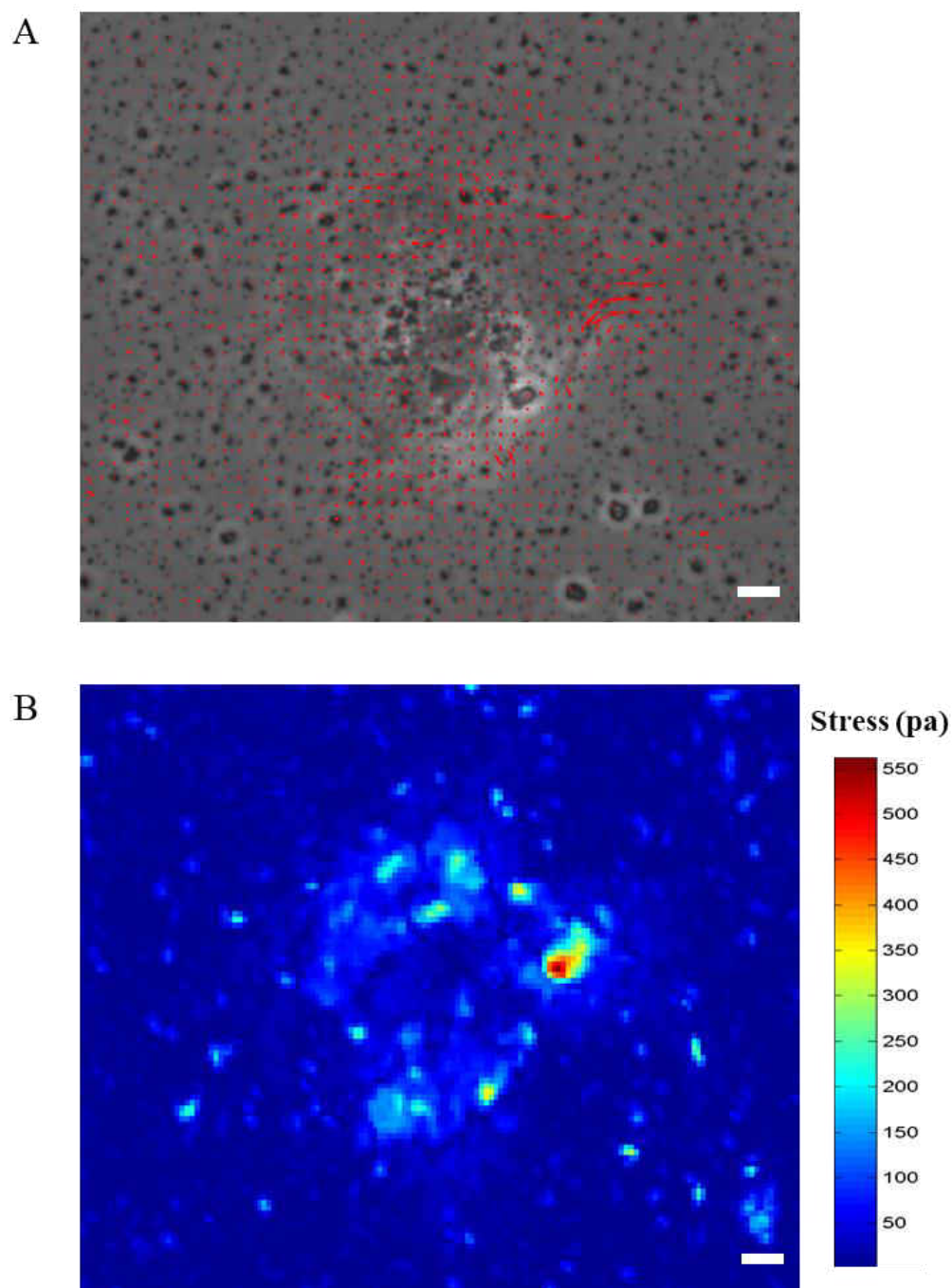
Figure 35: Traction forces within a MDCK α-catenin KO α-catenin-L344P rescue single cell. (A) Phase image of a single cell. Red arrows indicate traction stress vectors. (B) Heat map plot indicating the magnitudes of the traction stresses in (A). (Scale: 5 μm)
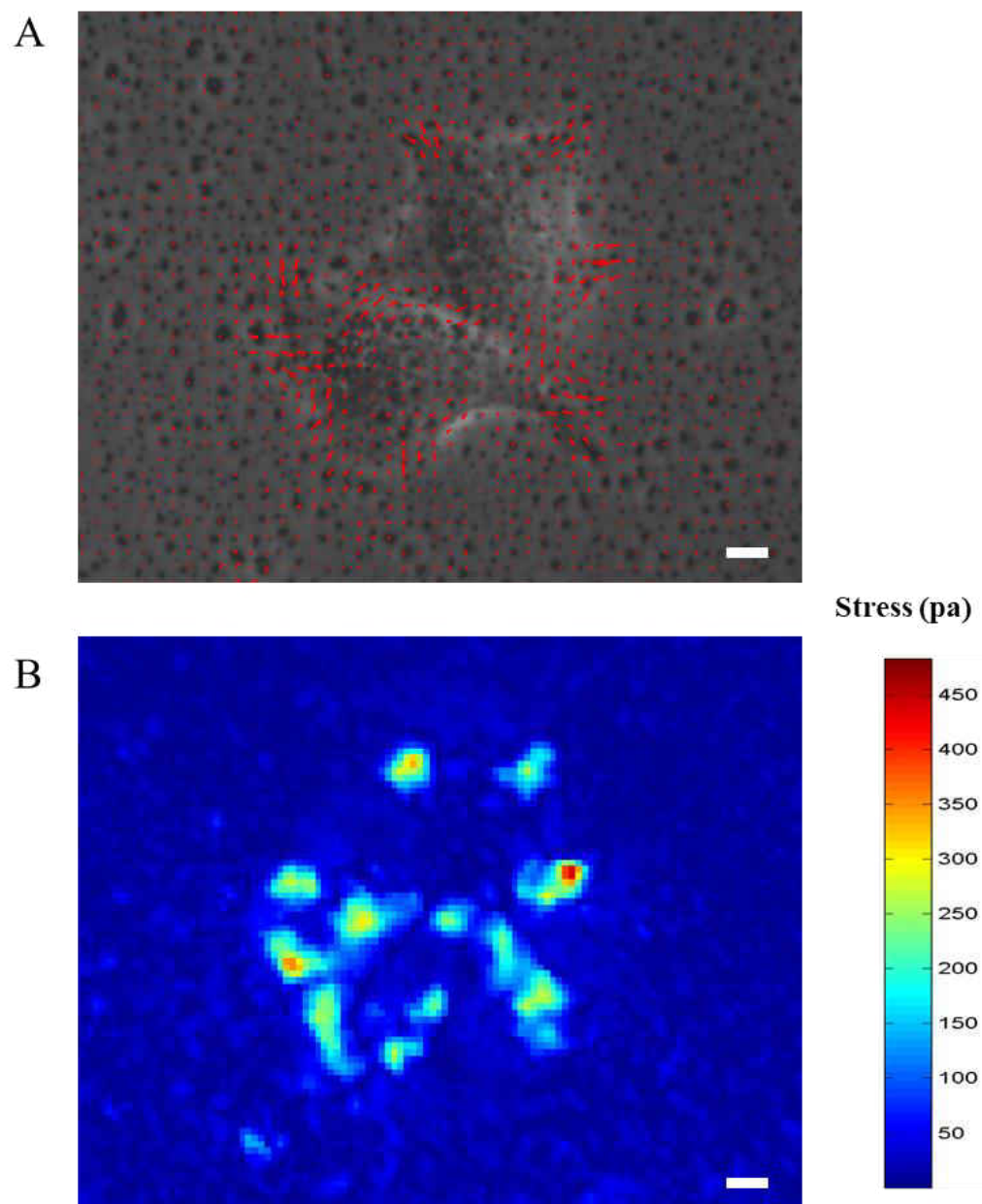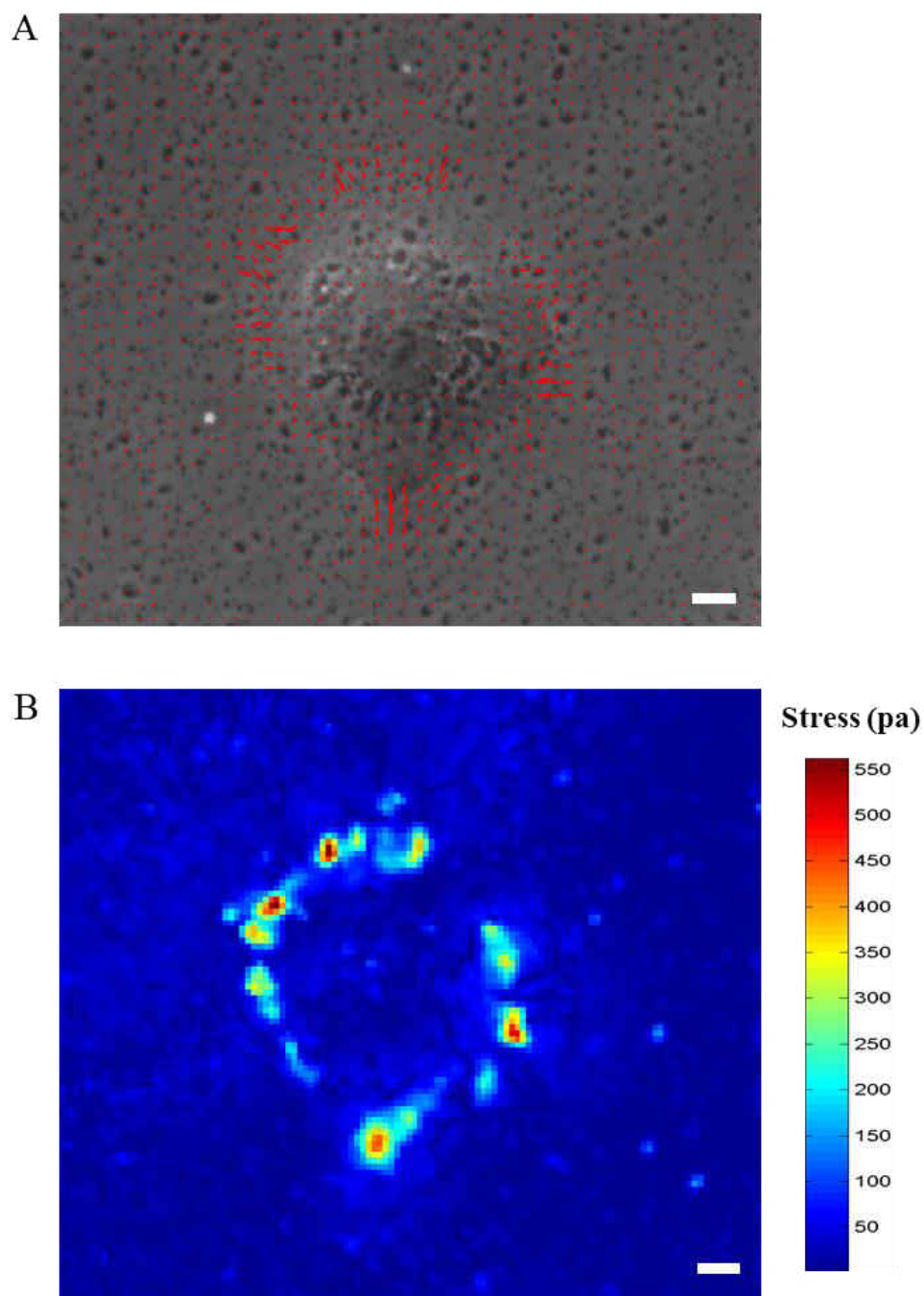
Figure 36: Traction forces within a MDCK α-catenin KO α-catenin-CA rescue single cell. (A) Phase image of a single cell. Red arrows indicate traction stress vectors. (B) Heat map plot indicating the magnitudes of the traction stresses in (A). (Scale: 5 µm)
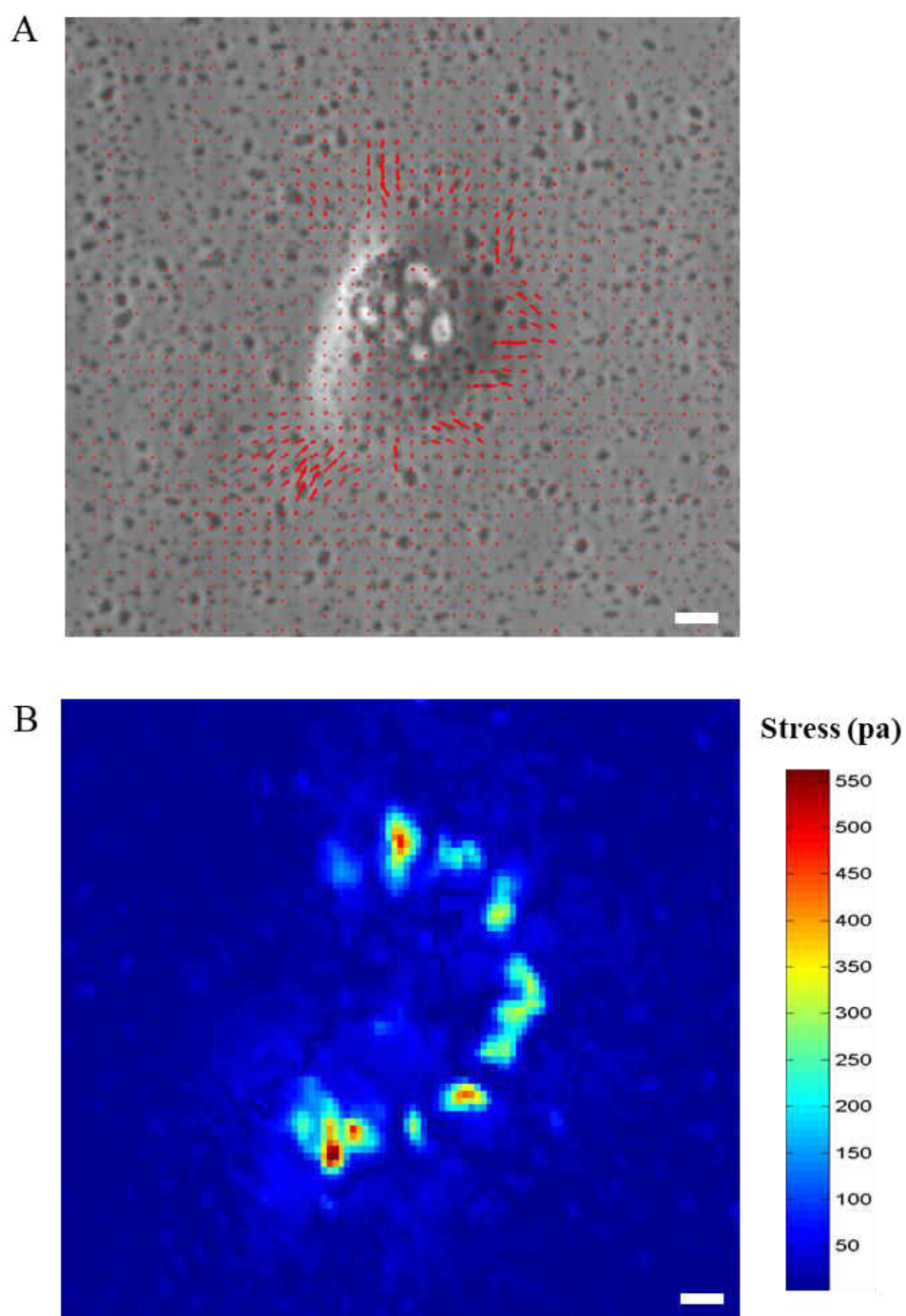
Figure 37: Traction forces within a MDCK α-catenin KO α-catenin-WT rescue single cell. (A) Phase image of a single cell. Red arrows indicate traction stress vectors. (B) Heat map plot indicating the magnitudes of the traction stresses in (A). (Scale: 5 μm)

In order to assess the localization of α-catenin and vinculin at cell-cell contacts, we performed immunofluorescence with cell pairs of rescue cells. Figures 38 and 39 present immunofluorescence images of the cell lines stained for α-catenin and vinculin (discussed further below). Intercellular forces were computed from traction maps for cell pairs for all rescue cell lines. The results (Figure 40) showed that the inter-cellular force was not significantly different for either the L344P α-catenin rescue or the CA α-catenin rescue cell pairs. Surprisingly, there was a statistically significant difference between MDCK and the WT α-catenin rescue, which could be possibly due to species-specific differences (the α-catenin rescue constructs were from chicken) or due to the fact that the 'WT rescue' expressing full length α-catenin in addition to the N-terminal region lacking truncated α-catenin.

I also computed the strain energy due to single cell traction forces. As the box plot in Figure 41 shows, all rescue constructs had lower levels of traction force (associated strain energy) than MDCK cells. This may reflect the altered extra-junctional roles of α-catenin, such as its role in inhibiting Arp2/3.

Immunofluorescence images showed that α-catenin was prominently localized in MDCK, L344P rescue cells and CA rescue cells, but was expectedly absent in α-catenin KO cells, as shown in Figure 38. As shown in Figure 39, vinculin was localized at cell-cell contacts levels in cell pairs

in all four cases (MDCK, L344P rescue cells, CA rescue cells and α-catenin KO cells). However, CA rescue cells appear to show slightly more prominent vinculin localization at cell-cell contacts (Figure 39). (We have not quantified the localization levels here, but there was significant heterogeneity for each case when considering several cell pairs.) Taken together with the inter-cellular force measurements, this means that vinculin levels are not particularly indicative of the level of inter-cellular force in cell pairs. It is worth noting that β-catenin can also recruit vinculin, independently of α-catenin. Thus, α-catenin-vinculin binding may not be the main determinant of endogenous force levels.
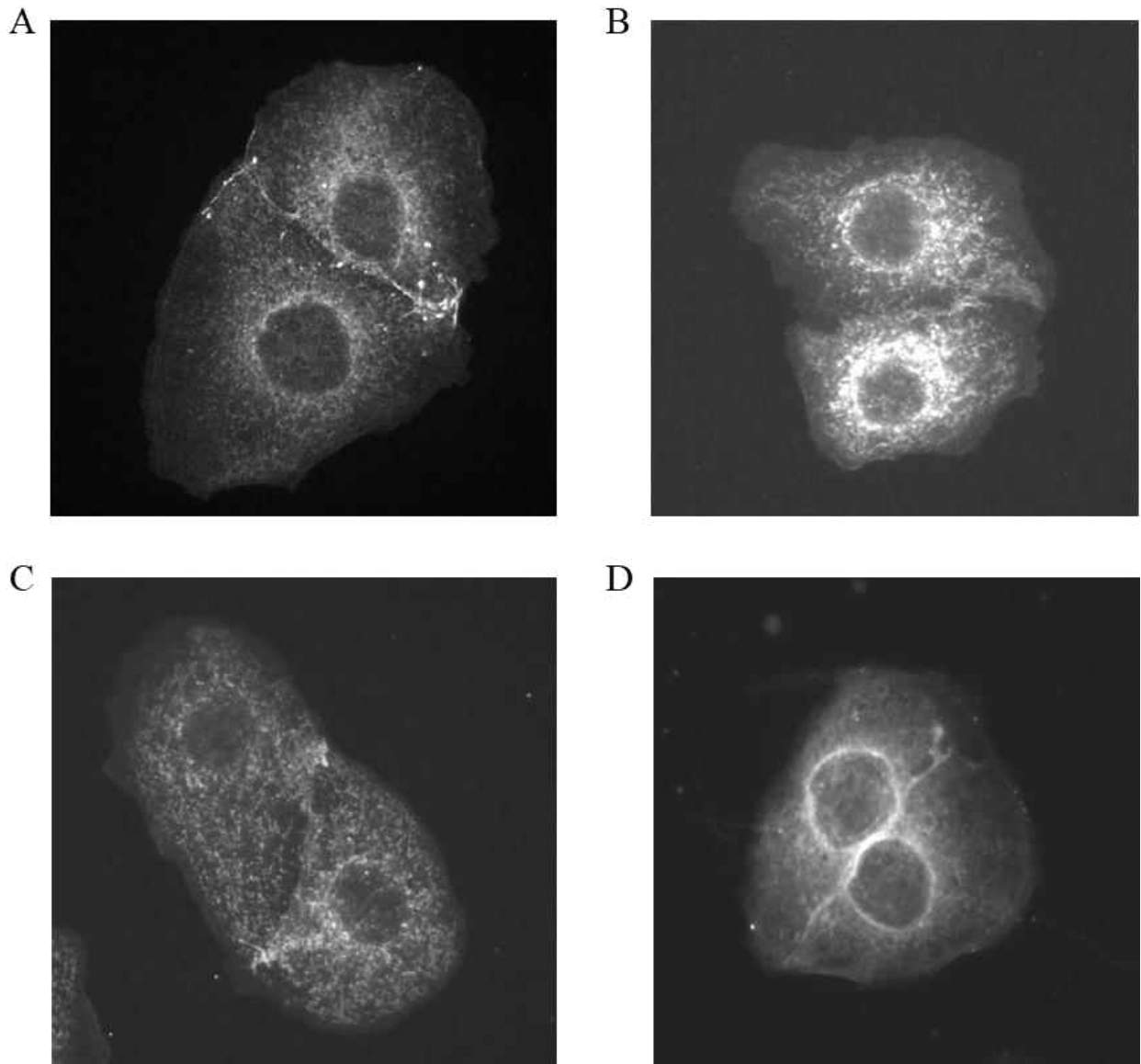
Figure 38: Immunofluorescence images of α-catenin expression levels within cell pairs of (A) MDCK, (B) MDCK α-catenin KO, (C) MDCK α-catenin KO α-catenin-L344P Rescue, (D) MDCK α-catenin KO α-catenin-CA Rescue.
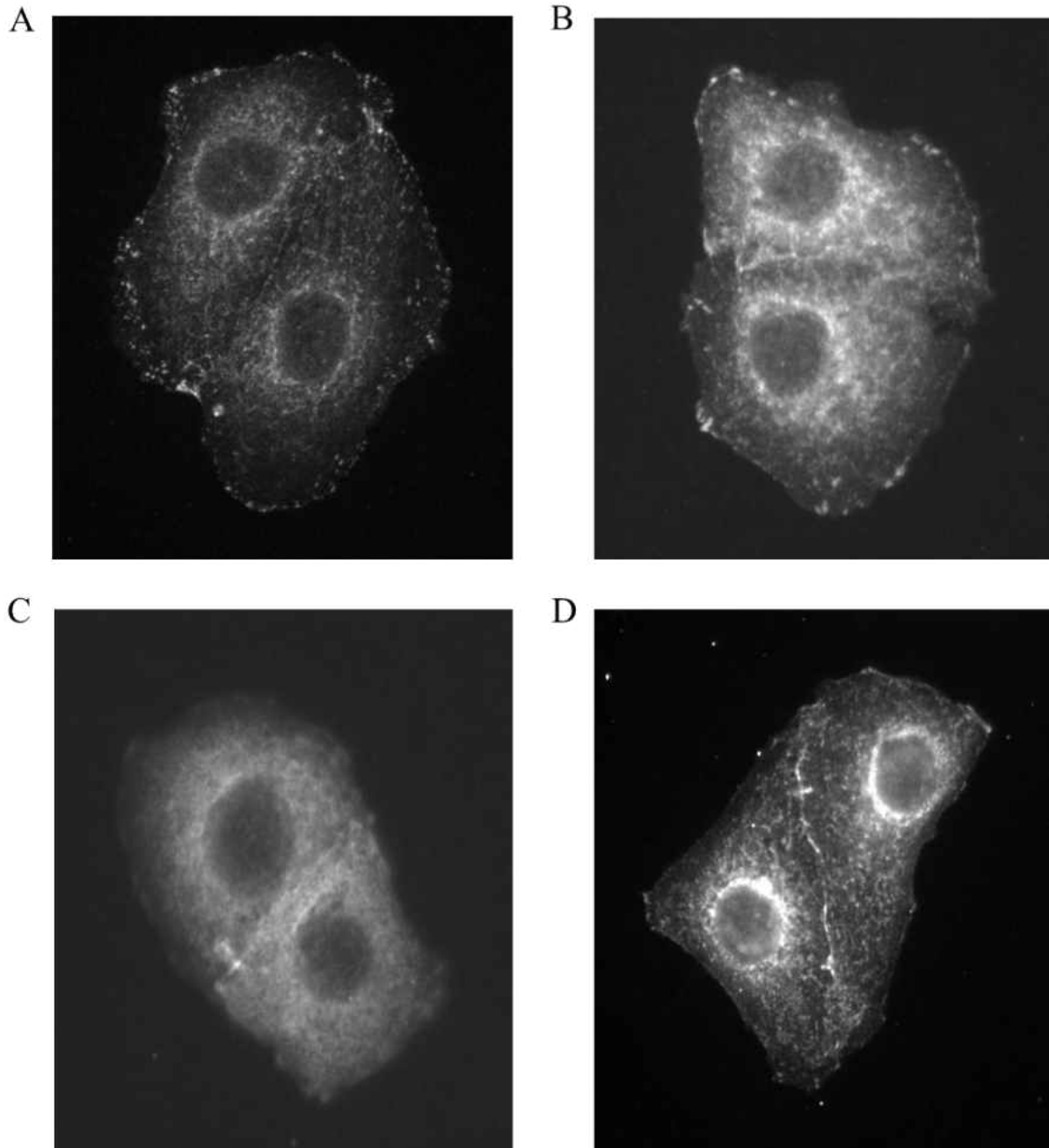
Figure 39: Immunofluorescence images of vinculin expression levels within cell pairs of (A) MDCK, (B) MDCK α-catenin KO, (C) MDCK α-catenin KO α-catenin-L344P Rescue, (D) MDCK α-catenin KO α-catenin-CA Rescue.

Statistical analysis using ANOVA and multiple-comparison of intercellular forces is shown in Table 1 and statistical analysis using ANOVA and multiple-comparison of single cell strain energies (associated with traction forces) is shown in Table 2.
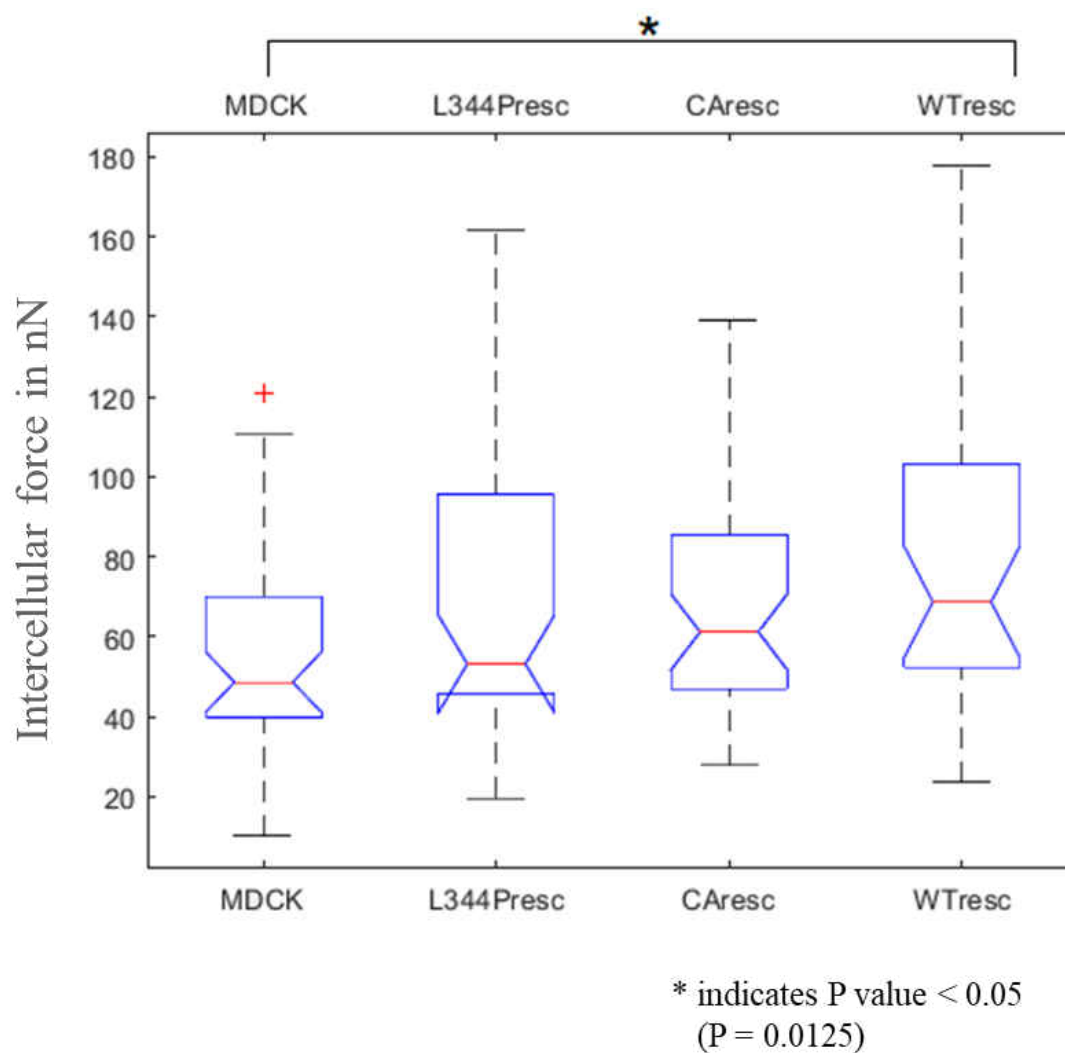
Figure 40: Box plot showing median intercellular force comparison between MDCK and MDCK α-catenin rescue mutant cell pairs. The boxes' notches of MDCK (control) and MDCK α-catenin

KO α-catenin-WT Rescue (control) showing no overlap which indicates is strong evidence of significant difference.

Cell Line Type	Cell Line Type	Lower Limit	Mean Difference	Upper Limit	P-value
1	2	-29.1309	-10.5171	8.0967	0.4671
1	3	-31.6444	-12.9176	5.8093	0.2868
1	4	-43.3714	-23.5225	-3.6736	0.0125
2	3	-20.8947	-2.4005	16.0937	0.9872
2	4	-32.6349	-13.0055	6.624	0.3225
3	4	-30.3417	-10.605	9.1318	0.5117

Table 1: ANOVA output for multiple comparison of intercellular forces. Cell types: (1) MDCK (2) MDCK α-catenin KO α-catenin-L344P Rescue (3) MDCK α-catenin KO α-catenin-CA Rescue (4) MDCK α-catenin KO α-catenin-WT Rescue.
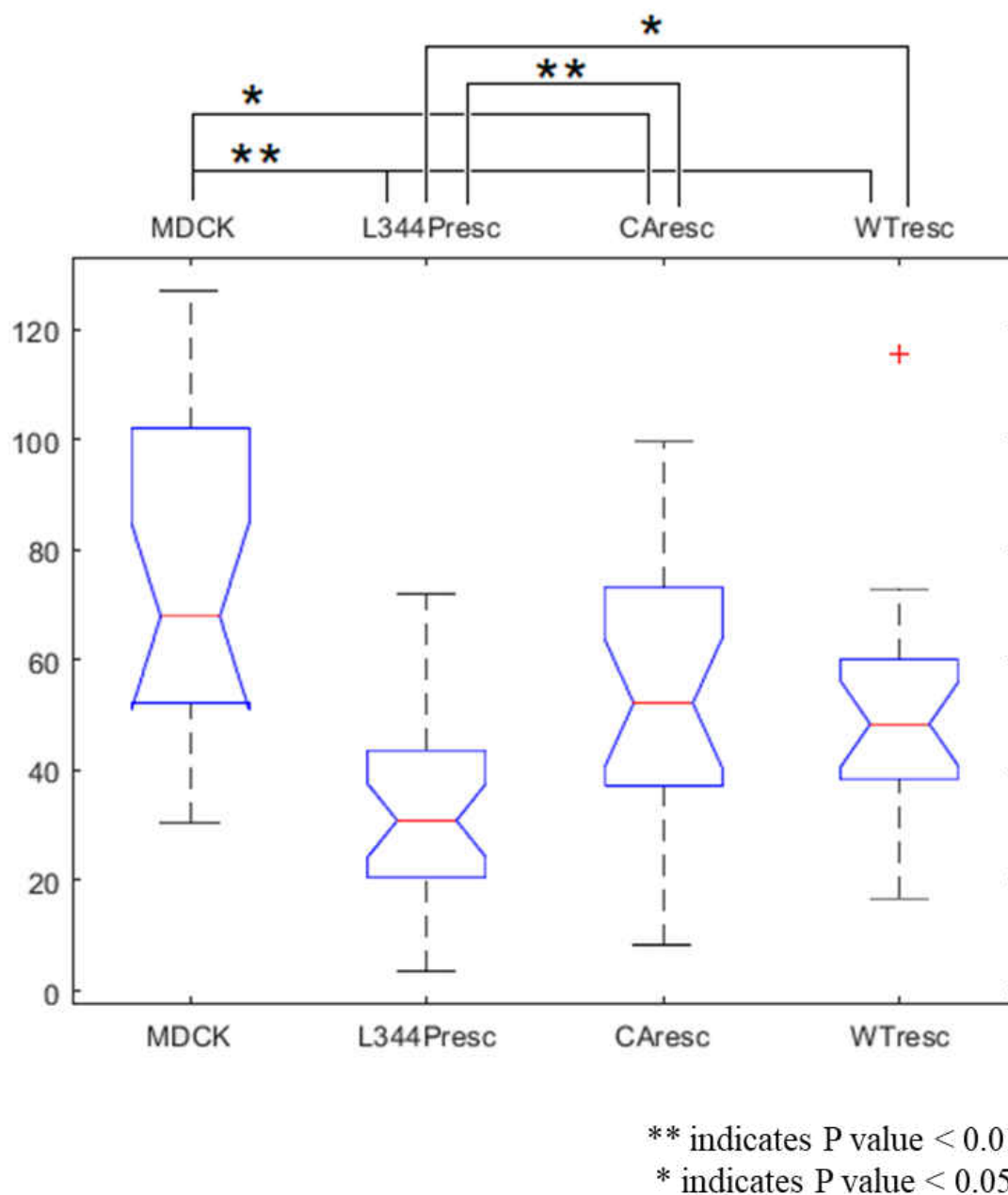
Figure 41 : Box plot showing median strain energy comparison between MDCK and MDCK α-catenin rescue mutant cell pairs. The boxes' notches for the cases MDCK (control) and MDCK α-catenin KO α-catenin-WT Rescue (control), and MDCK α-catenin KO α-catenin-L344P Rescue

(negative control) and MDCK α-catenin KO α-catenin-CA Rescue (negative control) showing no

overlap which indicates is strong evidence of significant difference, respectively.

	Cell Line Type	Cell Line Type	Lower Limit	Mean Difference	Upper Limit	P-value
	1	2	25.5461	42.6133	59.6806	0
	1	3	2.3775	20.4826	38.5877	0.0201
**	1	4	4.2702	23.2632	42.2561	0.0099
**	2	3	-38.7558	-22.1307	-5.5057	0.0042
	2	4	-36.9379	-19.3502	-1.7625	0.0252
	3	4	-15.816	2.7805	21.3771	0.9795

Table 2: ANOVA output for multiple comparison of strain energies. Cell types: (1) MDCK (2)

MDCK α-catenin KO α-catenin-L344P Rescue (3) MDCK α-catenin KO α-catenin-CA Rescue (4)

MDCK α-catenin KO α-catenin-WT Rescue.

CONCLUSION AND FUTURE SCOPE

Inter-cellular forces influence how cells mechanically communicate with each other. Thus, it is important to: (i) measure inter-cellular forces and (ii) understand what factors influence the level of these forces. In Chapter 3, we showed that the inter-cellular force at a single cell-cell contact in cell pairs is similar for MDCK cells exogenously expressing FRET constructs of full-length E-cadherin as well as E-cadherin mutants. Even though these constructs were recently shown to have different molecular tension levels, we found that the total inter-cellular force was similar. This means that the endogenous E-cadherin was still the important factor that determined inter-cellular force. This implies that, to see the effect of mutant constructs better, one needs to, preferably, deplete the endogenous pool of wildtype protein. This informed our studies in Chapter 5. Both the actin cytoskeleton and adhesion receptor proteins both influence intercellular junctional forces. Factors that affect the levels of cytoskeleton-adhesion linkages are thus important to study. My research thus focused on investigating key players of intercellular junctional proteins such as α-catenin and vinculin. Our results showed that knockout of α-catenin can significantly decrease both intercellular and traction forces. The fact that knockout of α-catenin even affected single cell traction forces suggests that the extra-junctional role of α-catenin is relatively under appreciated. One of the eligible candidates mediating this effect could be actin related protein Arp 2/3, which mediates the nucleation of branched actin filaments. Based on the literature discussed in section 5.2.2, it is evident that α-catenin, when expressed in higher amounts, can inhibit Arp 2/3 from forming branched actin filaments.

To study the effect of vinculin binding to α-catenin at intercellular junctions, I examined MDCK cells expressing α-catenin mutants, which can bind to vinculin to different extents. The inter-

cellular forces for the L344P and CA α-catenin rescue cells did not differ from MDCK, but the WT rescue, surprisingly, had slightly higher intercellular forces. As the α-catenin rescue mutants were constructed from chicken and transfected in dog kidney epithelial cells, there is a possibility of species-specific changes involved. The fact that the 'WT rescue' expressed the truncated and full length α-catenin may also be a possible explanation. In any case, the single cell traction forces for all rescue cells were lower than that for MDCK cells, suggesting that it is important to study and investigate the role of actin nucleators Arp 2/3 and formins, which may be involved in extra-junctional roles of α-catenin. Examining the role of vinculin further can also expand our understanding of intercellular and cell-ECM junctions and the forces that regulate these junctions. While inter-cellular force measurements with cell pairs are a useful system for understanding cell-cell force transmission, the use of larger systems, such as our micropatterned islands in Chapter 4, will enable us to understand force transmission in epithelial tissues better. Use of such large, but well defined, systems can help complement results obtained with approaches such as monolayer stress microscopy, but without the simplifying assumptions employed in the latter. Further improvements in inter-cellular force measurements and better understanding of the molecular factors that affect inter-cellular forces can be expected to advance fields such as developmental biology and tissue engineering.

REFERENCES

1. Bruce Alberts, A.J., Julain Lewis, Martin Raff, Keith Roberts, Peter Walter, *Molecular Biology of The Cell.* 2008.

2. Ananthakrishnan, R. and A. Ehrlicher, *The Forces Behind Cell Movement.* Int J Biol Sci, 2007. **3**(5): p. 303-17.

3. Heisenberg, C.P. and Y. Bellaiche, *Forces in tissue morphogenesis and patterning.* Cell, 2013. **153**(5): p. 948-62.

4. Lecuit, T., P.F. Lenne, and E. Munro, *Force generation, transmission, and integration during cell and tissue morphogenesis.* Annu Rev Cell Dev Biol, 2011. **27**: p. 157-84.

5. Wang, N., J.P. Butler, and D.E. Ingber, *Mechanotransduction across the cell surface and through the cytoskeleton.* Science, 1993. **260**(5111): p. 1124-7.

6. Sheetz, M.P., *Microtubule motor complexes moving membranous organelles.* Cell Struct Funct, 1996. **21**(5): p. 369-73.

7. Sims, J.R., S. Karp, and D.E. Ingber, *Altering the cellular mechanical force balance results in integrated changes in cell, cytoskeletal and nuclear shape.* J Cell Sci, 1992. **103 (Pt 4)**: p. 1215-22.

8. Gumbiner, B.M., *Regulation of cadherin-mediated adhesion in morphogenesis.* Nat Rev Mol Cell Biol, 2005. **6**(8): p. 622-34.

9. Wu, S.K., et al., *Active contractility at E-cadherin junctions and its implications for cell extrusion in cancer.* Cell Cycle, 2015. **14**(3): p. 315-22.

10. Wu, S.K., et al., *Cortical F-actin stabilization generates apical-lateral patterns of junctional contractility that integrate cells into epithelia.* Nat Cell Biol, 2014. **16**(2): p. 167-78.

11.   Mohan, A., et al., *Spatial Proliferation of Epithelial Cells Is Regulated by E-Cadherin Force.* Biophys J, 2018. **115**(5): p. 853-864.

12.   Kan, N.G., et al., *Gene replacement reveals a specific role for E-cadherin in the formation of a functional trophectoderm.* Development, 2007. **134**(1): p. 31-41.

13.   Wu, S.K. and A.S. Yap, *Patterns in Space: Coordinating Adhesion and Actomyosin Contractility at E-cadherin Junctions.* Cell Communication & Adhesion, 2013. **20**(6): p. 201-212.

14.   Rimm, D.L., et al., *Alpha 1(E)-catenin is an actin-binding and -bundling protein mediating the attachment of F-actin to the membrane adhesion complex.* Proc Natl Acad Sci U S A, 1995. **92**(19): p. 8813-7.

15.   Torres, M., et al., *An alpha-E-catenin gene trap mutation defines its function in preimplantation development.* Proc Natl Acad Sci U S A, 1997. **94**(3): p. 901-6.

16.   Kofron, M., et al., *The roles of maternal alpha-catenin and plakoglobin in the early Xenopus embryo.* Development, 1997. **124**(8): p. 1553-60.

17.   Hinck, L., et al., *Dynamics of cadherin/catenin complex formation: novel protein interactions and pathways of complex assembly.* J Cell Biol, 1994. **125**(6): p. 1327-40.

18.   Ozawa, M. and R. Kemler, *Molecular organization of the uvomorulin-catenin complex.* J Cell Biol, 1992. **116**(4): p. 989-96.

19.   Drees, F., et al., *Alpha-catenin is a molecular switch that binds E-cadherin-beta-catenin and regulates actin-filament assembly.* Cell, 2005. **123**(5): p. 903-15.

20.   Pokutta, S. and W.I. Weis, *Structure of the dimerization and beta-catenin-binding region of alpha-catenin.* Mol Cell, 2000. **5**(3): p. 533-43.

21.   Koslov, E.R., et al., *Alpha-catenin can form asymmetric homodimeric complexes and/or heterodimeric complexes with beta-catenin.* J Biol Chem, 1997. **272**(43): p. 27301-6.

22.   Yamada, S., et al., *Deconstructing the cadherin-catenin-actin complex.* Cell, 2005. **123**(5): p. 889-901.

23.   Cavey, M., et al., *A two-tiered mechanism for stabilization and immobilization of E-cadherin.* Nature, 2008. **453**(7196): p. 751-6.

24.   Buckley, C.D., et al., *Cell adhesion. The minimal cadherin-catenin complex binds to actin filaments under force.* Science, 2014. **346**(6209): p. 1254211.

25.   Schlegelmilch, K., et al., *Yap1 acts downstream of alpha-catenin to control epidermal proliferation.* Cell, 2011. **144**(5): p. 782-95.

26.   Benjamin, J.M., et al., *AlphaE-catenin regulates actin dynamics independently of cadherin-mediated cell-cell adhesion.* J Cell Biol, 2010. **189**(2): p. 339-52.

27.   Eyckmans, J., et al., *A hitchhiker's guide to mechanobiology.* Dev Cell, 2011. **21**(1): p. 35-47.

28.   Y., W., *Das Gesetz der Transformation der Knochen Verlag von August Hirschwald.* 1892.

29.   W., R., *Gesammelte Abhandlungen über Entwicklungsmechanik.* 1895.

30.   DW., T., *On Growth and Form.* 1917.

31.   Raab-Cullen, D.M., et al., *Mechanical loading stimulates rapid changes in periosteal gene expression.* Calcif Tissue Int, 1994. **55**(6): p. 473-8.

32.   el Haj, A.J., et al., *Cellular responses to mechanical loading in vitro.* J Bone Miner Res, 1990. **5**(9): p. 923-32.

33. David, V., et al., *Mechanical loading down-regulates peroxisome proliferator-activated receptor gamma in bone marrow stromal cells and favors osteoblastogenesis at the expense of adipogenesis.* Endocrinology, 2007. **148**(5): p. 2553-62.

34. Bancroft, G.N., et al., *Fluid flow increases mineralized matrix deposition in 3D perfusion culture of marrow stromal osteoblasts in a dose-dependent manner.* Proc Natl Acad Sci U S A, 2002. **99**(20): p. 12600-5.

35. Harris, A.K., P. Wild, and D. Stopak, *Silicone rubber substrata: a new wrinkle in the study of cell locomotion.* Science, 1980. **208**(4440): p. 177-9.

36. Harris, A.K., D. Stopak, and P. Wild, *Fibroblast traction as a mechanism for collagen morphogenesis.* Nature, 1981. **290**(5803): p. 249-51.

37. Civelekoglu-Scholey, G. and J.M. Scholey, *Mitotic force generators and chromosome segregation.* Cell Mol Life Sci, 2010. **67**(13): p. 2231-50.

38. Renkawitz, J. and M. Sixt, *Mechanisms of force generation and force transmission during interstitial leukocyte migration.* EMBO Rep, 2010. **11**(10): p. 744-50.

39. DeMali, K.A., X. Sun, and G.A. Bui, *Force Transmission at Cell–Cell and Cell–Matrix Adhesions.* Biochemistry, 2014. **53**(49): p. 7706-7717.

40. Barry, A.K., et al., *alpha-catenin cytomechanics--role in cadherin-dependent adhesion and mechanotransduction.* J Cell Sci, 2014. **127**(Pt 8): p. 1779-91.

41. Bazellières, E., et al., *Control of cell–cell forces and collective cell dynamics by the intercellular adhesome.* Nature Cell Biology, 2015. **17**: p. 409.

42. Valbuena, A., et al., *Mechanical properties of beta-catenin revealed by single-molecule experiments.* Biophys J, 2012. **103**(8): p. 1744-52.

43.   Avvisato, C.L., et al., *Mechanical force modulates global gene expression and beta-catenin signaling in colon cancer cells.* J Cell Sci, 2007. **120**(Pt 15): p. 2672-82.

44.   Lampugnani, M.G., et al., *VE-cadherin regulates endothelial actin activating Rac and increasing membrane association of Tiam.* Mol Biol Cell, 2002. **13**(4): p. 1175-89.

45.   Noren, N.K., et al., *Cadherin engagement regulates Rho family GTPases.* J Biol Chem, 2001. **276**(36): p. 33305-8.

46.   Nelson, C.M., et al., *Vascular endothelial-cadherin regulates cytoskeletal tension, cell spreading, and focal adhesions by stimulating RhoA.* Mol Biol Cell, 2004. **15**(6): p. 2943-53.

47.   Ratheesh, A., et al., *Centralspindlin and alpha-catenin regulate Rho signalling at the epithelial zonula adherens.* Nat Cell Biol, 2012. **14**(8): p. 818-828.

48.   Dumbali, S.P., et al., *Endogenous Sheet-Averaged Tension Within a Large Epithelial Cell Colony.* Journal of Biomechanical Engineering, 2017. **139**(10): p. 101008-101008-5.

49.   Fernandez-Gonzalez, R., et al., *Myosin II dynamics are regulated by tension in intercalating cells.* Dev Cell, 2009. **17**(5): p. 736-43.

50.   AF, B., *Applied Mechanics of Solids.* 2009.

51.   Maruthamuthu, V., et al., *Cell-ECM traction force modulates endogenous tension at cell–cell contacts.* Proceedings of the National Academy of Sciences, 2011. **108**(12): p. 4708.

52.   Polacheck, W.J. and C.S. Chen, *Measuring cell-generated forces: a guide to the available tools.* Nature methods, 2016. **13**(5): p. 415-423.

53.   Bell, E., B. Ivarsson, and C. Merrill, *Production of a tissue-like structure by contraction of collagen lattices by human fibroblasts of different proliferative potential in vitro.* Proc Natl Acad Sci U S A, 1979. **76**(3): p. 1274-8.

54.   Ehrlich, H.P. and J.B. Rajaratnam, *Cell locomotion forces versus cell contraction forces for collagen lattice contraction: an in vitro model of wound contraction.* Tissue Cell, 1990. **22**(4): p. 407-17.

55.   Dallon, J.C. and H.P. Ehrlich, *A review of fibroblast-populated collagen lattices.* Wound Repair Regen, 2008. **16**(4): p. 472-9.

56.   Stopak, D. and A.K. Harris, *Connective tissue morphogenesis by fibroblast traction. I. Tissue culture observations.* Dev Biol, 1982. **90**(2): p. 383-98.

57.   Ngo, P., et al., *Collagen gel contraction assay.* Methods Mol Biol, 2006. **341**: p. 103-9.

58.   Smith, K.D., A. Wells, and D.A. Lauffenburger, *Multiple signaling pathways mediate compaction of collagen matrices by EGF-stimulated fibroblasts.* Exp Cell Res, 2006. **312**(11): p. 1970-82.

59.   Fernandez-Gonzalez, R. and J.A. Zallen, *Wounded cells drive rapid epidermal repair in the early Drosophila embryo.* Mol Biol Cell, 2013. **24**(20): p. 3227-37.

60.   Farhadifar, R., et al., *The influence of cell mechanics, cell-cell interactions, and proliferation on epithelial packing.* Curr Biol, 2007. **17**(24): p. 2095-104.

61.   Vandenburgh, H., et al., *Automated drug screening with contractile muscle tissue engineered from dystrophic myoblasts.* Faseb j, 2009. **23**(10): p. 3325-34.

62.   Legant, W.R., et al., *Microfabricated tissue gauges to measure and manipulate forces from 3D microtissues.* Proc Natl Acad Sci U S A, 2009. **106**(25): p. 10097-102.

63.   Serrao, G.W., et al., *Myocyte-depleted engineered cardiac tissues support therapeutic potential of mesenchymal stem cells.* Tissue Eng Part A, 2012. **18**(13-14): p. 1322-33.

64.   Boudou, T., et al., *A microfabricated platform to measure and manipulate the mechanics of engineered cardiac microtissues.* Tissue Eng Part A, 2012. **18**(9-10): p. 910-9.

65. Sakar, M.S., et al., *Formation and optogenetic control of engineered 3D skeletal muscle bioactuators.* Lab Chip, 2012. **12**(23): p. 4976-85.

66. Puech, P.H., et al., *Measuring cell adhesion forces of primary gastrulating cells from zebrafish using atomic force microscopy.* J Cell Sci, 2005. **118**(Pt 18): p. 4199-206.

67. Krieg, M., et al., *Tensile forces govern germ-layer organization in zebrafish.* Nat Cell Biol, 2008. **10**(4): p. 429-36.

68. Maitre, J.L. and C.P. Heisenberg, *The role of adhesion energy in controlling cell-cell contacts.* Curr Opin Cell Biol, 2011. **23**(5): p. 508-14.

69. Stabley, D.R., et al., *Visualizing mechanical tension across membrane receptors with a fluorescent sensor.* Nat Methods, 2011. **9**(1): p. 64-7.

70. Campàs, O., et al., *Quantifying cell-generated mechanical forces within living embryonic tissues.* Nature methods, 2014. **11**(2): p. 183-189.

71. Baker, B.M. and C.S. Chen, *Deconstructing the third dimension: how 3D culture microenvironments alter cellular cues.* J Cell Sci, 2012. **125**(Pt 13): p. 3015-24.

72. Dai, J. and M.P. Sheetz, *Mechanical properties of neuronal growth cone membranes studied by tether formation with laser optical tweezers.* Biophysical journal, 1995. **68**(3): p. 988-996.

73. Kuo, S.C., D.A. Hammer, and D.A. Lauffenburger, *Simulation of detachment of specifically bound particles from surfaces by shear flow.* Biophysical journal, 1997. **73**(1): p. 517-531.

74. Thie, M., et al., *Cell adhesion to the apical pole of epithelium: a function of cell polarity.* Eur J Cell Biol, 1995. **66**(2): p. 180-91.

75. John, N.J., M. Linke, and H.W. Denker, *Quantitation of human choriocarcinoma spheroid attachment to uterine epithelial cell monolayers.* In Vitro Cell Dev Biol Anim, 1993. **29**(6): p. 461-8.

76. Alon, R., D.A. Hammer, and T.A. Springer, *Lifetime of the P-selectin-carbohydrate bond and its response to tensile force in hydrodynamic flow.* Nature, 1995. **374**(6522): p. 539-42.

77. Zahalak, G.I., W.B. McConnaughey, and E.L. Elson, *Determination of cellular mechanical properties by cell poking, with an application to leukocytes.* J Biomech Eng, 1990. **112**(3): p. 283-94.

78. Evans, E., et al., *Picoforce Method to Probe Submicroscopic Actions in Biomembrane Adhesion.* 1994. p. 125-139.

79. Benoit, M. and H.E. Gaub, *Measuring cell adhesion forces with the atomic force microscope at the molecular level.* Cells Tissues Organs, 2002. **172**(3): p. 174-89.

80. Gaub, H.E., J.M. Fernandez, *The molecular elasticity of individual proteins studied by AFM-related techniques.* AvH-Magazin, 1998. **71**: p. 11-18.

81. Clausen-Schaumann, H., et al., *Force spectroscopy with single bio-molecules.* Curr Opin Chem Biol, 2000. **4**(5): p. 524-30.

82. Huebsch, N.D. and D.J. Mooney, *Fluorescent resonance energy transfer: A tool for probing molecular cell-biomaterial interactions in three dimensions.* Biomaterials, 2007. **28**(15): p. 2424-2437.

83. Borghi, N., et al., *E-cadherin is under constitutive actomyosin-generated tension that is increased at cell-cell contacts upon externally applied stretch.* Proc Natl Acad Sci U S A, 2012. **109**(31): p. 12568-73.

84.   Kashef, J. and C.M. Franz, *Quantitative methods for analyzing cell-cell adhesion in development.* Dev Biol, 2015. **401**(1): p. 165-74.

85.   Grashoff, C., et al., *Measuring mechanical tension across vinculin reveals regulation of focal adhesion dynamics.* Nature, 2010. **466**: p. 263.

86.   Damsky, C.H. and Z. Werb, *Signal transduction by integrin receptors for extracellular matrix: cooperative processing of extracellular information.* Curr Opin Cell Biol, 1992. **4**(5): p. 772-81.

87.   DuBois, D.G.M.a.R.N., *Prostaglandins in Cancer Cell Adhesion, Migration, and Invasion.* International Journal of Cell Biology, 2012. **2012**.

88.   Evans, M.J., et al., *Postnatal development of the lamina reticularis in primate airways.* Anat Rec (Hoboken), 2010. **293**(6): p. 947-54.

89.   Melcher, A.H. and J. Chan, *Continuity of electron histochemically demonstrable substances in the basal lamina, the ground substance of the connective tissue and the intercellular spaces of eptihelial cells of rat gingiva.* J Anat, 1978. **127**(Pt 2): p. 261-71.

90.   Snodgrass, M.J., *Ultrastructural distinction between reticular and collagenous fibers with an ammoniacal silver stain.* Anat Rec, 1977. **187**(2): p. 191-205.

91.   Handorf, A.M., et al., *Tissue stiffness dictates development, homeostasis, and disease progression.* Organogenesis, 2015. **11**(1): p. 1-15.

92.   Burridge, K. and M. Chrzanowska-Wodnicka, *Focal adhesions, contractility, and signaling.* Annu Rev Cell Dev Biol, 1996. **12**: p. 463-518.

93.   Mege, R.M., J. Gavard, and M. Lambert, *Regulation of cell-cell junctions by the cytoskeleton.* Curr Opin Cell Biol, 2006. **18**(5): p. 541-8.

94.   Levental, I., P.C. Georges, and P.A. Janmey, *Soft biological materials and their impact on cell function.* Soft Matter, 2007. **3**(3): p. 299-306.

95.   Yeung, T., et al., *Effects of substrate stiffness on cell morphology, cytoskeletal structure, and adhesion.* Cell Motil Cytoskeleton, 2005. **60**(1): p. 24-34.

96.   Watt, F.M. and W.T. Huck, *Role of the extracellular matrix in regulating stem cell fate.* Nat Rev Mol Cell Biol, 2013. **14**(8): p. 467-73.

97.   Zustiak, S., R. Nossal, and D.L. Sackett, *Multiwell stiffness assay for the study of cell responsiveness to cytotoxic drugs.* Biotechnol Bioeng, 2014. **111**(2): p. 396-403.

98.   Mih, J.D., et al., *A multiwell platform for studying stiffness-dependent cell biology.* PLoS One, 2011. **6**(5): p. e19929.

99.   Herrick, W.G., et al., *PEG-phosphorylcholine hydrogels as tunable and versatile platforms for mechanobiology.* Biomacromolecules, 2013. **14**(7): p. 2294-304.

100.   Feng, J., et al., *Substrate stiffness influences the outcome of antitumor drug screening in vitro.* Clin Hemorheol Microcirc, 2013. **55**(1): p. 121-31.

101.   Bashirzadeh, Y., et al., *Stiffness Measurement of Soft Silicone Substrates for Mechanobiology Studies Using a Widefield Fluorescence Microscope.* JoVE, 2018(137): p. e57797.

102.   Pelham, R.J., Jr. and Y. Wang, *Cell locomotion and focal adhesions are regulated by substrate flexibility.* Proc Natl Acad Sci U S A, 1997. **94**(25): p. 13661-5.

103.   Young, D.A., et al., *Stimulation of adipogenesis of adult adipose-derived stem cells using substrates that mimic the stiffness of adipose tissue.* Biomaterials, 2013. **34**(34): p. 8581-8.

104. Oyen, M.L., *Mechanical characterisation of hydrogel materials.* International Materials Reviews, 2014. **59**(1): p. 44-59.

105. Tse, J.R. and A.J. Engler, *Preparation of Hydrogel Substrates with Tunable Mechanical Properties.* 2010. **47**(1): p. 10.16.1-10.16.16.

106. Johnson, A.W. and B. Harley, *Mechanobiology of cell-cell and cell-matrix interactions.* 2011: Springer Science & Business Media.

107. Janmey, P.A., J.P. Winer, and J.W. Weisel, *Fibrin gels and their clinical and bioengineering applications.* J R Soc Interface, 2009. **6**(30): p. 1-10.

108. Storm, C., et al., *Nonlinear elasticity in biological gels.* Nature, 2005. **435**(7039): p. 191-4.

109. Anseth, K.S., C.N. Bowman, and L. Brannon-Peppas, *Mechanical properties of hydrogels and their experimental determination.* Biomaterials, 1996. **17**(17): p. 1647-57.

110. Denisin, A.K. and B.L. Pruitt, *Tuning the Range of Polyacrylamide Gel Stiffness for Mechanobiology Applications.* ACS Applied Materials & Interfaces, 2016. **8**(34): p. 21893-21902.

111. Jacot, J.G., A.D. McCulloch, and J.H. Omens, *Substrate stiffness affects the functional maturation of neonatal rat ventricular myocytes.* Biophys J, 2008. **95**(7): p. 3479-87.

112. Engler, A.J., et al., *Matrix elasticity directs stem cell lineage specification.* Cell, 2006. **126**(4): p. 677-89.

113. Kandow, C.E., et al., *Polyacrylamide hydrogels for cell mechanics: steps toward optimization and alternative uses.* Methods Cell Biol, 2007. **83**: p. 29-46.

114. Kraning-Rush, C.M., et al., *Quantifying traction stresses in adherent cells.* Methods Cell Biol, 2012. **110**: p. 139-78.

115. Eftekharjoo, M., et al., *Fibrillar force generation by fibroblasts depends on formin.* Biochemical and Biophysical Research Communications, 2019. **510**(1): p. 72-77.

116. Bashirzadeh, Y., et al., *Mechanical response of an epithelial island subject to uniaxial stretch on a hybrid silicone substrate.* Cell Mol Bioeng, 2019. **12**(1): p. 33-40.

117. Frey, M.T., et al., *Microscopic methods for measuring the elasticity of gel substrates for cell culture: microspheres, microindenters, and atomic force microscopy.* Methods Cell Biol, 2007. **83**: p. 47-65.

118. Lee, D., et al., *Three-Dimensional Confocal Microscopy Indentation Method for Hydrogel Elasticity Measurement.* Langmuir, 2015. **31**(35): p. 9684-9693.

119. Dimitriadis, E.K., et al., *Determination of elastic moduli of thin layers of soft material using the atomic force microscope.* Biophysical journal, 2002. **82**(5): p. 2798-2810.

120. Hertz, H.R., *Über die Berührung fester elastischer Körper und über die Härte.* Verhandlungen des Vereins zur Beförderung des Gewerbfleißes, Berlin : Verein zur Beförderung des Gewerbefleisses, 2006. **1882**: p. 449-463.

121. Gardel, M.L., et al., *Traction stress in focal adhesions correlates biphasically with actin retrograde flow speed.* The Journal of Cell Biology, 2008. **183**(6): p. 999.

122. Sackmann, E., *How cells feel the force.* Nature Physics, 2010. **6**: p. 407.

123. Moeendarbary, E. and A.R. Harris, *Cell mechanics: principles, practices, and prospects.* 2014. **6**(5): p. 371-388.

124. Colin-York, H. and M. Fritzsche, *The future of traction force microscopy.* Current Opinion in Biomedical Engineering, 2018. **5**: p. 1-5.

125. Style, R.W., et al., *Traction force microscopy in physics and biology.* Soft Matter, 2014. **10**(23): p. 4047-4055.

126.   del Álamo, J.C., et al., *Spatio-temporal analysis of eukaryotic cell motility by improved force cytometry.* Proceedings of the National Academy of Sciences, 2007. **104**(33): p. 13343.

127.   Sabass, B., et al., *High resolution traction force microscopy based on experimental and computational advances.* Biophys J, 2008. **94**(1): p. 207-20.

128.   Munevar, S., Y. Wang, and M. Dembo, *Traction force microscopy of migrating normal and H-ras transformed 3T3 fibroblasts.* Biophysical journal, 2001. **80**(4): p. 1744-1757.

129.   Butler, J.P., et al., *Traction fields, moments, and strain energy that cells exert on their surroundings.* Am J Physiol Cell Physiol, 2002. **282**(3): p. C595-605.

130.   Kartenbeck, J., et al., *Different modes of internalization of proteins associated with adhaerens junctions and desmosomes: experimental separation of lateral contacts induces endocytosis of desmosomal plaque material*. Vol. 1. 1982. 725-32.

131.   Kartenbeck, J., et al., *Endocytosis of junctional cadherins in bovine kidney epithelial (MDBK) cells cultured in low Ca2+ ion medium.* J Cell Biol, 1991. **113**(4): p. 881-92.

132.   Martin, A.C., et al., *Integration of contractile forces during tissue invagination.* The Journal of Cell Biology, 2010. **188**(5): p. 735.

133.   Meng, W. and M. Takeichi, *Adherens junction: molecular architecture and regulation.* Cold Spring Harb Perspect Biol, 2009. **1**(6): p. a002899.

134.   Martin, A.C., et al., *Integration of contractile forces during tissue invagination.* J Cell Biol, 2010. **188**(5): p. 735-49.

135.   Bambardekar, K., et al., *Direct laser manipulation reveals the mechanics of cell contacts in vivo.* Proc Natl Acad Sci U S A, 2015. **112**(5): p. 1416-21.

136. Campas, O., et al., *Quantifying cell-generated mechanical forces within living embryonic tissues.* Nat Methods, 2014. **11**(2): p. 183-9.

137. Liu, Z., et al., *Mechanical tugging force regulates the size of cell-cell junctions.* Proc Natl Acad Sci U S A, 2010. **107**(22): p. 9944-9.

138. Muhamed, I., F. Chowdhury, and V. Maruthamuthu, *Biophysical Tools to Study Cellular Mechanotransduction.* Bioengineering (Basel), 2017. **4**(1).

139. Ng, M.R., et al., *Mapping the dynamics of force transduction at cell-cell junctions of epithelial clusters.* Elife, 2014. **3**: p. e03282.

140. Tambe, D.T., et al., *Collective cell guidance by cooperative intercellular forces.* Nat Mater, 2011. **10**(6): p. 469-75.

141. Tang, X., et al., *A novel cell traction force microscopy to study multi-cellular system.* PLoS Comput Biol, 2014. **10**(6): p. e1003631.

142. Maruthamuthu, V. and M.L. Gardel, *Protrusive activity guides changes in cell-cell tension during epithelial cell scattering.* Biophys J, 2014. **107**(3): p. 555-563.

143. Mertz, A.F., et al., *Scaling of traction forces with the size of cohesive cell colonies.* Phys Rev Lett, 2012. **108**(19): p. 198101.

144. Wang, N., et al., *Cell prestress. I. Stiffness and prestress are closely associated in adherent contractile cells.* Am J Physiol Cell Physiol, 2002. **282**(3): p. C606-16.

145. Vignaud, T., H. Ennomani, and M. Thery, *Polyacrylamide hydrogel micropatterning.* Methods Cell Biol, 2014. **120**: p. 93-116.

146. Martiel, J.L., et al., *Measurement of cell traction forces with ImageJ.* Methods Cell Biol, 2015. **125**: p. 269-87.

147. Plotnikov, S.V., et al., *High-resolution traction force microscopy.* Methods Cell Biol, 2014. **123**: p. 367-94.

148. Schwarz, U.S., et al., *Calculation of forces at focal adhesions from elastic substrate data: the effect of localized force and the need for regularization.* Biophys J, 2002. **83**(3): p. 1380-94.

149. Kimura, K., et al., *Regulation of myosin phosphatase by Rho and Rho-associated kinase (Rho-kinase).* Science, 1996. **273**(5272): p. 245-8.

150. Vincent, R., et al., *Active Tensile Modulus of an Epithelial Monolayer.* Phys Rev Lett, 2015. **115**(24): p. 248103.

151. Casares, L., et al., *Hydraulic fracture during epithelial stretching.* Nat Mater, 2015. **14**(3): p. 343-51.

152. Tambe, D.T., et al., *Monolayer stress microscopy: limitations, artifacts, and accuracy of recovered intercellular stresses.* PLoS One, 2013. **8**(2): p. e55172.

153. Benjamin, J.M. and W.J. Nelson, *Bench to bedside and back again: molecular mechanisms of alpha-catenin function and roles in tumorigenesis.* Semin Cancer Biol, 2008. **18**(1): p. 53-64.

154. Hajra, K.M. and E.R. Fearon, *Cadherin and catenin alterations in human cancer.* 2002. **34**(3): p. 255-268.

155. Yu, J., et al., *α-Catenin expression is decreased in human gastric cancers and in the gastric mucosa of first degree relatives.* 2000. **46**(5): p. 639-644.

156. Matsuzawa, K., et al., *alpha-Catenin Controls the Anisotropy of Force Distribution at Cell-Cell Junctions during Collective Cell Migration.* Cell Rep, 2018. **23**(12): p. 3447-3456.

157. Buckley, C.D., et al., *The minimal cadherin-catenin complex binds to actin filaments under force.* Science, 2014. **346**(6209): p. 1254211.

158. Ishiyama, N., et al., *An autoinhibited structure of alpha-catenin and its implications for vinculin recruitment to adherens junctions.* J Biol Chem, 2013. **288**(22): p. 15913-25.

159. Seddiki, R., et al., *Force-dependent binding of vinculin to alpha-catenin regulates cell-cell contact stability and collective cell behavior.* Mol Biol Cell, 2018. **29**(4): p. 380-388.

160. Hazan, R.B., et al., *Vinculin is associated with the E-cadherin adhesion complex.* J Biol Chem, 1997. **272**(51): p. 32448-53.

161. Chen, H., D.M. Choudhury, and S.W. Craig, *Coincidence of actin filaments and talin is required to activate vinculin.* J Biol Chem, 2006. **281**(52): p. 40389-98.

162. Ziegler, W.H., R.C. Liddington, and D.R. Critchley, *The structure and regulation of vinculin.* Trends in Cell Biology, 2006. **16**(9): p. 453-460.

163. Chen, H., et al., *Spatial distribution and functional significance of activated vinculin in living cells.* J Cell Biol, 2005. **169**(3): p. 459-70.

164. Peng, X., et al., *α-Catenin uses a novel mechanism to activate vinculin.* The Journal of biological chemistry, 2012. **287**(10): p. 7728-7737.

VITA

SANDEEP DUMBALI

Dr. Maruthamuthu's Cellular Mechanobiology Lab, Old Dominion University, Norfolk VA
✉ sdumb001@odu.edu, sandeepdumbali@gmail.com ☏ 979-922-9119

EDUCATION

PhD. Mechanical Engineering	Old Dominion University (ODU), USA	2015-2019
M.Tech. in Computer Integrated Manufacturing	Visvesvaraya Technological University, India	2009-2011
B.E. Production Engineering	Solapur University, India	2005-2009

RESEARCH EXPERIENCE

Cell Mechanobiology Lab 2120 ESB, Mechanical and Aerospace Engineering Department, ODU
Projects:
- E-cadherin Force Regulation in Cell Proliferation – Collaborated with VCU (2015-2017)
- Endogenous Force Transmission within Large Epithelial Colony (2016-2018)
- Characterization of Cell Substrates (2017-2018)
- Mechanical Virtues within Supracellular Collectives (2017-2018)
- Levels of Cytoskeletal Elements Affecting Intercellular Force (2018-2019)

SKILLS AND TECHNIQUES

Lab:	**Computer:**
Mammalian Cell Culture	MATLAB
DNA/siRNA Transfection	Image Processing Software: Image J, Adobe Photoshop, Gimp
Immunofluorescence Staining	Inkscape, SciDAVis,
Fluorescence Microscopy	**Post Graduate Diploma in Computer Aided Engineering**
Traction Force Microscopy	(2012-2013):
Cell Substrate Fabrication	Finite Element Modeling – HyperMesh
Substrate Micro-patterning	Finite Element Analysis – ANSYS & Workbench
Atomic Force Microscopy	Computational Fluid Dynamics - ICEM & FLUENT

PUBLICATIONS

- **Sandeep Dumbali**, Lanju Mei, Shizhi Qian, Venkat Maruthamuthu, Endogenous Sheet-Averaged Tension Within a Large Epithelial Cell Colony. ASME. Journal of Biomechanical Engineering. 18th August 2017, 139 (10):101008-101008-5. doi:10.1115/1.4037404
- Yashar Bashirzadeh*, Siddharth Chatterji*, Dakota Palmer*, **Sandeep Dumbali***, Shizhi Qian, Venkat Maruthamuthu, Stiffness Measurement of Soft Silicone Substrates for Mechanobiology Studies Using a Widefield Fluorescence Microscope, Journal of Visualized Experiments (137), 3rd July 2018, e57797, doi: 10.3791/57797 (*These authors contributed equally)
- Abhinav Mohan, Kyle Schlue, Alex Kniffin, Ashley Duke, Vani Narayanan, Paul Arsenovic, **Sandeep Dumbali**, Venkat Maruthamuthu, Daniel Conway. Spatial proliferation of epithelial cells is regulated by E-cadherin force, Biophysical Journal. 23rd July 2018, doi: 10.1016/j.bpj.2018.07.030
- Yashar Bashirzadeh, **Sandeep Dumbali**, Shizhi Qian, Venkat Maruthamuthu. Mechanical response of an epithelial island subject to uniaxial stretch on a hybrid silicone substrate, Journal of Cellular and Molecular Bioengineering, 19th October 2018, doi.org/10.1007/s12195-018-00560-1